KU LEUVEN

ARENBERG DOCTORAL SCHOOL
FACULTY OF SCIENCE

ELECTRO-OPTICAL SWITCHING OF PLASMONIC NANOPARTICLES INSIDE CAPACITOR-LIKE NANOSTRUCTURES

Milan OBRADOVIC

Supervisor:
Prof. Dr. Peter Lievens
Co-supervisor:
Prof. Dr. Marcel Di Vece, University of Milan

Members of the Examination Committee:
Prof. Dr. Chris Van Haesendonck, KU Leuven, chair
Prof. Dr. Gustaaf Borghs, KU Leuven
Prof. Dr. Koen Clays, KU Leuven
Prof. Dr. Jean-Pierre Locquet, KU Leuven
Prof. Dr. Zoran Popovic, University of Belgrade

Dissertation presented in partial fulfilment of the requirements for the degree of Doctor of Science

May 2017

Мојим вољеним:
прецима (Србима Лике и Црне Горе),
жени Олги и
чедима: Сави, Василији, Даници, ...[i]

[i] To my beloved: ancestors (Serbs from Lika and Montenegro), wife Olga and children: Sava, Vasilija, Danica, …

Acknowledgements

My PhD research may be split into two parts. The first one is the time I have spent in Belgium, where I did experimental work, along with other researchers. The second part is the time that, although unwillingly, I have spent in Serbia (because I preferred to finalise my PhD while being in Belgium). Yet, in Serbia I have been spending quite some time in both a beautiful town Inđija and a beautiful village Lovćenac, while connected via Wi-Fi to the publications database, immersed in scientific articles, reading, writing, working on calculations and simulations.

Starting to thank as many people as I came across during my research career, who consciously or unconsciously have helped me on that journey, I believe, would be a formidable task since here or there, due to the long list, I would surely inadvertently omit someone. Yet, I would like to mention all essential persons on both my research and life road and to attempt to thank them all. First, to my supervisor Prof. Dr. Peter Lievens, who, along with his everyday struggle to keep up successfully on his two roads by being a devoted dean and an organiser, as well as a successful scientist, found time to scientifically guide me to the successful end. Also, a great thank to my co-supervisor Prof. Dr. Marcel Di Vece who was mentoring me both on location (in Belgium) and "online" (from Argonne (USA), Denmark, Utrecht and Italy) and whose ideas have outstandingly inspired me. Above all, I thank them for giving me the opportunity of doing my doctoral research in a strongly scientific and irreplaceable environment for research in one of the most important, as well as intriguing scientific fields of electro-optical and plasmonic properties of small metal nanoparticles. I also thank Dr. Didier Grandjean for having

many fruitful discussions and talks about planned and realized experiments.

I would like to express a great gratitude to the Research Foundation-Flanders (FWO, Belgium), Flemish Concerted Action (BOF KU Leuven), as well as IMEC vereniging zonder winstoogmerk (association without lucrative purpose) for their financial support and great possibilities to work in this cutting-edge research.

I also thank the members of the doctoral committee: Prof. Dr. Gustaaf Borghs, Prof. Dr. Koen Clays, Prof. Dr. Jean-Pierre Locquet, Prof. Dr. Chris Haesendonck and Prof. Dr. Zoran Popovic for their interest in my research and their time spent in reading and efforts in improving the thesis. I thank Prof. Dr. Koen Clays for giving me the opportunity to work in the chemistry lab of his group where I employed an absorption spectrometer virtually in all my experiments, as well as mastered chemistry while performing electrochemical experiments. I thank Dr. Inge Asselberghs for experimental assistance and help, Prof. Dr. Chris Haesendonck for allowing me to use and master atomic force microscopy which was essential in my experiments, as well as Prof. Dr Gustaaf Borghs for his inspiring lessons on optical properties of solids.

I would also like to thank all other people with whom I worked and collaborated (Branko, Kelly, Christian, Koen), as well as those who were from our vivid CLASS group or with whom I shared time and facility, discussed, talked and those who helped me in any way: Prof. Dr. Roger Silverans, Prof. Dr. Margriet Van Bael, Prof. Dr. Ewald Janssens, Jorg and Thuy, Christian, Dries, Nico, Aurélie, Kenneth, Thomas, Wim, Ayele, David, Pieterjan, Yejun, Zhe, Jo, Sandra, Tobias, Tom, Maarten, Katrien, Sabina, Vladimir, Tung, Li, Thomas, Zhe, David, Koen, Stijn, Edith, Monique, Liliane, Jeroen, Bas, Philip, Phillipe, Stijn, but also those whose lives somehow were bound to mine (Dmitry and Arezou, Alessandro and Ester, Prof. Dr. Dejan Rakovic, Prof. Dr. Branislav Jelenkovic, Jovan Polovina (teacher in physics), Denise, Abey and Marta, Ivana, Mario, Vladimir and Biljana, Fr. Viktor and Judith, Luc and Francoise, Dorin, Jeremy, Dr. Žarko Vidović...). In addition, I thank all

people that I know, who somehow influenced my life, whether being + or -, since both influences make anyone stronger and fit.

I thank my grandparents: Milan (Mile), Sava (Saja), Marko and Vukosava; my father Stanko and my mother Đina, who made, brought up and taught me such as I am; my sister Bojana, brother-in-law Predrag, and nieces Maša, Anastasija and Mila, my both paternal and maternal relatives who have supported, and at least a bit affected not only my career, but my life (prababe Maša and Gospava, deda Špiro, Dr. Mitar Pešikan, Sofija Pekic, Vesna, Božidar, Marko, Branko, Dr. Zoran M. Obradović, Nevenka, Bosiljka, Zorica...), as well as Fr. Vojislav.

I thank my "perpetuum mobile" - my beloved children: Faith, Hope and Love, i.e. Sava (8), Vasilija (6) and Danica (4) ... ... … who are a great inspiration for my moves in this full-of-surprises life. I thank my ever-increasingly beloved wife Olga who has supported me unreservedly… Thank thee, God, for giving me everything I am and for teaching me to use the gifts thou gave me. I apologise those people whose names by chance I failed to mention here; I thank them too.

The PhD is a big bite which is eventually finilised. However, my research, as well as my life, has just started... at least looking from eternity, where the light is just an untouchable property...

Milan (Stankov) Obradović
February 2017

„ *I am your immortal spark*
– a bright idea said to me –
I shall lead thee to the eternal hearth
Wherefrom I have likewise flown."

From The Ray of the Microcosm,
by Peter II Petrovic Njegos (1813-1851)

Abbrevations	*Full Name*
APSiO	amine-terminated siloxane
a.u. / arb.u.	arbritary units
AFM	Atomic Force Microscopy
CBD	Cluster Beam Deposition (technique)
CDA	Cluster beam Deposition Apparatus
CB	conduction band
DNA	deoxyribonucleic acid
DLVO	Derjaguin-Landau-Verwey-Overbeek (theory)
EELS	Electron-Energy-Loss Spectroscopy
FWHM	Full Width at Half Maximum
ITO	Indium Tin Oxide
MBE	Molecular Beam Epitaxy
NC	nanocluster
NP	nanoparticle
NIR	Near Infra Red
PL	photoluminescence
PMT	photomultiplier tube
RF	radiofrequency
RIU	Refractive Index Unit
RNA	ribonucleic acid
SCCM	Standard Cubic Centimeters per Minute
3D	three-dimensional
TOF	time-of-flight
UHV	ultra high vacuum
UV	ultraviolet
VB	valence band
VIS	visible
XRD	X-ray diffraction

Contents

Preface

" A single ray of light from a distant star falling upon the eye of a tyrant in bygone times may have altered the course of his life, may have changed the destiny of nations, may have transformed the surface of the globe, so intricate, so inconceivably complex are the processes in Nature."

Nikola Tesla

Colours, as a consequence of light-matter interaction, were as one of the superb impressions for the early man. Although he has very early mastered extracting and smelting metals from the ores [1], it is only a few centuries ago that light has been increasingly understood and indispensibly employed. Even the ancient Romans have known this interaction, but have also lacked in-depth knowledge to understand it more profoundly. However, although the light-matter interaction was inconceivable in that time, ancient man was astonished by the interaction thanks to material extraction from its ore. The highlight of the "unconscious" knowledge and the ancient Roman's longing for decoration and propelling to a more profound intellect was incorporated in the Lycurgus Cup, see Fig. 1. The ancient Roman has made this cup in the 4^{th} century and it is preserved and stored in the British Museum in London.
It was made of glass and gold/silver alloy nanoparticles giving rise to a fantastic colour pattern; the size of the gold/silver alloy particles are claimed to be ~70 nm [3] which is small enough to render *the plasmon resonance effect* (which is to be described

and used as one of the crucial parameters in the thesis). Although the ancient Romans have not understood the nanophysics of the Lycurgus cup, they knew how to make artefacts with noble metal nanoparticles whose intense colours inspired many artists and fascinated scientists for centuries to come.

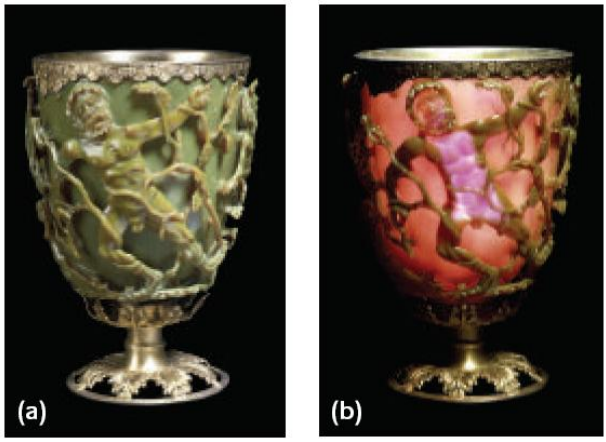

Fig. 1. The Lycurgus cup (continuously exhibited at the British Museum, London). When a light source stands outside the cup (a), the olive colour is a result of the reflection of light, and when the light source stands in the cup (b), the red and olive colour is a result of transmission of light and light scattering, respectively [2].

It is only for a few last decades that the electro-optical properties of metal nanoparticles were considerably studied. This scientific engagement is not unexpected since more than 80 per cent of information from the external world, we receive throughout our eyes [4]. This fact expresses by itself how important it is to study the optical properties of nanoparticles and their changes caused by diverse physical phenomena. However, these changes are not in general detectable with the naked eye and modern facilities and techniques must be evolved and employed to disentangle the world of light-matter interaction.

A great upsurge of interest in an attempt to understand the electro-optical properties of noble metal nanoparticles relies

on their extraordinary and very attractive features which are not present in other metals. Gold is the noblest of all the metals [5] which, reducing its size to as low as a few nanometers, loses its luster, but starts exhibiting *plasmon resonances* in the visible part of the electromagnetic spectrum. In general, the optical properties of nanoparticles significantly depend on particle shape, size and environment [6, 7]. To attain the finest optical properties of nanoparticles in a bottom-up method, a controllable deposition is required. The advent of lasers in the last century has created new techniques to deposit nanoparticles in a fine and controllable way which enabled clearer conception of the absorption spectrum of the deposited metal nanoparticles. However, at the same time, this development increased the number of new and unknown electro-optical properties waiting to be resolved and disentangled, especially when the particle size reached the nanometer size. At first glance, there is an increasing number of research groups which are investigating the optical properties of metal nanoparticles more profoundly; this increase is likely exponential, as illustrated in Fig. 2. However, there have yet been some research gaps and some phenomena are underestimated despite there is plenty of room for research. Fortunately, in the last few years considerable attention was given to collecting and merging up-to-date knowledge on the optical properties of metal nanoparticles, both theoretically and experimentally [8]. There are many investigations of electro-optical properties of metal nanoparticles ongoing. For example, a compelling aspect is certainly how metal nanoparticles, possessing intrinsic memory (storing, charging) effects, behave electro-optically in a capacitor-like structure. To this end, more then a decade ago, a very interesting pioneering work on capacitance variation with nanometric-sized metal nanoparticles has been theoretically elaborated [9, 10], also stating the lack of research in this field. This fact is still not much changed up till now, however.

Objectives and short summary of the thesis

In this thesis the electro-optical behaviour of capacitor-like nanostructures containing 1-10 nm sized noble metal nanoparticles is studied. The plasmonic properties of the metal particles are controlled by changing the charge density which results in a change of the optical absorption and photoluminescence. Due to its nobleness gold nanoparticles are a convenient choice as they do not oxidize and have a well defined plasmon resonance [5]. The main objective of the thesis is to study the effect of charge on the plasmonic properties of metal (gold and silver) nanoparticles. This was achieved by constructing a capacitor-like nanostructure in which the plasmonic nanoparticles act as electron storing islands, i.e. electron receptors. When the entire nanostructure is electrically charged, the plasmonic particles, embedded within the nanocapacitor, store electrons from the immediate surroundings, as provided by the electrical potential difference, giving rise to a shift of the plasmon resonance. The subtle correlation between electric charging and optical spectra makes it possible to use such nanodevices for electro-optical switching. While the nanoparticle samples were electrically charged in a different manner, the optical changes were simultaneously examined by measuring the optical absorption or photoluminescence. Nanoparticles were deposited on a conductive support and covered by diverse layers such as ZnO. By immersing the sample in a solution or by covering it with an electrode layer, it acts as a capacitor nanodevice with interesting and novel electro-optical switching properties.

The interaction between the ZnO semiconducting properties and the plasmonic properties of gold nanoparticles were investigated leading to the important discovery of charge transfer from defects in the ZnO to the gold, shifting the plasmon resonance energy. This provides a novel method to control the optical properties of gold nanoparticles with charge. Furthermore, the thesis explores the electro-optical properties of ~ 2 nm sized noble metal nanoparticles, which may exhibit quantum confinement properties due to its very small size.

The research topic of plasmonic nanoparticles is very timely as indicated by Fig. 2, which illustrates an increase of the research interest with the relevant key words. It indicates a prospective trend for further research that may lead to applications indiverse nanodevices and nanostructures.

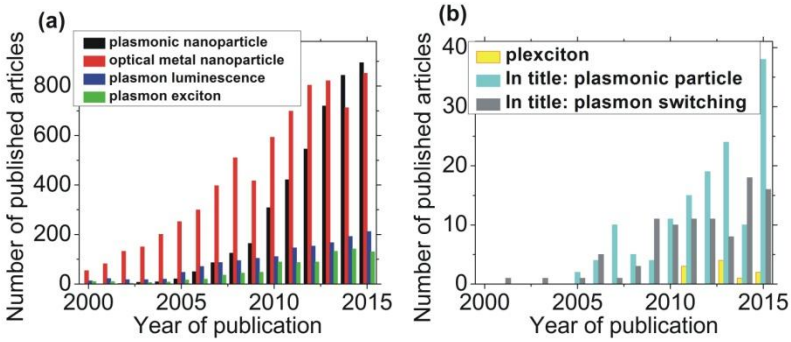

Fig. 2. The annual number of published articles containing distinctive words (in the thesis) according to Web of Science database (2016). "*In title*" in (b) means that the words appear in the titles of articles).

The first part of the thesis, along with the theoretical and experimental sections, is devoted to the distinction between two concepts of being small in nanoparticles, i.e. "small" and "very small". Due to the importance of quantum confinement at the nanometer scale, significant differences in the electronic and optical characteristics may be expected. We consider metal (gold) particles with diameters as large as 100 nm to be "*large*", those with diameters lower than 3-5 nm to be "*small*" and those in the range of 1-2 nm to be *"very small"* (the main reason is the non-scalable change of properties with size, see later in the thesis), although slightly different definitions do exist [11]. The very small particles are often named clusters or nanoclusters.

The Leuven cluster beam deposition apparatus can produce very small uncoated nanoclusters (nanoparticles) in a fine island-like pattern, allowing for constructing a bottom-up nanodevice with specific electro-optical features. The second part of the thesis is focused on the prime aim – tuning of the electro-optical properties of noble metal nanoparticles; this was accomplished either by changing the pH of the nanostructure

surrounding or by applying a voltage to it. The external changes give rise to an electron redistribution onto the embedded nanoparticles which accordingly modifies the plasmonic and electro-optical properties as a whole. This mechanism makes gold nanoparticles so attractive for applications in nanotechnology.

Although it is still a challenge to discriminate the effective and the dominating background signal, nanoplasmonics does not only enable to overcome the classical diffraction barrier, but is also an ideal platform for electro-optical switching necessary in many applications [12]. Optical devices, along with embedded (nano)plasmonic metal nanoparticles, are quintessential in near future high density optical data storage and high-speed signal processing [13, 14, 15, 16], catalysis [17], data storage [18], computer chips [19], plasmon-assisted solar energy conversion [6], tele-communications [20], consumer electronics and environment [21], as well as in nascent applications in biophysics [12, 22] and biosensing [6, 13, 23, 24, 25, 26, 27, 28]. This thesis contributes to the study of switching gold nanoparticles as well as to nanodevices based thereon.

Chapter overview

Chaper 1 gives the theoretical background for understanding the phenomena observed in the performed experiments. It sweeps through equations, necessary to understand and account for the electro-optical properties of metal nanoparticles. Approximations were also shown since they enable relatively simplified calculations, without losing much of accuracy, thus facilitating the overall understanding. Eventually, the electronic structure and electronic behaviour in nanoparticles is also envisioned.

Chapter 2 gives an overview of the setups employed during the experiments, e.g. the cluster deposition setup and the optical characterization techniques which have been extensively employed. The former represents a state-of-the-art deposition facility available in our research group and the latter was used to

examine and account for electro-optical behaviour of the studied nanodevices. Additional experimental details, employed in a particular experiment, are described in the relevant chapter where the new technique or setup is utilized.

Chapter 3 explains how the absorption spectrum of metal nanoparticles (gold) is affected by the nanoparticle size variation, indicating that the optical properties of 1-2 nm sized gold nanoparticlesare differentfrom slightly larger ones. A further distinction is reflected in a peculiar absorption spectrum of *"very small nanoparticles"* (around 1-2 nm in diameter) which may be explained by particle plasmon coupling or effects associated with the discretized electronic levels. Although the chapter does not investigate the differences in detail, it demonstrates that there is a great opportunity for the future research to better understand the very meaning of the frontier between "small" and "very small".

In **Chapter 4**, the possibility of the electric charge variation around differently deposited metal nanoparticles by pH variation of the surroundings is described. It relates changes of the plasmonic properties (via absorption spectra) upon changing the surrounding pH value as a consequence of the electric charge change in the environment. The behaviour of both the gold colloidal solution and the laser-deposited gold clusters is compared and a trend of plasmonic behaviour upon electric charges via pH alteration is highlighted. Further research directions have also been suggested.

Chapter 5 demonstrates that electro-optical switching in metal nanoparticles can be achieved by adding or removing electrical charge. The capacitor-like structure was electrochemically charged. Here, an interesting approach is taken, i.e. changing the photoluminescence properties as a function of electrical charge on gold nanoparticles. A relation between absorption and photoluminescence has revealed an influence of the charge state on the electronic properties, and therefore on the optical transition probability, opening a new way for electro-optical switching.

Chapter 6 reports on a capacitor-like nanodevice built with gold clusters embedded in a ZnO layer. The plasmon resonance frequency shifts when the electric charge on a metal

nano-object is altered. We thus indirectly vary the number of free electrons in gold nanoparticles embedded within a ZnO layer, by applying an electrical potential difference over the entire heterostructure. This potential difference consequently induces shifts of defect energy levels in the ZnO resulting in electron exchange between particles and surrounding matrix which in turn modifies the gold nanoparticle plasmon properties. In addition, the study was supported with a calculation which was compared with recent studies. This electro-optical effect is a promising way to obtain fast optical switching in the visible spectrum in a solid state composition. This also holds a promise for both fundamental and applied research in optics, e.g. in the study of the phenomenon of light trapping by coupling to electrons near a metal surface.

Chapter 7 continues with an analogous nanostructure where silver clusters are deposited instead of gold. This chapter emphasizes the importance of a broader research of similar capacitor-like nanostructures to unravel their electro-optical (switching) properties. Silver nanoclusters were deposited by the cluster deposition apparatus and later covered by a ZnO layer. An overlap of the excitonic and plasmonic peaks of this nanostructure shows distinctive switching features when electrically charged, which could have benefits in amplifying and sensing applications.

Chapter 1

Optical properties of metal nanoparticles

"The scientific man does not aim at an immediate result. He does not expect that his advanced ideas will be readily taken up. His work is like that of the planter - for the future. His duty is to lay the foundation for those who are to come, and point the way. He lives and labours and hopes."

Nikola Tesla

This chapter introduces the underlying concepts of electro-optical properties of noble metal nanoparticles used further on in the thesis. Calculations in the following chapters are based upon relations and approximations given here. In addition, important terminology is also introduced. The introduction of concepts and terminology starts with the main principles; in case of the electromagnetic and opto-electrical properties of materials, these are the equations of Maxwell.

1.1 Maxwell's equations

The theoretical basis and explanatory tool of diverse electro-optical phenomena in a nanostructure are the Maxwell's equations. They also represent the starting point for many approximations which facilitate calculation, still keeping considerable accuracy. Two field vectors: the electric displacement field, $\boldsymbol{D}$ and the magnetizing field, $\boldsymbol{H}$, respectively, are defined in vacuum as (vectors are henceforth represented by bold fonts):

$$\boldsymbol{D} = \varepsilon_0 \cdot \boldsymbol{E} + \boldsymbol{P} \tag{1.1}$$

$$\boldsymbol{H} = \frac{1}{\mu_0} \cdot \boldsymbol{B} - \boldsymbol{M} \tag{1.2}$$

where $\boldsymbol{E}$ is the electric field, $\boldsymbol{P}$ is the local electric polarization of matter, $\boldsymbol{B}$ is the magnetic field, $\boldsymbol{M}$ is the local magnetization, ε_0 is the permittivity of free space, and μ_0 is the permeability of free space. By these two vectors, $\boldsymbol{D}$ and $\boldsymbol{H}$, the free charge density, ρ_F and the current density,j_f, respectively, can be accounted for by means of Maxwell's equations:

$$\nabla \cdot \boldsymbol{D} = \rho_F \tag{1.3}$$

$$\nabla \cdot \boldsymbol{B} = 0 \tag{1.4}$$

$$\nabla \times \boldsymbol{H} = j_F + \frac{\partial}{\partial t}\boldsymbol{D} \tag{1.5}$$

$$\nabla \times \boldsymbol{E} = -\frac{\partial}{\partial t}\boldsymbol{B} \tag{1.6}$$

For simplicity, the external electric field is henceforth assumed to be harmonic:

$$\boldsymbol{E}(\boldsymbol{r}, t) = \boldsymbol{E}_0 \cdot e^{-i\omega t} \tag{1.7}$$

Although in practice many fields are quite intricate, any complex field can be portrayed as a superposition of such fields by Fourier transformation.

1.2 Drude model

The Drude model is an approximation which assumes free coherent movement of individual electrons in a metal nanoparticle upon perturbation. This coherent electron movement leads to a macroscopic response, comprising a sheer sum of the effects of all electrons of a nanoparticle. These electrons collide with each other and other collision centres. The electron (carrier) lifetime, τ, is commonly called the relaxation time. The average rate of collision processes, $\Gamma = \tau^{-1}$, is commonly called the relaxation (damping) constant which represents the electron collision rate. Importantly, this model only considers the valence atomic orbitals: 6*s*, 5*s* and 4*s* for gold, silver and copper, respectively. If a nanoparticle is smaller than the bulk mean free path, the wavelength becomes dependent upon *r* and an extra term must be added to the bulk damping constant [29, 30]:

$$\Gamma(r) = \Gamma + A\frac{v_F}{r} \tag{1.8}$$

where v_F is the Fermi velocity and *A* is the proportionality factor which takes the following values: 1, ¾ and 0, if the scattering is assumed to be isotropic, diffusive and elastic, respectively [29]. This factor is not devoid of controversy [30] and ranges between theoretically justified values: 0.1 and 2 [31].

The Full Width at Half Maximum (FWHM) of the absorption spectrum is strongly related to the dephasing time τ of free electrons which constitutes the plasmon resonance, as a result of coherent oscillations of the free electrons; the plasmon decay rate (plasmon life time) can thus be determined by the FWHM [32]:

$$\tau_{plasmon} = \frac{1}{\pi c\left[\frac{1}{\lambda_{left}} - \frac{1}{\lambda_{right}}\right]} \tag{1.9}$$

Kreibig et al. [11] have elegantly presented the Drude model and the penetration depth of electromagnetic waves in metals, which is partly paraphrased in the following lines:

When the external field (equation (1.7)) affects a nanoparticle, it actually affects its free electrons with the mass, m_e, and the charge, e:

$$m_e \frac{\partial^2 \boldsymbol{r}}{\partial t^2} + m_e \Gamma \frac{\partial \boldsymbol{r}}{\partial t} = e\boldsymbol{E_0} e^{-i\omega t} \tag{1.10}$$

This differential equation is valid without eigenfrequencies for $\omega > 0$ and corresponds only to the free conduction band electrons; to involve the bound electrons, a linear restoring force determining the eigenfrequency of the oscillating electron should be added to equation (1.10) [11]. By solving zero of equation (1.10), one can easily get the dipole moment of an electron $p = er_0$ and the polarization $\boldsymbol{P} = n\boldsymbol{p}$, where n is the number of electrons per unit volume. The polarization $\boldsymbol{P}$ and the dielectric function $\varepsilon(\omega)$ are related as $\varepsilon = 1 + \boldsymbol{P}/(\varepsilon_0 \boldsymbol{E})$, and ε is related to the complex index of refraction by $n + ik = \sqrt{\varepsilon}$. The electronic polarizability, α is defined by $\boldsymbol{P} = n\alpha\boldsymbol{E}$ (within an isotropic media) and has the following relation with ε [11]:

$$\varepsilon - 1 = \frac{1}{\varepsilon_0} n\alpha \tag{1.11}$$

The complex dielectric function $\varepsilon(\omega) = \varepsilon_1(\omega) + i\varepsilon_2(\omega)$ of a system of n free electrons per unit volume can be written as [11]:

$$\begin{aligned} \varepsilon(\omega) &= 1 - \frac{\omega_p^2}{\omega^2 + i\Gamma\omega} = \\ &= 1 - \frac{\omega_p^2}{\omega^2 + \Gamma^2} + i\frac{\omega_p^2 \Gamma}{\omega(\omega^2 + \Gamma^2)} \end{aligned} \tag{1.12}$$

where

$$\omega_p = \sqrt{\frac{ne^2}{\varepsilon_0 m_e}} \tag{1.13}$$

is the Drude plasma frequency. In addition to the Drude plasma frequency, Table 1.1 shows additional and important electro-optical parameters of some noble metals.

Table 1.1. The volume (bulk) plasma frequency, ω_p, the damping constant, Γ and the Fermi velocity, v_F of some noble metals [37].

Metal	$\boldsymbol{\omega_p}$ **[eV]**	$\boldsymbol{\Gamma}$ **[eV]**	$\boldsymbol{v_F}$ **[10^6 m/s]**
Silver	9.2	0.021	1.4
Gold	9.1	0.072	1.4
Copper	8.8	0.092	1.6
Aluminum	15.1	0.605	2

If $\omega \gg \Gamma$, the real and imaginary part of $\varepsilon(\omega)$ for free-electron metals (equation (1.12)) can be approximated, respectively, as [11]:

$$\varepsilon_1(\omega) \approx 1 - \frac{\omega_p^2}{\omega^2},\ \varepsilon_2(\omega) \approx 1 - \frac{\omega_p^2}{\omega^3}\Gamma \tag{1.14}$$

From the Drude approximation, equation (1.14), one can see that for $\varepsilon_1(\omega) = 0$, $\omega = \omega_p$. This particular frequency is called the volume (bulk) plasma frequency or merely the Drude frequency. The dielectric function $\varepsilon(\omega)$ can be represented in terms of the dielectric susceptibility, χ [11]:

$$\varepsilon(\omega) = 1 + \chi^{DS}(\omega) \tag{1.15}$$

where χ^{DS} is the free-electron Drude (-Sommerfeld) susceptibility [11].

In general, there are two assumed independent components of the dielectric function (absorption): the free

conduction electrons within one band (intraband absorption) and the bound electrons from one band to another (interband absorption) [33]. The coupling of free and core (deep level) electrons is accounted for by replacing the electron mass, m_e, with the effective mass of the electron, m^*. The disadvantage of the model is the assumption that all electrons are effectively the conduction electrons. However, there is indeed a considerable contribution of electrons from the deep levels (via interband transition) to the dielectric function, i.e. electrons undergoing the interband transition gives an additional contribution to the susceptibility and thus to the plasma oscillations (plasmon resonance) [34]. For example, this influence is more pronounced for gold and especially for copper than for silver nanoparticles [35], since the plasmon and the interband transition wavelength regions are respectively more and less overlapped. It is still a challenge to appropriately model the complex dielectric function of gold nanoparticles and to properly represent the frequency dependence of their dielectric function [36].

The dielectric function of the interband contribution in the standard Lorentz form is given as [37]:

$$\varepsilon_{IB} = 1 + \frac{\omega_1^2}{\omega_0^2 - \omega^2 - i\gamma\omega} \tag{1.16}$$

where ω_0 is the central oscillation frequency of a bound electron under an applied electric field, and ω_1 and γ are respectively related to the density and damping of bound electrons. Inserting corresponding parameters for gold: ω_0=2.8 *eV* (λ_0=450 *nm*), ω_1=3.0 eV and γ=0.6 eV [37] in equations (1.12) and (1.16), the dielectric function (permittivity) of gold nanoparticles, both with and without the interband transition contribution, can be calculated. Fig. 1.1(a) shows the free electron and the interband transition contributions to the complex dielectric function separately, while Fig. 1.1(b) shows the sum of the both contributions [37]. The constant values were taken from ref. [37] where a gold film was measured. However, the real plasmon resonance frequency strongly depends on size, geometry and environment [11, 38, 39]. This implies that, depending on the investigated system, the plasmon peak wavelength positions can

deviate from the one shown in Fig. 1.1 for as much as 100 nm. Numerous attempts to solve the problem of this inaccuracy were proposed [40, 41, 42]. Although these attempts included a large number of parameters, a recent study used a relatively simplified model based upon the Drude model [36].

The importance of the real part χ_1^{IB} comes into play for the lower frequencies, whereas the imaginary part χ_2^{IB} portrays the energy dissipation [11]. The complex dielectric function, with both the free and the bound electron contribution, can be written as:

$$\varepsilon(\omega) = 1 + \chi^{DS} + \chi^{IB} \tag{1.17}$$

Since bulk plasmons are longitudinally polarized charge-density waves [43], they cannot be coupled with transverse electro-magnetic fields, i.e. they cannot be excited optically. However, observing bulk plasmons can be performed by Electron-Energy-Loss Spectroscopy (EELS). The concept of surface plasmons has been introduced by Ritchie [44], shortly after the discovery of bulk plasmons in metals. Surface plasmons, i.e. surface plasmon polaritons are electro-magnetic excitations, i.e. delocalized electron oscillations at the interface between a metal and a dielectric which has lower energy than bulk plasmons. In small nanoparticles, when the surface-to-volume ratio is markedly high, electron oscillations (surface plasmons) can be detected by optical spectroscopy due to increased interface (boundary surface) with the surrounding dielectric [45]. Furthermore, whereas the surface plasmon dispersion relation for planar configurations is unique and thoroughly explained [46, 47], numerous surface plasmon dispersion relations for very small metal nanoparticles have been theoretically developed [48, 49, 50, 51] and understanding is constantly improving by taking into account quantum size effects of the particles [52, 53, 54].

1.3 Penetration depth of electromagnetic waves in metals

When an electromagnetic wave impinges on a metal particle, it penetrates through the particle to a certain point owing to energy dissipation. This holds for particles large enough so that the penetrated electron is relaxed within its relaxation time [11].

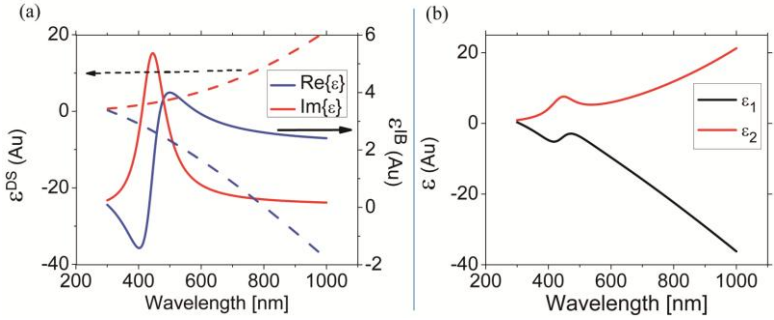

Fig. 1.1. Based on ref. [37]. (a) The real (blue) and the imaginary (red) part of the dielectric function for the free (dashed lines) and the interband transition (solid lines) electrons in gold. (b) The real (black) and the imaginary part (red) of the dielectric function of gold when both the free electron (Drude) and the interband transition contribution are taken into account.

If an electric field of the following form $\boldsymbol{E}(\boldsymbol{r},t) = \boldsymbol{E_0}e^{i(\boldsymbol{kr}-\omega t)}$ is assumed, where the wavevector, $\boldsymbol{k}$ can be written as $|\boldsymbol{k}| = \frac{\omega}{c}(n_r + ik)$, and if $\boldsymbol{kr} = |\boldsymbol{k}|z$ is assumed, the electric field obtains the following form [11]:

$$\boldsymbol{E}(\boldsymbol{r},t) = \boldsymbol{E_0}(\boldsymbol{r},t)e^{i\omega\left(\frac{zn_r}{c}-t\right)}e^{-\frac{z}{\delta}} \tag{1.18}$$

where δ is the skin depth, determining attenuation of the field [11]:

$$\delta = \frac{c}{\omega k} = \frac{\lambda}{2\pi k}. \tag{1.19}$$

The skin depth loses its significance while the particle size is decreasing; the attenuation is eventually negligible in small nanoparticles. There is a correlation between the absorption coefficient, k and the complex dielectric function, $\varepsilon(\omega)$ as [11]:

$$n + ik = \sqrt{\varepsilon_1(\omega)}. \tag{1.20}$$

As already mentioned, this holds only for larger and is negligible for smaller nanoparticles. However, when $\delta \leq l$, the nonlocal anomalous skin effect occurs, the formulae above do not hold anymore and some corrections have to be applied to properly account for this effect, see appendix A.2. In this case, only electrons moving nearly parallel to the surface are effective in absorbing and screening the electromagnetic radiation, since carriers moving perpendicular to the surface leave the skin depth before they scatter [55]. Table 1.2 shows skin depths and the respective bulk mean free paths for selected metals for a few different wavelengths at 273 K [11].

There is also another type of penetration depth which has nothing to do with energy dissipation. When considering the boundary of two different environments, i.e. at their surfaces, classically the electric field is discontinuous [11] and Maxwell's boundary conditions can elegantly account for this effect [56].

Table 1.2. Skin depth δ [nm] for selected metals as a function of wavelength, and the respective bulk mean free paths, l_∞ of the conduction electrons at 273 K [11].

Element	δ_{Au}	δ_{Ag}	δ_{Cu}	δ_{Al}
~ 620 nm	31	24	30	13
~ 415 nm	37	29	30	13
~ 310 nm	27	82	29	13
l_∞	42	52	42	16

1.4 Optical response of metal nanoparticles

1.4.1 Mie theory

Ludvig Lorenz and Gustav Mie independently calculated the response of a neutral metal nanoparticle to the external electromagnetic field by solving Maxwell's equations [11]. The dielectric function, $\varepsilon(\omega, R)$ may differ from ε_{bulk} since diverse effects, like spill-out of the negative charge density beyond the sphere radius of the positive charges (see appendix A.2), as well as the intrinsic size effects which affect Γ (equation (1.8)), have to be taken into account [57]. The dielectric function $\varepsilon(\omega, R)$ of a particle averages contributions of all electronic and atomic constituents of the particle [11].

The optical properties of nanoparticles are usually expressed by absorption, scattering, and extinction cross section, where the latter equals the sum of the first two [11]:

$$\sigma_{ext} = \sigma_{abs} + \sigma_{sca}. \tag{1.21}$$

According to the Lambert-Beer law [11]:

$$\Delta I_{abs}(z) = I_0(1 - e^{-\#\sigma_{abs} z}), \tag{1.22}$$

$$\Delta I_{sca}(z) = I_0(1 - e^{-\#\sigma_{sca} z}), \tag{1.23}$$

if respectively purely absorbing and purely scattering particles are assumed. In both cases, # represents the number density of clusters [11].

According to Mie's calculation, extinction, scattering and absorption cross sections are respectively [11]:

$$\sigma_{ext} = \frac{2\pi}{|\boldsymbol{k}|^2} \sum_{L=1}^{\infty} (2L+1)\, Re\{a_L + b_L\} \tag{1.24}$$

$$\sigma_{sca} = \frac{2\pi}{|\boldsymbol{k}|^2} \sum_{L=1}^{\infty} (2L+1)\, (|a_L|^2 + |b_L|^2) \tag{1.25}$$

$$\sigma_{abs} = \sigma_{ext} - \sigma_{sca}, \tag{1.26}$$

with Mie coefficients from the multipole expansion being [11, 36]:

$$a_L = \frac{m\psi_L(mx)\psi_L^{'}(x) - \psi_L^{'}(mx)\psi_L(x)}{m\psi_L(mx)\xi_L^{'}(x) - \psi_L^{'}(mx)\xi_L(x)} \tag{1.27}$$

$$b_L = \frac{\psi_L(mx)\psi_L^{'}(x) - m\psi_L^{'}(mx)\psi_L(x)}{\psi_L(mx)\xi_L^{'}(x) - m\psi_L^{'}(mx)\xi_L(x)}. \tag{1.28}$$

$m = n_{particle}/n_{medium}$, $\boldsymbol{k}$ is the wavevector, $x = |\boldsymbol{k}|r$ is the size parameter, $\psi_L(z)$ and $\xi_L(z)$ are the Riccati-Bessel cylindrical functions [11, 58].
L denotes the order of multipole expansion. In case of spheres, L=1, which is called the dipole mode, whereas in case of ellipsoid (rod-like) structures, L=2, which is called the quadrupole plasmon mode.

In contrast to reality, Mie theory does not anticipate a blueshift in the absorption spectrum while the noble particle size is decreasing. However, this discrepancy is accounted for by the quasi-static approximation which will be discussed in the following lines.

1.4.2 Quasi-static approximation

If the diameter of a spherical particle is within the order of penetration depth of the electromagnetic waves in metals, the excitation light can penetrate the particle. The field inside the particle collectively shifts the conduction electrons with respect to the fixed positive charge of the lattice ions resulting in a dipole nanoparticle. The difference in electrical potentials at two opposite sides of a particle leads to the restoring force. The frequency of light coincides with the eigenfrequency of the collective oscillations leading to strong oscillations even at low excitation energy. The restoring force is one of the crucial factors in determining the resonance frequency; it depends on the number of separated electrons and ions, i.e. particle size,

shape (electrons tend to redistribute more intensely at the sharper edges) and polarizability of the medium around the particle which all affect the separated charges [6].

The quasi-static approximation applies for small nanoparticles with respect to the wavelength irradiated on the particles, meaning that the particle "feels" the electromagnetic field of light with a constant phase. This proves to be applicable for particle sizes (diameters) below 30 nm. Electrostatics holds in cases when a particle radius relates as $R \ll \lambda$. This simplifies the concept of the electro-optical response of small metal nanoparticles. If it is assumed that the positive charge and the negative charge are immobile and mobile, respectively, while the nanoparticle is placed in an electric field, only displacement of the negative charges (electrons) can occur. Using the boundary conditions on a spherical particle interface, the resulting electric field inside the particle equals [11]:

$$E_i = E_0 \frac{3\varepsilon_m}{\varepsilon + 2\varepsilon_m}, \tag{1.29}$$

where ε_m is the dielectric constant of the embedding medium. Using the definition of the polarizability, $p = \alpha\varepsilon_m E_0$ and equation (1.29), one can obtain the static polarizability of a spherical metal nanoparticle [11]:

$$\alpha = 4\pi R^3 \varepsilon_0 \frac{\varepsilon - \varepsilon_m}{\varepsilon + 2\varepsilon_m} \tag{1.30}$$

For metals, $\varepsilon(0) = -\infty$, this leads to an equation for the classical static electric polarizability of a metal sphere [11]:

$$\alpha = 4\pi\varepsilon_0 R^3. \tag{1.31}$$

Equation (1.31) keeps its validity only in the quasi-static regime when the field is spatially constant and phase-coordinated, as cartooned in Fig.1.2.

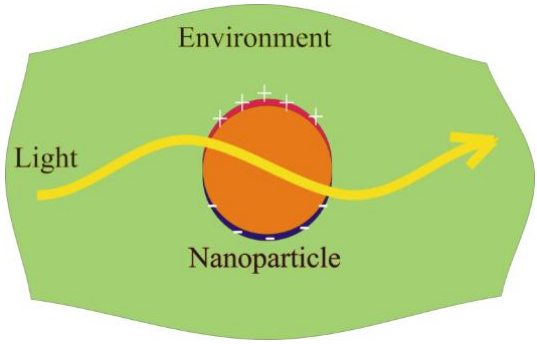

Fig. 1.2. Plasma oscillation of a particle excited by light wave (the yellow line). This particle "feels" the light (electromagnetic field) spatially constant, but time-dependent (phase-coordinated).

The internal electrical field, defined by equation (1.29), as well as the static polarizability in equation (1.30), have the resonance behaviour only when [11]:

$$|\varepsilon + 2\varepsilon_m| = min, \tag{1.32}$$

$$\text{i.e. } (\varepsilon_1(\omega) + 2\varepsilon_m)^2 + (\varepsilon_2(\omega))^2 = min. \tag{1.33}$$

Equation (1.33) means that a negative $\varepsilon_1(\omega)$ (the real part of the dielectric function) is necessary for the resonance to occur, i.e. the field and the polarization to be in a phase relation. Only in case of small $\varepsilon_2(\omega)$ (the imaginary part of the dielectric function) $\varepsilon_2 \ll 1$ or in case of weakly frequency dependence, $\frac{\partial \varepsilon_2}{\partial \omega} \approx 0$, equation (1.33) approximates to [11]:

$$\varepsilon_1 = -2\varepsilon_m. \tag{1.34}$$

Using the Drude approximation (1.14) for the free-electron metals and$\varepsilon_m = 1$, the surface plasmon resonance position (for spherical particles in vacuum) can be represented as [11]:

$$\omega_1 = \frac{\omega_p}{\sqrt{3}}, \tag{1.35}$$

More generally, in case of metal nanoparticles embedded in a dielectric matrix with the dielectric function, ε_m, by using equations (1.14) and (1.34), the correlation between the Drude and the plasma frequency is given as [59]:

$$\omega_1 = \frac{\omega_p}{\sqrt{1+2\varepsilon_m}}. \tag{1.36}$$

The plasma frequency and its wavelength are related as:

$$\lambda_1 = \frac{2\pi c}{\omega_1}, \tag{1.37}$$

where c is the speed of light.

1.4.3 Electro-optical correlations

Assuming the Drude model (see sec. 1.2) and employing equations (1.13) and (1.36), the free electron density, n_D is given as:

$$n_D = \frac{\omega_1^2(1+2\varepsilon_m)\varepsilon_0 m_e}{e^2} \tag{1.38}$$

and the number of free electrons, N, is given by:

$$N = n_D V, \tag{1.39}$$

where the subscript D in equation (1.38) denotes the Drude approximation condition. Equations (1.38) and (1.39) give a relation between the number of free electrons and the plasmon peak position, i.e. the plasma frequency change is a result of variation of the number of transferred electrons to or from a metal particle.

Because electrons are fermions, obeying the Pauli exclusion principle, they fill all the energy levels up to the Fermi energy and are related as [60]:

$$n = \frac{8\sqrt{2}\pi m_e^{2/3}}{h^3} \cdot \left(\frac{2}{3} E_F^{3/2}\right) \tag{1.40}$$

where n is the free density of electrons, m_e^* is the effective mass of an electron, E_F is the Fermi energy and h is the Planck constant.

In addition, the Fermi energy dependence upon the free electron density is given by [60]:

$$E_F = \left(\frac{(hc)^2}{8mc^2}\right) \cdot \left(\frac{3V}{\pi}\right)^{2/3} N^{2/3}. \tag{1.41}$$

Chapter 2

Experimental details

"Money does not represent such a value as men have placed upon it. All my money has been invested into experiments with which I have made new discoveries enabling mankind to have a little easier life."

Nikola Tesla

In this chapter, a short description of a few techniques and setups utilized for sample deposition, characterization and measurement is given. A state-of-the-art cluster beam deposition (CBD) apparatus, including its consisting parts, will be discussed. This apparatus enables deposition of diverse nanoparticle materials on various substrates. In addition, it enables a fine and controlled deposition of clusters in different patterns.

Absorption and photoluminescence spectroscopies, along with the equipment by which the samples were electrically charged, are also explained in this chapter. The size of the deposited clusters was determined with atomic force microscopy (AFM). Since the particle and the tip provide a convoluted image of the particles, the height was used to determine the nanoparticle size. Since ZnO is an important material in this thesis, the average ZnO grain size was characterized with X-ray diffraction (XRD) by determining the width of the Bragg peak,

which is a measure of the object size [61]. A considerable part of the study in the thesis is devoted to the photoluminescence and optical absorption properties of the samples while being electrically charged in different fashions. Hence, this chapter explains the principles of how these spectroscopies, as well as the equipment used to electrically charge the samples, work.

To study the electro-optical properties of gold, silver and gold/silver alloy nanoparticles, the CBD setup was employed as reported in chapter 3, chapter 4, chapter 6 and chapter 7. AFM and XRD were used as characterization techniques: AFM in chapter 3, chapter 4, chapter 5, chapter 6 and chapter 7, and XRD in chapter 6 and chapter 7. To study the electro-optical properties, photoluminescence and photoabsorption spectroscopies were employed.

Photoluminescence of the gold nanoparticles was measured for the study reported in chapter 5 and optical absorption was measured for the studies reported in chapter 3, chapter 4, chapter 5, chapter 6 and chapter 7. Photoluminescence and absorption spectra were employed as complementary techniques in chapter 5. Although very small metal nanoparticles may lose their plasmonic properties, they still can exhibit photoluminescence. To investigate how electro-optical properties vary by applying electric charge in chapter 5, chapter 6 and chapter 7, it was crucial to apply an electrical potential difference. A potentiostat used in the electro-chemical experiment reported in chapter 5 and a power supply employed in the studies reported in chapter 6 and chapter 7 are briefly described in this chapter.

2.1 Cluster beam deposition apparatus

The Cluster beam Deposition Apparatus (CDA) is situated at KU Leuven (within the Clusters and Laser Spectroscopy (CLASS) group) and is used for bottom-up synthesis and deposition of clusters on diverse substrates in ultra high vacuum (UHV). It can produce both metallic and bi-metallic clusters consisting of 2 to ~2000 atoms [62]. The source of the CDA produces cluster beams with low energy (< 1

eV/atom), thus avoiding cluster fragmentation upon hitting the target substrate and considerably reducing the cluster deformation. This regime is called the soft landing regime, where the kinetic energy per atom is lower than the binding energy of each atom in the cluster. As a matter of fact, low energy limits influence of the cluster impact on the substrate and the interaction is hence boiled down to the cluster-substrate interaction.

The CDA consists of four parts: the source chamber, the excitation chamber, the deposition chamber and the load chamber; its cross section is shown in Fig. 2.1. The source and extraction chambers are separated by a skimmer with a diameter of 2 mm. Another diaphragm, with a diameter of 10 to 20 mm, stands between the extraction and the deposition chamber. The load chamber, lying posteriorly in Fig. 2.1, is connected to the deposition chamber via a valve.

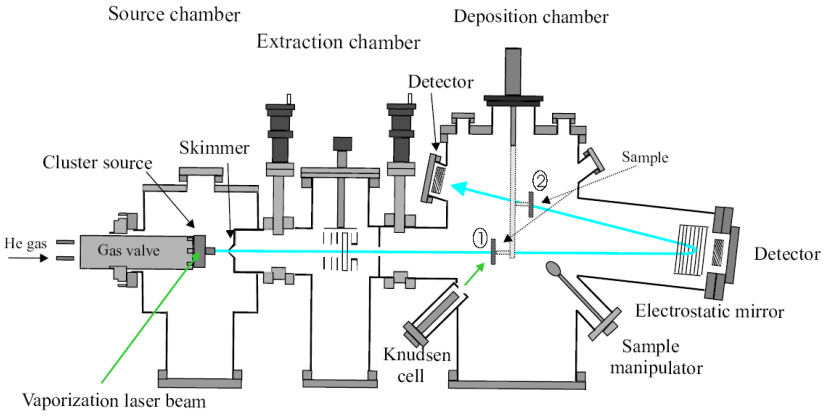

Fig. 2.1. Schematic cross section of the CDA divided in four chambers (the load chamber lying posteriorly is invisible) with the laser light (the green line) and cluster beam (the blue line) indicated.

2.1.1 Cluster source

The cluster source enables production and deposition of the clusters via laser ablation and vaporization. Vaporization of target material can be achieved by one or two pulsed vaporizing Nd:YAG (neodymium-doped yttrium aluminum garnet) lasers. Both lasers work on the second harmonic (λ=532 nm, pulse width=7ns). The hot vaporized atoms of a material condense while being in contact with the cold surrounding inert (noble) gas (purity=99.9999% He). The role of helium (He) is to facilitate cluster formation, simultaneously disabling chemical reaction with the cluster species.

2.1.2 Source chamber

The cluster source is attached to a pulsed gas valve. The entire source chamber is pumped toward vacuum by a 3200 l/s turbomolecular pump (Pfeifer, TPU 2200) resulting in a base pressure of $10^{-8}\ hPa$. However, when He gas is introduced in the chamber, pressure is increased to $\sim 4 \cdot 10^{-5}\ hPa$.

As soon as the vaporizing laser light impinges on the target material (depositing material), the He gas, introduced by a synchronized pulse in the source chamber, carries the atoms and helps them to condense to larger aggregates – clusters. Much of the condensed matter is pushed via a nozzle in vacuum and directed by a skimmer to the extraction chamber as a directional supersonic cluster beam toward the deposition chamber. The cluster source, i.e. the compartment in which the clusters are generated, along with a photograph of the entire source chamber, is given in Fig. 2.2. In more detail, one can see that the vaporizing laser light passes through the insert channels (numbered 4) and impinges on the target of interest (X,Y), whereby the vaporized material is mixed with the carrier gas (He) which synchronizingly enters the formation chamber (numbered 3) through the pulsed gas valve (numbered 1). The condensed matter is thereafter carried to vacuum of the extraction chamber through a nozzle (numbered 6). While the laser light is hitting the target of interest, the entire target holder

(numbered 7) is moving by an engine system, thus preventing inhomogeneous ablation of the target material which could lead to reduced performance of cluster production. The speed and movement pattern of the engine system can be adjusted via synchronization of the target holder movements and the laser shots to provide stability of the cluster production.

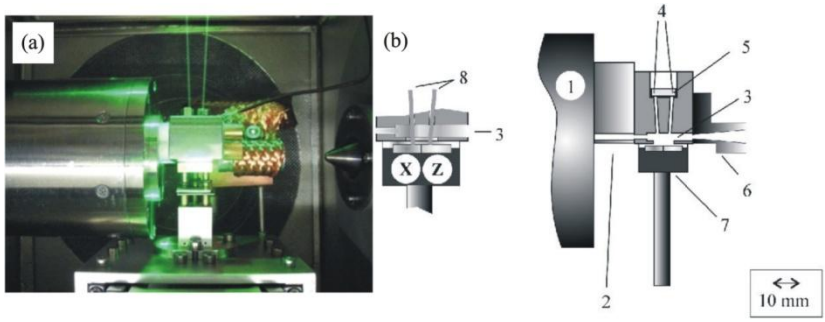

Fig. 2.2. (a) Photograph (made by the CLASS group at KU Leuven) of the source chamber with the laser-irradiated cluster source in the middle. (b) Schematic overview of the dual-target, dual-laser vaporization cluster source: (1) pulsed gas valve, (2) teflon spacer, (3) formation chamber, (4) laser beam insert channels, (5) glass plate, (6) nozzle, (7) target holder, (8) laser beams, (X and Y) targets [63].

2.1.3 Extraction chamber

The extraction chamber is pumped with a turbomolecular drag pump (Pfeiffer, TMU 1600), with a pumping capacity of 1320 l/s. Without the load, a pressure of the order of $10^{-9}\ hPa$ is reached. However, when the source is in operation, the pressure in the extraction chamber increases to $5 \cdot 10^{-7}\ hPa$, which is approximately two orders of magnitude lower as compared to the pressure in the source chamber. Other features of this chamber are detailed elsewhere [63, 64].

2.1.4 Deposition chamber

The clusters, i.e. condensed aggregates, are supersonically led from the source chamber to a substrate mounted in the deposition chamber under optimal vacuum conditions. The deposition chamber is connected to the load chamber from which the samples were previously moved with a transport system to the deposition chamber. The samples are thereafter mounted onto a deposition holder utilizing a manipulation and transport system after which this system is retracted to the load chamber. By a noble-gas-stable ion pump (Varian, VacIon plus 500 Star Cell), including a titanium sublimation pump, the entire chamber is pumped to below $10^{-10}\ hPa$ and during cluster source operation to $5 \cdot 10^{-7}\ hPa$. This vacuum reduction was caused by the presence of residual He gas.

2.1.5 Load lock chamber

The load chamber is pumped by a turbo molecular drag pump (Pfeiffer, TMU 520) reaching a pressure of the order of $1 \cdot 10^{-8}\ hPa$. The samples from ambient to the vacuum system are loaded or retracted through this chamber via the load lock chamber.

2.1.6 Sample transport system

This system places the sample holder from the load lock chamber to the deposition chamber where the samples are handled by pincers. The sample holder and the carrousel are shown in details in Fig. 2.3.

The size of the sample holders is $5x10\ mm^2$. A carrousel has four places provided for the sample holders, which is also the maximum number of depositions without pulling the samples out of the CDA. The clusters can also be deposited on larger substrates; in this case, maximum two larger substrates can be mounted in the carrousel, leaving the other two places, if

necessary, for the normal size sample holders. The carrousel with a mounted sample is transferred to the deposition chamber where it can be further manipulated. If needed, depositions can be performed one after another without using the load-lock or breaking the vacuum.

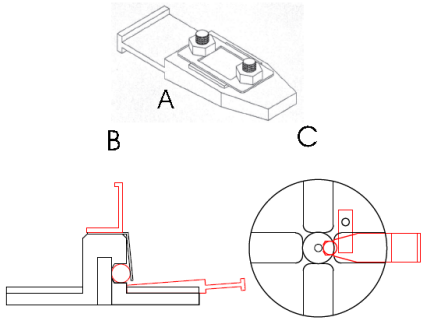

Fig. 2.3. The substrate holder ready for the cluster deposition is fixed on a sample holder (A) after which the sample holder is placed on a sample transport carrousel (B). There are four places for the substrates in the carrousel (C) [63].

2.1.7 Time-of-flight mass spectrometer

To measure the mass distribution of the produced clusters, the deposition chamber is equipped with a reflectron time-of-flight (TOF) mass spectrometer [65]. This spectrometer works on the following principle: the mass of the charged particles with the same kinetic energy is calculated according to their flight time necessary to reach the detector. The charged particles fly through a reflectron which consists of an electrostatic mirror (reflectron) and an ion detector. The charged particles are accelerated by electrodes of the extraction optics. After passing a potential difference, V, the velocity of particles with mass, m and charge, q can be written as:

$$v = \sqrt{\frac{2qV}{m}} \tag{2.1}$$

This equation establishes the relation between the charge-to-mass ratio of a cluster and its speed. Heavier particles have a longer flight time through the field-free zone of the detector before being detected. The particle's impact on the detector with sufficient kinetic energy results in a pulse of electrons registered and amplified by a digital oscilloscope.

Once the mass distribution is retrieved from the TOF mass spectrometer, the size distribution can be calculated, assuming that the deposited clusters are spherical. Therefore, knowing the number of atoms in the deposited clusters, N and the Wigner-Seitz radius of the atoms, r, the cluster diameter, d can be estimated in the following manner:

$$d = 2r\sqrt[3]{N}, \tag{2.2}$$

which represents a conversion formula from the cluster mass spectrum to the cluster size spectrum.

2.1.8 Vaporization laser system

Two independent Q-switched lasers (Spectra Physics, INDI) are employed to ablate and vaporize metal clusters. The lasers work on 532 nm wavelength. The pulse duration lasts 7 ns, with a repetition rate of 10 Hz. Pulse energies can reach as much as 240 mJ. However, typical working energy values, sufficient for a proper vaporization, range between 20 and 40 mJ per pulse. The typical beam diameter is around 7 mm, focused and reduced to 1 mm on the very target surface.

Further details about the CDA are described in ref. [63].

2.2 Sample characterization techniques

2.2.1 Atomic force microscopy

AFM gives information about the surface topography of a sample with ~1 nm resolution. In contrast to the scanning

tunnelling microscope technique, AFM is not limited to conductive and semi-conductive samples because its working principle relies on the interaction forces between atoms at the tip apex and the sample surface rather than on the tunnelling current. This feature makes AFM indispensable in observing nonconductive samples and structures which is important not only for physics and chemistry, but also for biophysics and neuroscience [66, 67]. This characterization is one of the many techniques associated with scanning force microscopy developed by Binnig, Quate and Gerber [68].

In principle, an AFM probe consists of a sharp tip attached to the end of a spring which is called cantilever, Fig. 2.4(a). The interaction force, F which the tip experiences at small distances between the tip and the atoms of a sample gives rise to bending of the cantilever occurring due to Hooke's law:

$$\Delta x = \frac{F}{k}, \tag{2.3}$$

where k is a force constant of the cantilever spring and x is a deflection perpendicular to the substrate at the end of the cantilever. The bending of the cantilever is optically detected by laser beam deflection; deflection of as low as 0.1 nm could be detected.

Because the attractive forces are 10 times weaker than the repulsive ones, Fig. 2.4(b), for the noncontact tapping mode, a piezoelectric crystal is employed to apply an external force $F_{ext}(t)$ to the cantilever, giving rise to a cantilever oscillation of ~200 kHz. This crystal is at a certain, but very small distance above the sample. While approaching a surface, the resonant frequency or vibration amplitude of the cantilever changes due to van der Waals interactions between atoms of the sample and the tip. These changes are detected by using the laser deflection system. To keep the vibration amplitude constant during the scan, a feedback system provides a topographic image of the scanned area.

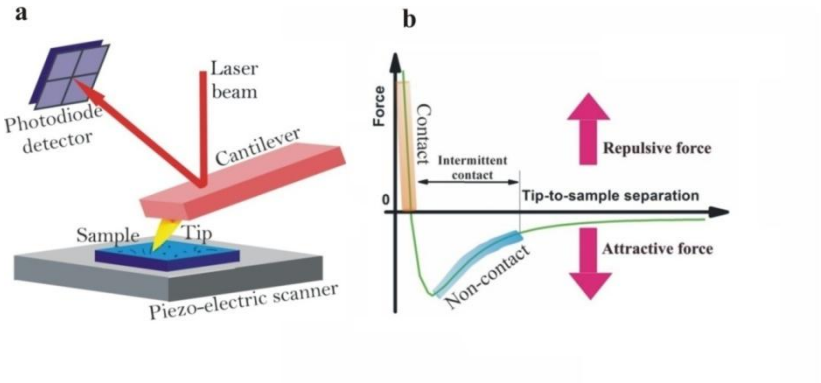

Fig. 2.4. (a) Schematic overview of the AFM setup. (b) Depicted forces on the tip when the tip is moving away from the sample. Illustrations based on ref. [69].

2.2.2 X-Ray diffraction

X-Ray diffraction is a widely used technique to attain several important features of a sample, e.g. sample thickness, recognition of different components, grain size, crystal orientation, etc. For the experiments reported in chapters 6 and 7, we have used this technique to obtain the grain size of ZnO. The XRD spectrum represents a set of peaks for which a condition must be fulfilled. This condition is named after two Braggs, father and son, who have discovered it. This condition, i.e. Bragg's law can be represented as [71]:

$$2dsin\theta = n\lambda_{XRD}\,(n = 1,2,3,\dots) \qquad (2.4)$$

where d is the interplanar spacing between the consecutive planes parallel to the film surface and λ_{XRD} is the wavelength of the incident X-ray beam, n is the integer. Equation 2.3 reflects the periodicity of the structure which helps determine crystal orientation, crystal size, etc.

2.3 Setups for the electro-optical measurements

2.3.1 Photoluminescence spectroscopy

Photoluminescence (PL) spectroscopy is a contactless and harmless method to probe the electronic structure of material. The principle of PL spectroscopy is based on excitation of a sample by monochromatic laser light and thereafter detecting the emitted light. Being excited by a wavelength, the sample subsequently emits photons of different energies which are then detected step by step, i.e. wavelength per wavelength. Eventually, the entire recorded wavelength range represents the emission or photoluminescence spectrum of a sample. This spectroscopy is a distinctive method whose spectrum also indicates the crystal quality of the material. The process of photoluminescence is illustrated with an example of a direct bandgap semiconductor, as shown in Fig. 2.5. However, this process is not restricted to semiconductors. For example, metal nanoparticles also luminescence due to both interband [72] and intraband transition [73].

The used photoluminescence setup is depicted in Fig. 2.6. It consists of the excitation pulsed Nd:YAG laser (Spectra Physics GCR-11-2) at 355 nm (the third harmonic) with duration of 10 ns and a repetition rate of 10 Hz. The laser pulses were focused onto the samples with a lens having a focal length of 10 cm and an intensity of 5 mJ per pulse. The resulting photoluminescence signal is guided through the entrance slit of a 60 cm focal length monochromator (HR 640, Jobin Yvon), with a 1800 g/mm grating and using slit widths of 2 mm, which can yield a spectral resolution of less than 1 nm. The monochromator can range wavelengths between 260 nm and 1060 nm. Emission signal is detected by a photomultiplier tube (PMT C3531, Hamamatsu), mounted at the outer slit of the monochromator. Its photocurrent was preamplified and recorded/digitized using a 500 MHz bandwidth oscilloscope (TDS5052, Tektronix). To calibrate the power fluctuations of

the excitation laser, a small part of the excitation light was picked off and routed to a Si photodiode; the laser light intensity was simultaneously measured and all sample signals were accordingly intensity-corrected.

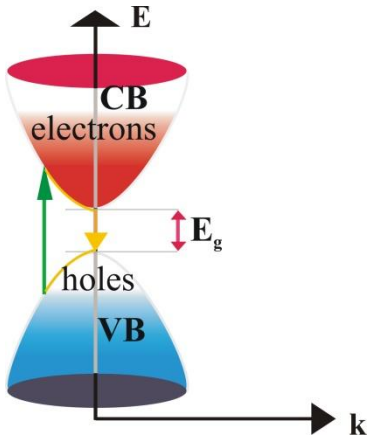

Fig. 2.5. Cartooned bandgap diagram in *k*-space (crystal momentum space), describing the photoluminescence in a direct bandgap semiconductor. The red-coloured states at the bottom of the conduction band (CB) and empty states (the white states within the blue) at the top of the valence band (VB), respectively, represent the electrons and holes created by the absorption of photons with energy $E_{exc}>E_g$, where E_g is the bandgap energy. Exciting the direct bandgap semiconductor with E_{exc} (the green arrow line), the electrons are excited to the peak of the green arrow, leaving a hole in the valence band. Subsequently, when this energy drops to the energy of the bottom of the conduction band (via phonon relaxation), a photon will be emitted with the energy of the bandgap (the red double arrow line) as a result of electron-hole radiative recombination (the yellow arrow line).

The measured steady-state photoluminescence spectra provided valuable information about the electro-optical properties of gold nanoparticles. However, time-resolved photoluminescence spectra for gold nanoparticles were not measured since the photoluminescence setup had a time resolution of only a few nanoseconds while the luminescence

decay times of large and small gold nanoparticles are much faster (picoseconds) [74].

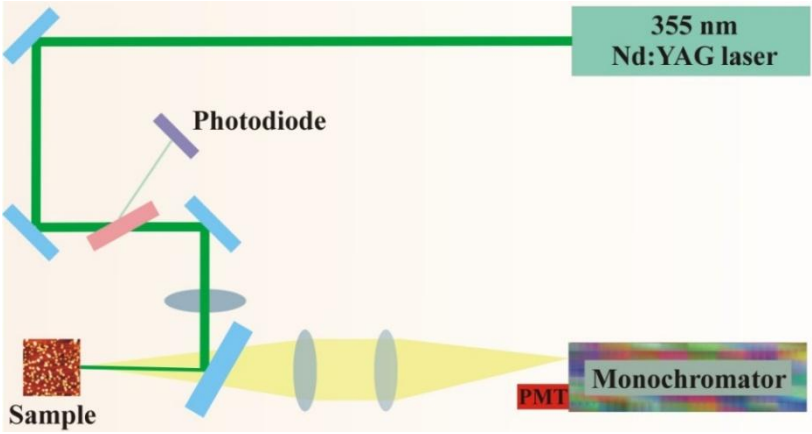

Fig. 2.6. Schematic overview of the photoluminescence setup. The laser light beam (the green line) is guided to the sample. As a result, the excited sample emits photons, being guided to the monochromator (the yellow broad beam) and is thereafter detected by a photomultiplier tube.

2.3.2 Optical absorption spectroscopy

The principle of a linear absorption spectrometer is based upon the Beer-Lambert law, as shown by equation (1.22). This law relates the attenuation of light to the electro-optical properties of the material through which the light passes. This relation is expressed as:

$$I = I_0 e^{-\frac{l}{x}} \tag{2.5}$$

where I and I_0 represent the input light intensity (in front of the material) and the output light intensity (passed through the material), respectively. Fig. 2.7 illustrates how the (optical) absorption of particles of interest is detected; if there are two identical substrates whereas only one of them has additionally deposited material, the principle of absorption measurement of

the deposited material is based on subtraction of the output light intensity of the sample of interest and the output light intensity of the reference sample, according to equation (2.5). This subtraction will be henceforth termed "*optical subtraction*" in this thesis.

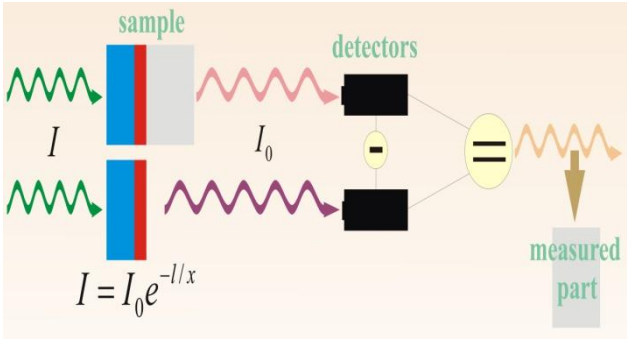

Fig. 2.7. Schematic overview of how the double-channel spectrometer measures absorption. There are two samples – the lower sample (blue-red) and the upper one (blue-red-gray) which is the reference, i.e. substrate and the sample of interest, respectively. By subtracting corresponding two signals travelling through these two samples within the spectrometer, the absorption spectrum of the added part (the gray part) is detected.

Our optical absorption experiments have been performed at the Department of Chemistry, Laboratory for Molecular Electronics and Photonics, with a spectrometer (Perkin Elmer Lambda 900 UV/VIS/NIR Spectrometer) at a working wavelength range between 175 and 3300 nm with an accuracy of 0.08 nm in UV-visible region and 0.3 nm in the NIR region. It is a double-beam, double monochromator ratio recording system with tungsten-halogen and deuterium lamps as sources. This double-channel instrument has the advantage that it eliminates the influence of cuvettes, solvents or other undesired surrounding parts of the sample. In addition, it can measure transmittance, absorbance or reflectance, although our experiments were focused on absorbance. The scattering component of the final signal in the spectrometer can be

recognized within the extended absorption tails in the absorption spectrum whose contribution is proportional to $1/\lambda^4$ and can be thus corrected, if necessary.

2.4 Equipment for applying electric potential

For the samples in chapter 5 (a wet electrochemical experiment), a potentiostat/galvanostat 263A (Princeton Applied Research) has been employed. It consists of three electrodes: an Ag-wire acted as pseudo-reference, a Pt-wire as counter electrode and ITO on glass as working electrode. For the dry samples (chapter 6 and chapter 7), a power supply (Thurlby Thandar Instruments Ltd. EL30) has been used; it consists of two electrodes.

Chapter 3

Electronic structure and optical properties of very small gold nanoclusters

> *"The day when we shall know exactly what electricity is will chronicle an event probably greater more important, than any other recorded in the history of the human race."*
>
> Nikola Tesla

The electro-optical properties of noble metal nanoparticles are important to understand the experiments of the further chapters. Therefore, this chapter summarizes the knowledge on electro-optical properties of noble metals. It also provides an experimental result which sets a size below which gold particles behave markedly different with respect to their larger counterparts; in the thesis, nanoparticles smaller than this size are referred to as *very small nanoparticles*.

3.1 Interband transition of noble metals

In metals, the onset of interband absorption is associated with transitions either from the Fermi surface to the next higher empty band or from a lower filled band to the Fermi surface [75]. The noble metals belong to the eleventh group of the Mendelyeev periodic table, representing an exception of Mandelung's rule, which describes filling of atomic subshells. Copper, silver and gold (coinage metals) have the following orbital structure:

Copper: $1s^2\ 2s^2\ 2p^6\ 3s^2\ 3p^6\ 3d^{10}\ 4s^1$
Silver: $1s^2\ 2s^2\ 2p^6\ 3s^2\ 3p^6\ 3d^{10}\ 4s^2\ 4p^6\ 4d^{10}\ 5s^1$
Gold: $1s^2\ 2s^2\ 2p^6\ 3s^2\ 3p^6\ 3d^{10}\ 4s^2\ 4p^6\ 4d^{10}\ 4f^{14}\ 5s^2\ 5p^6\ 5d^{10}\ 6s^1$

One can see that the *s*-subshell of these metals is only half filled, i.e. it has only one electron. Together with the empty p-orbitals, this leads in bulk to a *sp*-hybridized band which is filled up to the Fermi level. The *sp*-hybridized band gives rise to the unique electronic and optical properties of noble metals. In this band, electrons are viewed as free electrons which make metals conductive. However, when the energy of exciting photons is larger, the deeper level electrons from the valence band are excited to the conduction band. Depending on the transition energy, different points in the Brillouin zone are considered; when an electron is excited to an unoccupied state in the conduction band, leaving a *d*-band hole in the valence band, it will be radiatively or nonradiatively recombined with an electron from the conduction band. The peak energy of the emitted electrons is related to the energy separation between the *d*-band holes and the Fermi level, which for gold particles near the *X* and *L* point in the Brillouin zone equals 1.8 eV (Fig. 3.1(a)) and 2.4 eV (Fig. 3.1(b)), respectively [73].

The photoluminescence of gold nanoparticles at 2.5 eV (~500 nm) [72] is ascribed to the interband transition near the *L* point in the Brillouin zone [73, 76], although there are also other mechanisms ascribed to the photoluminescence of gold nanoparticles in both the blue [77, 78] and the red part of the spectrum [79, 80, 81].

The proximity of the plasmon resonance to the interband transition onset can prevent identification of the interband transition edge in the absorption spectrum [29], thus giving rise to the plasmon resonance damping [11, 82, 83].

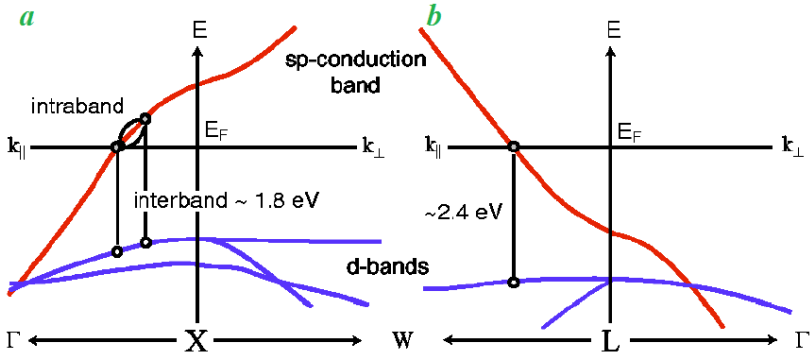

Fig. 3.1. Interband transitions in gold near (a) the *X* point and (b) the *L* points in the first Brillouin zone [73].

Gold spherical nanoparticles have the plasmon resonance at 520 nm, very close to the onset of the interband transition region (~2.5 eV) [35, 84]. The plasmon resonance of silver nanoparticles, for example, peaks at ~3.8 eV (326 nm) [35, 84], rather different from the interband transition, contributing to greater plasmon resonance oscillations; copper has the weakest oscillator strength of the plasmon among the coinage metals, due to an overlap of the plasmon resonance with the interband transition region [35]. By shifting the plasmonic peak out of the interband transition region, the plasmon oscillator strength enhances [11]; this tuning can be performed by different means: making core/shell structures [35] or changing the surrounding dielectric properties and geometry of the particle [85], etc. For example, if a noble metal particle size decreases, its plasmon resonance blueshifts and approaches the interband energy, thus weakening the plasma oscillations.

Furthermore, it was shown that quantum effects are not strictly related to very small nanoparticles [86], but also to those having a diameter as large as 10 nm [52, 53, 54, 87, 88] where the plasmon resonance is more subject to the quantum nature of

the conduction electrons. Yet, this effect becomes more significant in smaller particles (clusters), when the particle size is markedly (~10%) below the electron mean free path, leading to a change in particle permittivity [51, 52, 89, 90]. Therefore, a very important parameter in the electronic and optical properties of a metal particle is its size; with decrease of the particle size, the Kubo gap, i.e. the average spacing between adjacent energy levels in a metal particle, increases, thus contributing also to the oscillator strength. However, with significant cluster size increase, the energy levels start to overlap, evoluting from the *d*-band to the continuous plasmon resonance band. Having less free electrons, smaller particles have greater sensitivity to various changes [11, 91] which is desirable in nanometer-scale sensing. However, the changes in the electronic properties (absorption) of smaller particles become more complex to detect in this case. Moreover, depositing very small gold nanoclusters (~ 1 nm) is a formidable task due to the surface effects since more atoms are opened to the influence of environment in contrast to their larger counterparts [92]. Very small gold nanoclusters are supposed to be very attractive as intrinsic one-event transducers and sensors due to their increased sensitivity [91]. They have a wider spacing of the energy levels [93, 94], facilitating identification of the absorption peaks.

Table 3.1 approximates how the Kubo gap varies with increasing the number of atoms in gold nanoclusters which are assumed to be spherical; the Kubo gap is determinant for both the photoluminescence and plasmon resonance, as well as for magnetic properties in noble metal nanoparticles [92]. Gold clusters are assumed to have dense packing of the atoms within an atomic shell. There is a magic number of the surrounding atoms, i.e. every atom is surrounded by the 12 nearest neighbours where the n^{th} shell has $10n^2+2$ atoms [95]. Table 3.1 shows that the smallest cluster size (one-shell cluster) has an atom surrounded by 12 additional atoms within the first layer. When this structure is further fully surrounded by an additional atomic shell of 42 atoms, in an ideal case (the structure symmetry), there are 55 atoms in the double shell cluster, etc.

Table 3.1. The Kubo gap dependence upon cluster size (the number of atoms), after ref. [96, 97, 98, 99], although the Kubo gap, along with the magic numbers of atoms within a cluster, may be subject to slight changes depending on the surroundings which can lead to a distorted hexagonal close-packed core and therefore intermediate magic numbers [96, 100].

Atomic shell, n	Atoms per shell	Atoms per cluster	Cluster size [nm]	Kubo gap [eV]
1	12	13	0.7	200
2	42	55	1	170
3	92	147	1.7	70
4	162	309	2.1	50
5	252	561	2.5	25
6	362	923	3.4	9
7	492	1415	4.2	8
8	642	2057	5.5	7
9	812	2869	7.1	6

3.2 Three different gold particle samples

Three different gold samples were prepared to compare their absorption spectra. The first sample, a 15 nm thick gold film, was grown on glass by the Riber Molecular Beam Epitaxy (MBE) system at KU Leuven. A 2 nm thick Cr layer was first deposited by an e-beam evaporator to increase the adhesion of gold to glass.

The deposition was controlled by a mass spectrometer and a quartz crystal (growth rate 0.2 Å/s). The base pressure was $2.1 \cdot 10^{-10} hPa$. Thereafter, gold was grown from a Knudsen cell at 1460 °C with a growth rate of 0.35 Å/s. All depositions were performed at room temperature. To achieve UHV conditions, an ion pump was used, combined with a titanium sublimation pump and a cryoshield with liquid nitrogen. Fig. 3.2 illustrates the sample (the left sample), as well as how the absorption spectrum of the gold nanofilm was measured. Optical

absorption spectra were measured by two detectors (above), one for the sample and one for the reference (the right sample), which provides the spectrum of the sample by subtraction of the reference signal.

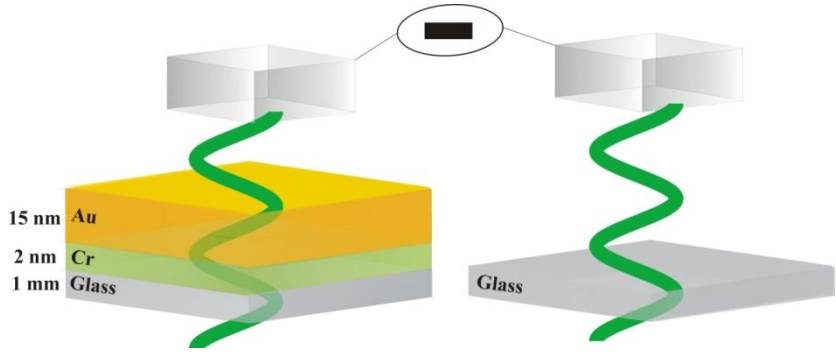

Fig. 3.2. Schematic diagram depicting the sample produced by MBE (the left sample) with given thicknesses and schematic overview of how the double-channel spectrometer measures absorption of the gold nanofilm; there are two samples: the right sample without gold deposition, as reference, and the left one, with a gold nanofilm. Identical light beams (green wave lines) pass through both samples. Absorption spectra of the samples are detected by two (gray) detectors above and absorption spectra were constructed by subtracting the corresponding signal and reference which allows to attribute the spectrum resulting from the subtraction to the gold nanofilm.

The second sample was a 10 nm sized gold colloidal aqeous solution (purchased by the Sigma Aldrich) placed in a quartz cuvette. The solution consisted of highly monodisperse ($< 12\%$ variability in size and shape) 10 nm spherical gold nanoparticles which were surrounded by additional components and ligands: tannic acid (< 0.01 %), sodium citrate ($< 0.04\%$), choloroauric acid ($< 0.01\%$) and sodium azide ($< 0.02\%$), as preservative.

The concentration of gold nanoparticles in the colloidal solution was $c = 3.82 \cdot 10^{12}$ particles/ml. An enlarged gold nanoparticle from the solution is shown to the very right side of

Fig. 3.3. In addition, a schematic overview of how the absorption spectrum of gold colloidal nanoparticles was measured is also illustrated in Fig. 3.3. The optical spectrometer subtracted the background signal (i.e. reference, the left cell) from the cell of interest (the right cell).

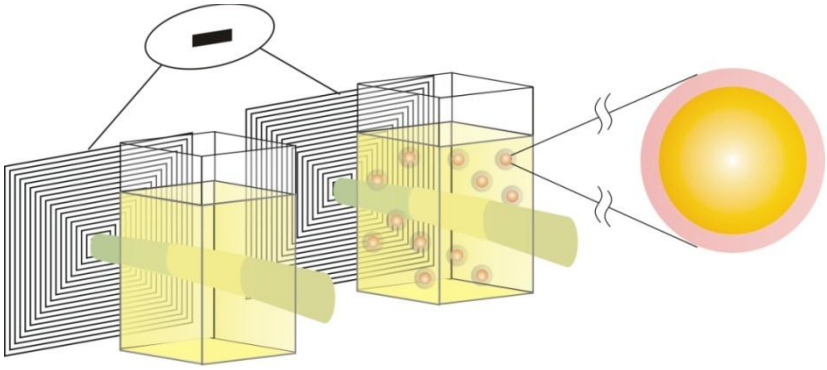

Fig. 3.3. Schematic overview of how the double-channel spectrometer measures absorption of the gold colloidal solution. There are two samples: the left sample without particles, as reference, and the right, with gold colloidal nanoparticles surrounded by citrate. A nanoparticle is enlarged (to the very right side) with the (yellow) metal core and (pink) citrate layer around it). The identical light beams (green lines) pass through both samples. Absorption spectra are detected by two detectors (represented by concentric squares). The aqueous solution of gold nanoparticles with Milli-Q water are respectively equal for signal and reference, which allows to attribute the spectrum to the nanoparticles.

The third sample consists of gold nanoclusters deposited on glass by the CDA. Commercially available microscopic slide (dimensions: 1 mm x 26 mm x 75 mm) was cut to size of a CDA sample holder which is presented in Fig. 2.3 (see sec. 2.1.6). After cutting, the sample was immersed in copious amounts of methanol under supersonic vibration for 15 minutes. During deposition, the cluster flux was ~ 3 Hz/min and the deposition time was chosen to be 4 minutes which allowed for deposition

of ~ 0.3 equivalent monolayer of gold. Fig. 3.4 represents a schematic overview of the sample with deposited gold nanoclusters (the right sample), as well as how its absorption spectrum was measured. Absorption was measured by two detectors above the samples; i.e. it is equal for signal (the left sample) and reference (the right sample), which allows to attribute the spectrum resulting from the subtraction to the gold nanofilm.

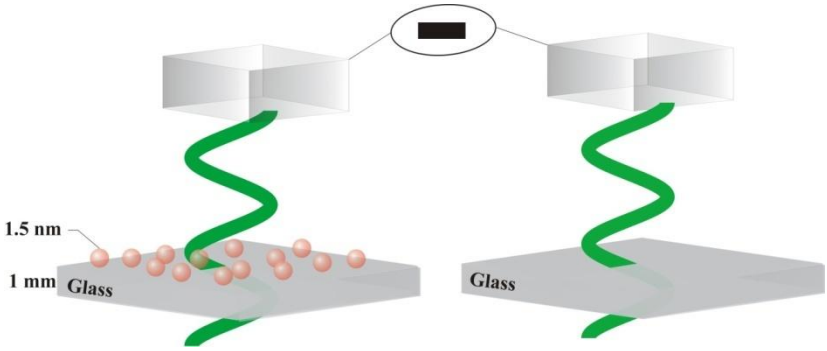

Fig. 3.4. Schematic diagram depicting the sample produced by CDA (the left sample) and an overall schematic overview of how the doublechannel spectrometer measures absorption of the gold nanofilm; there are two samples: the right sample without gold nanoclusters, as reference, and the left one, with gold nanoclusters. Identical light beams (green wave lines) pass through both samples. The absorption spectra of the samples were detected by two detectors above and absorption spectra were constructed by subtracting the corresponding signal and reference which provides the spectrum resulting from the gold nanoclusters.

For the AFM visualization of the gold nanoparticles, silicium wafer with grown oxide layer was chosen as substrate, as the adhesion is stronger and therefore the nanoparticles withstand the AFM lateral force better. In addition, it is easier to distinguish nanoparticles on a smooth substrate as compared to the rough ones. The AFM image was processed with the WSxM program [70], as shown in Fig. 3.5.

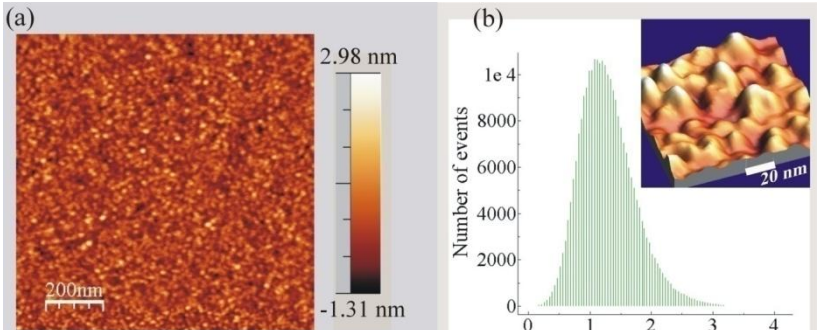

Fig. 3.5. (a) AFM image of the deposited gold clusters. The bar at the right hand side represents a colour-coded height scale. (b) The WSxM program [70] calculated the average cluster height (diameter) of ~1.5 nm, although the size distribution is broader. An inset (in (b)) represents a zoomed 3D region with tens of clusters from the AFM image in (a).

3.3 Optical absorption of a gold film, nanoparticles and clusters

Figs. 3.6 (a), (b) and (c) represent the absorption spectrum of the 15 nm thick gold layer, 10 nm sized gold colloidal solution and 1.5-2 nm sized gold nanoclusters, respectively. It is clear from Fig. 3.6(a) that the thin gold nanofilm shows a dip in its spectrum (~500 nm). The right flank of the spectrum grows at longer wavelengths [101], i.e. at the near infrared where it forms a broad plasmon peak [101, 102, 103].

If the interparticle distance between deposited island-like particles becomes smaller, a significant redshift of the plasmon can be noticed [104], ending up to the markedly redshifted plasmon for touching particles [101, 102, 103, 105, 106]. Further slight thickening of the thin film does not significantly influence the shape and position of the plasmon resonance [107].

The 10 nm sized colloidal gold nanoparticles show a plasmon peak at ~ 516 nm, as expected [108], see Fig. 3.6(b).

Because of its large size, the gold nanoparticles with a concentration of $c = 3.82 \cdot 10^{12}$ particles/ml, surrounded with a ligand (citrate), gives a pronounced plasmon peak.

In contrast, very small nanoclusters, deposited by the CDA, do not have such a pronounced absorption peak. Yet, their absorption has particularly interesting features and a relatively unexpected absorption spectrum. Therefore, we will henceforth focus on the result in Fig. 3.6(c). The blue curve in Fig. 3.6(c) represents the absorption spectrum of nanoclusters deposited by the CDA whose average height is 1.5-2 nm according to AFM image in Fig. 3.5. Interestingly, the absorption of very small gold nanoclusters in Fig. 3.6(c) is ~50 times lower as compared to the absorption of 10 nm sized gold nanoparticles in Fig. 3.6(b) and has two peaks: at ~460 nm and ~500 nm. The 50 times lower absorption peak of very small gold nanoclusters as compared to the absorption peak of 10 nm sized gold nanoparticles may suggest that the plasmon resonance energy, when the cluster size is sufficiently reduced, reaches the onset of interband transitions, leading to an oscillator strength decrease [109, 110].

To understand the 50 times lower absorption, the number of excited gold colloids (Fig. 3.6(b)) and the number of the excited deposited clusters (Fig. 3.6(c)) have to be compared. These numbers were calculated, knowing the light beam dimension and the concentration of nanoparticles. The light beam passes through a volume of the gold colloidal (aqueous) solution (Sigma Aldrich) of $1.96 \cdot 10^{-7}$ m^3. Since the concentration of the nanoparticles is $3.82 \cdot 10^{12}$ particles/ml, the light is estimated to excite $\sim 7.5 \cdot 10^{11}$ gold colloidal nanoparticles. These nanoparticles give rise to the plasmon peak in Fig. 3.6(b). Approximating that all the deposited nanoclusters have a diameter of 1.4 nm, see Fig. 3.5(b), the number of nanoclusters through which the light beam passes is estimated to be $\sim 6.9 \cdot 10^9$. It can now be noted that the number of nanoclusters is about two orders of magnitude lower, which explains why the spectrum in Fig. 3.6(c) is ~50 times lower in intensity than the spectrum of the colloidal solution in Fig. 3.6(b). The scales were adjusted for clarity by taking arbitrary

units. Furthermore, the lower intensity in Fig. 3.6(c) may also originate from the difference in size of the deposited nanoclusters; it is well-known that smaller clusters have a much lower optical absorption (and scattering) cross section [11, 52, 111].

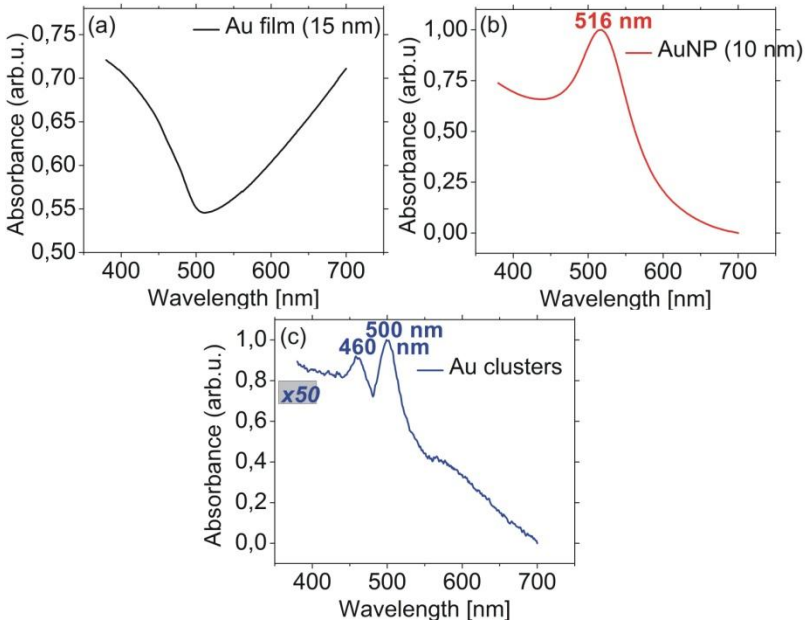

Fig. 3.6. Absorption spectrum of (a) a gold nanofilm with thickness of 15 nm, (b) gold colloidal solution (d=10 nm), and (c) gold nanoclusters with an average height of 1.5-2 nm.

The AFM cannot measure the particle shape due to tip convolution [112]. However, the particle density can be determined by AFM measurements [112]. Fig. 3.7 gives an approximation of the interparticle distance based upon stochastically taking 335 clusters from different particles of the AFM image in Fig. 3.5(a). The interparticle distance distribution represents a lateral dimension, i.e. the distance between the two neighbouring peaks from Fig. 3.5(a). The lower threshold nanoparticle size was 0.5 nm, i.e. nanoparticles smaller than 0.5 nm were not taken into account since the effect of tip convolution is larger than this size. The distribution is approximated by a Lorentzian in Fig. 3.7 (the red curve), with

the most frequent interparticle distance of $\sim(10 \pm 1)$ nm. Also relatively frequent interparticle distances are those of $\sim(22 \pm 1)$ nm and those with the smallest interparticle distance of 3 nm which is yet low-frequent. The lateral error of ± 1 nm is taken due to tip convolution (tip size) effect which enlarges the lateral dimension of the particle.

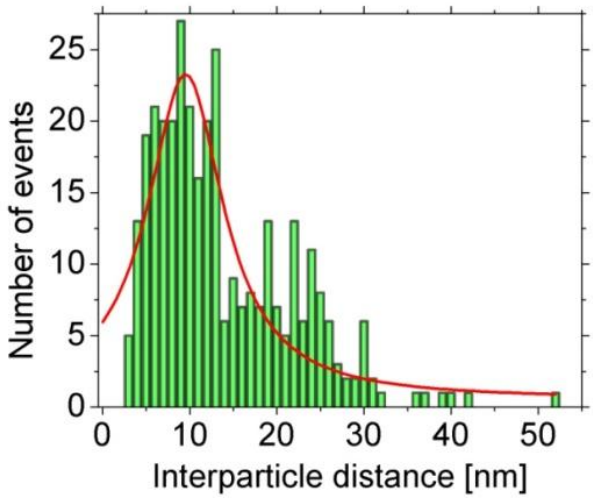

Fig. 3.7. Interparticle distance distribution of stochastically taking 335 nanoclusters (deduced from the AFM image in Fig. 3.5(a)). The red curve represents a Lorentzian curve based upon interparticle distance distribution for selected nanoclusters from the sample.

As we know from the cluster beam deposition sample preparation, where a quartz microbalance was used to measure the cluster fluence, the deposition contains ~0.3 equivalent monolayers. Roughly speaking, estimating the size of nanoparticles from Fig. 3.5 and interparticle distance from Fig. 3.7, the sample coverage by gold nanoparticles is ~0.15 (equivalent monolayers). The disagreement in sample coverage likely originates from several factors: 1) particles smaller than 0.5 nm were not taken into account, 2) there is a relatively broad particle distribution rather than just 1.5 nm sized nanoparticles, 3) accuracy of the calculation of the number of equivalent

monolayers by the CDA. However, this approximation can yet provide additional information about the interparticle distance.

Concerning the position of the plasmon resonance peaks of the very small gold nanoparticles, for particles larger than 2 nm the plasmon wavelength begins to peak from around 500 nm in vacuum [29], and moves to the red depending on the refractive index of its surroundings. Our gold clusters were partially surrounded with a glass substrate and air. A combined effect of the dielectric constants of glass and air gives the effective dielectric constant [11]:

$$\varepsilon_m = \frac{\varepsilon_{air} + \varepsilon_{glass}}{2} = \frac{1 + 2.25}{2} \approx 1.6 \qquad (3.1)$$

This value is too low to cause a significantly detuning (redshift) of the plasmon resonance of gold from the onset of the interband transition wavelength region of about 500 nm [52, 85, 113]. The plasmon resonance peak should therefore remain close to the interband transition region and, since the cluster size is very small (causing a blushift of the plasmon resonance [114]), the plasmon resonance strength is significantly reduced [11].

The presence of the two observed peaks in Fig. 3.6(c) could have various explanations. A first explanation is the presence of two distinct gold particle sizes; the small particle has a plasmon resonance wavelength which is smaller than that of the large particle.

Alternatively, the nanoclusters slightly deforms upon impact, which results in a slightly flattened (oblate) particle which was not possible to observe by AFM imaging due to the tip convolution effect. The cluster shape becomes a very important parameter for diameters below 2 nm [11].
The double peak may also result from plasmonic coupling of "kissing particles" (particles which are almost or just touching) [115, 116, 117] which becomes markedly pronounced for the sub-nanometer distance between particles [117, 118, 119].

According to Fig. 3.7, the average distance between particles is rather large, which makes the phenomenon of "kissing particles" (interparticle distance $\leq$ 3 nm) less probable. Because less than 2% of the particles can be considered

"kissing", the double peak in the optical absorption originating from this reason is thus less probable, although it cannot be excluded. However, although small in size and low frequent (Fig. 3.5), 0.5 nm sized gold nanoparticles may also influence the spectra, at least by smaller interparticle distances.

In general, when the plasmon resonance reaches the onset of interband transition, for example by decreasing the particle size, the plasmon peak dampens [11, 82, 83]. However, relatively new findings indicate that the optical absorption associated with the local interband transition is enhanced owing to an interaction of the interband transition and a dipolar plasmon resonance [34, 35]. When the plasmon resonance reaches and overlaps the interband transition threshold, a double-peaked resonance may appear, owing to the electromagnetic interference of the plasmon resonances with a local interband transition [34, 35]. This depends on the spectral width of the plasmon resonance and that of the interband transitions. However, at this point the data cannot provide a satisfactory estimate of these values.

Gold particles have the onset of interband transition (the *d*-band to the Fermi surface transitions) near the *L* point in the first Brillouin zone at 2.45 eV (506 nm), peaking at ~2.68 eV (462 nm) [84, 109]. These values are in a rough agreement with the peak positions in the absorption spectrum of our gold nanoparticles, see Fig. 3.6(c). Contribution of the *X* point and *L* point to the absorption at room temperature is shown in Fig. 3.8; it can be inferred that the interband transition at the *L* point overlaps the plasmon resonance and considerably contributes to the absorption spectrum.

It is however very clear that the interband transitions do not have a strong peak value but instead are a gradual function of energy (wavelength). Because of this spectral shape, the smooth curve is not able to indent the plasmon resonance.

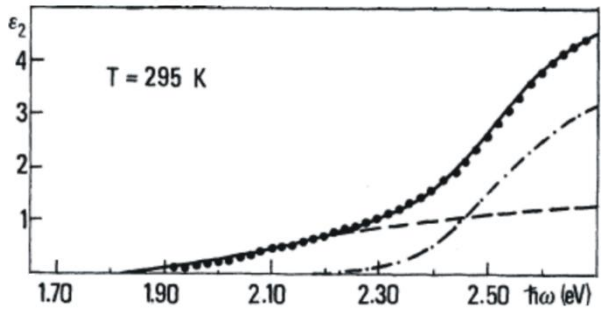

Fig. 3.8. Interband contribution of the imaginary part, ε_2 (absorption) of the dielectric function for Au at room temperature: experimental (triangles), *X*-transitions contribution (dashed line), *L*-transitions contribution (dot-dashed line), total theoretical (solid line), (intraband contribution has been subtracted assuming a Drude-like behaviour) [109].

In case of $Au_{25}(SH)_{18}$ (thiol-protected gold), Zhu et al. [120] have attributed the peak at 2.63 eV (471 nm) to the mixed intraband (*sp* to *sp*) and interband transition (*d* to *sp*) and the peak at 2.91 eV (426 nm) to an interband (*d* to *sp*) transition. However, these nanoparticles are much smaller than our deposited nanoclusters and the optical properties may thus be markedly altered when varying the cluster size.

Although it was recently shown that metal nanoparticles, larger than 60-70 atoms, resemble the bulk metals [100], Alvarez et al. [29] have detected the peculiar step-like features of very small gold nanoparticles (for d = 1.7 nm and 1.4 nm, the latter having more expressive step-like features) within the derivative absorption spectrum (see sect. 2.4.2).

Further experiments are needed to give an accurate explanation for the presence of the double peaks. At this point it is difficult to infer which mechanism produces the two plasmon absorption peaks at ~460 nm and ~500 nm.

3.4 Conclusions

We compared the optical absorption spectra of very small gold nanoclusters with respect to gold colloids and a gold thin film. While a thick gold film has its plasmon frequency resonance in the infrared region, showing a dip at around 520 nm, 10 nm sized gold colloidal solution shows a pronounced plasmon resonance at around 516 nm. In contrast, 1.5-2 nm sized gold nanoclusters show two peculiar small absorption peaks for which currently multiple explanations are considered: 1) plasmonic coupling of neighbouring particles, 2) oblate shape of the particles, 3) interband transition near the *L* point of the first Brillouin zone contribution of the smallest clusters in the sample and an overlap of the gold plasmon resonance with the interband transition threshold. This study indicates how important it is to accurately control the size of gold nanoclusters and the distances between them. Further experiments are needed to understand the observed phenomena which are a platform for the electro-optical switching study. This study emphasizes that very small features in the absorption spectrum of the very small metal nanoparticles should not be underestimated. The research pathways to provide well defined conditions should include controlling the cluster size distribution [121, 122] and the cluster coverage. Moreover, perfect spherical clusters will likely provide results which are better to model [123, 124].

Chapter 4

Prospects of pH-induced electro-optical tuning and sensing in gold particles nano-systems

Gold and silver nanoparticles are increasingly used as pH sensors [125, 126, 127]. Determining pH is not only important in nanosensing, but also during gold nanoparticles' growth [128, 129, 130] and for controlling the distance between gold nanoparticles [131]. Nanostructure materials can be formed top-down or bottom-up. Traditional top-down methods based on lithography have as advantage that interparticle distances can be controlled precisely, but lacks spatial resolution (tens of nanometer) [115, 132, 133], although there are good prospects to improve resolution in the future [133, 134, 135]. The bottom-up methods cannot be employed to fabricate nanostructures as large as a few tens of nanometers in a well-controlled way. However, this method has much potential in fabrication of

smaller nanostructures (a few nanometers) where interparticle distances can be smaller than one nanometer. To achieve even more precise control of interparticle distance and strong immobilization, Li et al. [131] have employed methods based on pH variation around gold nanoparticles. Noble metal nanoparticles, due to their plasmonic effects, have a great potential in biophysics for biomolecular manipulation, labeling and detection [136, 137, 138], especially as detection centres for affinity between biomolecules [139, 140], e.g. in glucose sensing [141]. They could also overcome the technological limitations of optical tweezers in trapping of single molecules [142, 143, 144] and nanoparticles [145] at the nanometer scale around the particles.

In the reported references, the sizes of nanoparticles are typically a few tens of nanometer. Since the size dependence of the surface plasmon resonances is markedly pronounced for smaller gold nanoparticles (<10 nm), these small sizes are also more sensitive to any surface modifications [129]. pH-induced shifts in the absorption spectrum of nanoparticles smaller than 10 nm are also of interest since the particles could control the smaller parts of larger biomolecules, e.g. DNA and RNA [140, 146, 147] and thus can be used in nucleic acid delivery [148]. For example, it was shown that 2.2 nm ligand-protected Au nanoparticles create a stable photoluminescent material which exhibits reversible pH-dependent photoluminescence and absorption, suggesting that the pH value and the electric charge responses are related [149].

This chapter explores the effect of charge on plasmonic particles by change of the pH. This has been achieved by studying two kinds of samples: gold colloidal solutions (ligand-protected) and gold clusters (unprotected) deposited on glass by the CDA. The absorption spectra of both systems are compared, which allows the elucidation of the involved mechanisms via absorption spectrum changes during pH variation. Although these two systems, i.e. ligand-protected and unprotected gold nanoparticles have different physio-chemical properties, they have their own advantages and disadvantages, which, if fully grasped, can play an important role in a wide range of the

standalone sensing nanodevices including nano-pH-meters [150].

4.1 Theoretical

Water contains, besides H_2O molecules, also H^+ and OH^- ions. When a surplus of H^+ is present, the solution is acidic, while when a surplus of OH^- is present, the solution is alkaline. The amount of H^+ and HO^- is expressed by the pH. The pH is notionally defined as the decimal logarithm of the reciprocal of the (relative) hydrogen ion activity, a_{H^+}, (which is proportional to concentration) in a solution [151]:

$$pH = -log_{10} a_{H^+}, \tag{4.1}$$

which can also be written as:

$$pH = -log_{10} \frac{m_H \gamma_H}{m^e}, \tag{4.2}$$

where m^e is arbitrary constant representing the standard state condition, numerically equal to 1 mol/kg, m_H is the molality of hydrogen ions and γ_H is the single ion activity coefficient of the hydrogen ion [151]. The hydrogen activity, a_{H^+} is defined as: $a_{H^+} = \gamma[H^+]$, where γ is the activity coefficient and $[H^+]$, is the hydrogen-ion concentration.

The pH value accounts for the activity of hydrogen ions in an environment, which is proportional to its concentration. If these ions are very active (inactive), the environment is acidic (basic, i.e. alkaline) having pH values between 0 and 7 (7 and 14). Immersed in such environments, ligand-protected gold nanoparticles can accumulate protons from the acidic environment or expel them to an alkaline environment [152].
Although there is a lack of in-depth knowledge and controversy on pH dependent plasmon resonance shifts [150, 153, 154, 155], it is well-established that the plasmon resonance of noble metal nanoparticles blueshifts when extra electrons are introduced onto the particle, and redshifts when the particles are decharged [108, 156]. Therefore, we have investigated how the optical

properties of gold nanoparticles in diverse configurations are altered while the pH of the local environment, including the ligands protective layer and the pH of the solution in which the nanoparticles are immersed, is being varied. Beforehand, we first define a few terms of importance in colloid and nanoparticle science. The following definitions are paraphrased from definitions by Ross and Morrison [157]:

- *Agglomeration* is a process of collecting nanoparticles joined at the edges and corners in larger units (agglomerates) whose specific surface area does not differ much from the sum of the areas of the involved particles. This process could be reversible.
- *Aggregation* is a process of collecting nanoparticles joined at the faces in larger units (agglomerates), with the surface area markedly less than the sum of the areas of the particles involved, resulting in irreversibility of the aggregation to the primary particles.
- *Flocculation* is a process of forming flocs which represent any form of close particle collections, whether it is as agglomerate or aggregate.

To quantitatively determine the flocculation process of gold nanoparticles within a sample, we have spectrally defined the flocculation parameter, analogous to the definition in ref. [158]: The absorption spectra of the gold nanoparticles for all the applied pH values were normalized to the plasmon peak, after which it was integrated, starting from the plasmon resonance to the appropriate wavelength to the red part of the spectrum. Similarly, this was done for the control measurement (while the sample is not immersed in a buffer). The flocculation parameter is obtained by subtracting the two integrated absorption spectra and thus represents the flocculation parameter for the appropriate pH value. This empirical parameter is a reasonable quantification and is used for a comparison among the different samples.

4.2 5 nm sized gold colloidal solution

The variation of the pH around ligand-protected gold colloidal nanoparticles has three effects: 1) on the ligand, which is stronger since it is directly exposed to the environment, 2) on the gold core particle "protected" by the ligand, and 3) on the dielectric environment [159, 160, 161, 162]. Since the core and ligand are electronically coupled [163], changes in one of them cannot be observed independently, nor those in their surrounding environment. Yet, the gold plasmon peak offers an observable that reflects the electronic structure of the gold cores. The gold particle charge state strongly depends on the surrounding pH [164, 165] and pH can thus be used to control the charge on the core, which is more convenient than traditional methods [165]. When ligand molecular orbitals are filled, charge transfer may occur from ligand's molecular orbitals to partially fill *d*-orbitals of the core, leading to a spilling-in effect in the core. This particulary happens as a result of pH variation in the presence of weakly passivating ligands such as citrate [165, 166]. Since citrate forms weak bonds with the gold core, rather than a covalent bond [155], electron transfer between the ligand and the core occurs. This effect can lead to flocculation of the particles via protonation/deprotonation of the ligand [158, 167]. It was shown in chapter 3 that the double peak resonance may originate from a rod-like structure, since geometry of a particle affects the electron distribution, i.e. plasmonic oscillations [127, 168]. Therefore, pH variations can give rise to electron redistribution which can be reversible (agglomeration) [158], as well as to irreversible particle growth (core growth) [158, 165].

As soon as the particles come closer to each other, ending up with touching each other, a significant redshift of the plasmon can be noticed (as a result of particle elongation) [101, 102, 103, 105, 106, 168, 169]. Therefore, if a metal nanoparticle is elongated in one or two dimensions, by pH variation, a redshift and broadening of the spectrum occurs which is also expected by Mie theory [170]. Kreibig et al. [171] have also shown that when the distance between the flocs is smaller than

the radius of the sphere, an additional resonance occurs at longer wavelengths (longitudinal peak).

4.2.1 Experimental

For the pH experiment, the following commercial pH buffer solutions were used:

1. pH=8.5; Trimethylammonium bicarbonate buffer solution (Sigma Aldrich);
2. pH=5.5; based on Na-citrate (Sigma Aldrich).

The gold colloidal solution with the particles having diameter of 5 nm (Sigma Aldrich) and concentration of $c = 4.4 \cdot 10^{13}$ particles/ml were purchased. The gold particles were already protected by a ligand, i.e. citrate.

Fig. 4.1 illustrates how a gold nanoparticle is stabilized by a citrate molecule (ligand). The ligand is bound to a nanoparticle via the Lewis (loosely) bond. This results in a weak reaction between citrate and gold nanoparticles, leading to formation of slightly negatively charged (citrate-stabilized) gold nanoparticles. The negative carriers play a role in counterbalancing the flocculation process in gold particles.

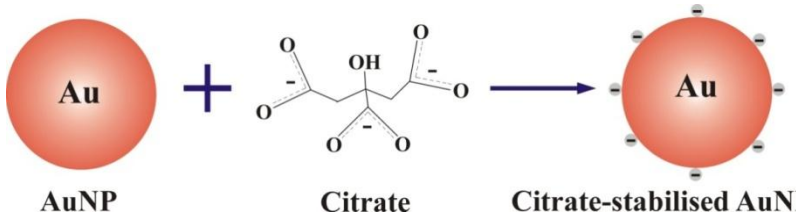

Fig. 4.1. Formation of a ligand-coated gold nanoparticle which is slightly negatively charged enabling counterbalancing flocculation.

A schematic overview of how the absorption spectrum of gold colloidal nanoparticles was measured is illustrated in Fig. 4.2. The optical spectrometer subtracted the background signal (the left cell) from the cell of interest (the right cell).

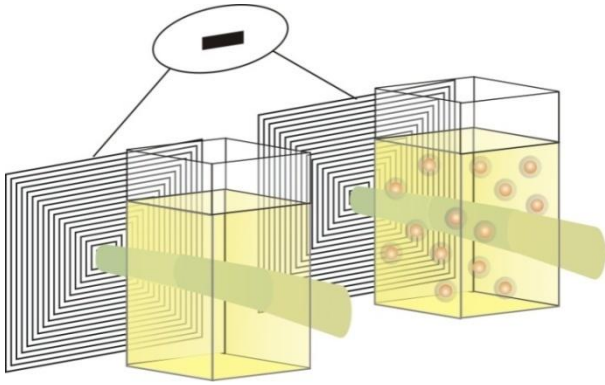

Fig. 4.2. Schematic overview of how the double-channel spectrometer measures absorption of gold colloidal solution. There are two samples – the left sample without particles, as reference, and the right, with gold colloidal nanoparticles surrounded by citrate (represented by grey rings around them). The identical light beams (green lines) pass through both samples. Absorption spectra are detected by two detectors (represented by squares) and absorption spectra are constructed by subtracting the corresponding colloidal nanoparticle signal and solution background spectra (represented by the minus sign). The aqueous solution with buffer solution are equal for signal and reference, which allows to attribute the spectrum resulting from the subtraction to the nanoparticles.

4.2.2 Results and Discussion

Fig. 4.3 shows the absorption spectrum of the 5 nm sized gold colloidal solution. Fig. 4.3(a) shows an increased absorption in the red part of the spectrum at pH=8.5 which is ascribed to the process of flocculation. In additon, the plasmon peak of gold colloids slightly shifts upon pH variation, as shown in Fig. 4.3(b). It can be seen that the plasmon resonance peaks at 516 nm for an unchanged pH. When the gold colloids are surrounded by the acidic environment (pH=5.5), the peak blueshifts to 512 nm, and when the gold colloidal is surrounded by the alkaline environment (pH=8.5), the plasmon peak redshifts to 518 nm. It is likely that the minute plasmon peak

shift occurs as a result of small citrate chains in the gold colloids, since recent studies have shown that the longer ligand chains cause larger plasmonic shifts [154, 172]. Toh et al. [153] have shown similar results in 11-mercaptoundecanoic acid modified gold nanorods; with increasing pH (between 6.41 and 8.88) the longitudinal plasmon resonance peak redshifted.

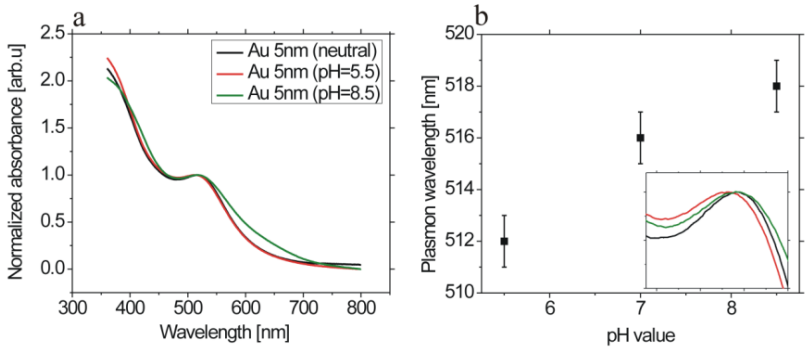

Fig. 4.3. (a) Absorption spectra (normalized at the plasmon peak) for the 5 nm sized gold colloidal solution: without changing pH (the black curve), with the acidic environment (the red curve) and with the alkaline environment (the green curve). (b) Plot of the extracted plasmon peak shifts from (a) for three different pH values (pH=7 is assumed initially when there was no pH change); the inset represents the zoomed plasmon peak range from plot (a).

According to [173], the plasmonic shift of a nanoparticle can be empirically calculated as:

$$\Delta\lambda_{max} = m\Delta n(1 - e^{-2t/l}) \tag{4.3}$$

where m is the refractive index sensitivity, $\Delta n = n_{COOH} - n_{COO^-}$ is the difference of local refractive index of protonated (n_{COOH}) and deprotonated (n_{COO^-}) citrate, t is the thickness of the surrounding citrate and l is the evanescent field decay length of the plasmon resonance. For gold nanoparticles, $m = 200$ nm/RIU (RIU: Refractive Index Unit) [174, 175, 176], t ranges between 0.7 and 1 nm for a citrate layer on Au, depending on the facets of gold nanoparticles [155], l ranges between 5 and 35

nm [174, 175, 176, 177, 178] and for approximately fully protonated citrate, $n_{citrate} = 1.44$ [179].

According to the mentioned literature, the observed blueshift for lower pH occurs because additional electrons are gained, while the redshift is the result of electron loss from the citrate-stabilized gold nanoparticles. This process is illustrated in Fig. 4.4; note the removed proton at the headgroup of the ligand in the lower cartoon.

Protonation and deprotonation of citrate likely trigger various degrees of electron-pulling forces via reduced and extended dipole moment, respectively [158, 167]. In addition, hapticity of the citrate [155] may also affect citrate-stabilized electron-donating nature, thus affecting also its absorption response.

According to equation (4.3), with the measured shift of ~6 nm as a result of reducing the pH value from 5.5 to 8.5, one can obtain Δn which is thus ~0.03, i.e. $n_{COOH} = 1.44$ and $n_{COO^-} = 1.47$. However, for a precise calculation, an accurate *t* and *l* are necessary which are still unknown [180]. With an empirical estimate (according to eq. (4.3)) of $\Delta n \approx 0.03$, the corresponding changes in the local dielectric environment when protonated/deprotonated citrate-stabilized gold nanoparticles are small, implying that other mechanisms could be involved.

Protonation (at lower pH) and deprotonation (at higher pH) reduces and enhances the Debye radius, respectively [153], which determines a charge-carrier electrostatic effect in the solution.

The Debye radius (length), r_D is given by:

$$r_D = \sqrt{\frac{\varepsilon_r \varepsilon_0 k_B T}{n e^2}} \tag{4.4}$$

where k_B is the Boltzmann constant, T is the absolute temperature and n is the electron density in the core particle. For our 5 nm colloidal gold solution, according to equation (4.4), the Debye radius is $r_D = 5.39 \cdot 10^{-12}$ m and the dipole moment is 0.26 D (Debye).

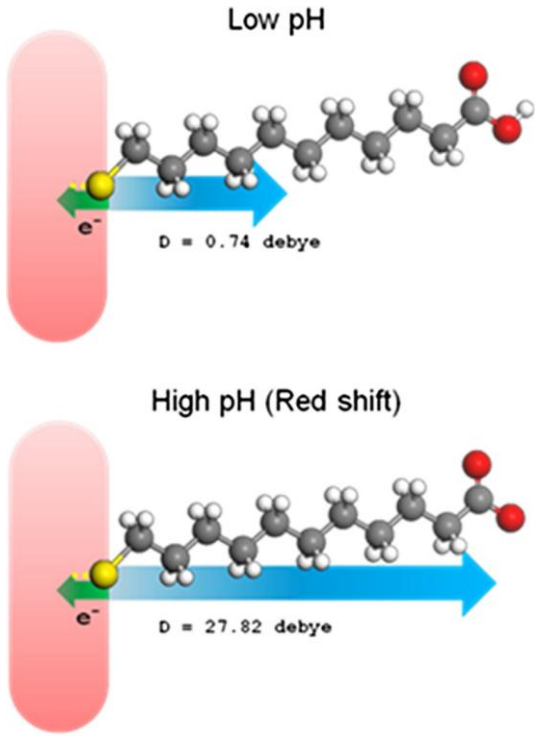

Fig. 4.4. Schematic cartoon model [158] (not to scale) based on ref. [158]. (a) A gold nanoparticle is surrounded by the ligand headgroup which has a carboxyl ending, electrically altered by pH variation. With the pH decrease from neutral to acidic, the ligand is protonized and the Debye radius is reduced which leads to an increased number of electrons on the particle (represented by the green with respect to the initial yellow column). (b) Increasing pH from neutral to alkaline, the ligand headgroups of the gold particle are deprotonized and the Debye radius consequently extends.

Being in a water solution, citrate has a carboxylic acid terminal functionality headgroup, as illustrated in Fig. 4.1, and exhibits an electron-donating nature [129, 181] and thus can be electrically charged to various degrees by controlling the pH of the nanoparticles' ligands.

The broadening to the red part of the spectrum in Fig. 4.3(a) occurs as soon as the dipole moment reaches the length of

the citrate chain, caused by deprotonation (when the pH is increased), thus resulting in gold particles' flocculation due to the van der Waals forces operating at small distances, in accordance with the Derjaguin-Landau-Verwey-Overbeek (DLVO) theory [182, 183]. Namely, with deprotonation (higher pH), the Debye radius is extended and electrostatic forces are screened outside the Debye radius so that the other neighbouring dipoles feel this dipole as a neutral centre. Therefore, these dipoles have very low or no repelling forces during their Brownian motion, being consequently ruled by the fully expressed van der Waals forces which lead them to flocculate. On the other hand, when the Debye length is reduced during protonation (low pH), appropriately charged citrate headgroups of the particles disable their flocculation, thanks to the repulsive and stabilizing Coulombic forces.

It can be also seen in Fig. 4.3 (b) that the redshift is not as pronounced as the blueshift which likely occurs due to the flocculation process, i.e. elongation process (rod-like structures) because the Debye length of the citrate headgroups likely depends on the two axes (aspect ratio dependence) and electrons normally tend to accumulate at the sharp edges in rod-like particle cores [184, 185].

4.3 2 nm sized gold nanoclusters deposited on glass by CDA

4.3.1 Experimental

Gold nanoclusters with sizes of ~2 nm were deposited by the CDA which is detailed in sec. 2.1. The gold nanoparticles were deposited under the same conditions on a glass substrate and on a silicium wafer with grown oxide layer substrate. The clusters on silicium wafer with grown oxide layer were imaged with AFM, see Fig. 4.5(a), from which the cluster size distribution is processed with the WSxM program [70], see Fig. 4.5(b).

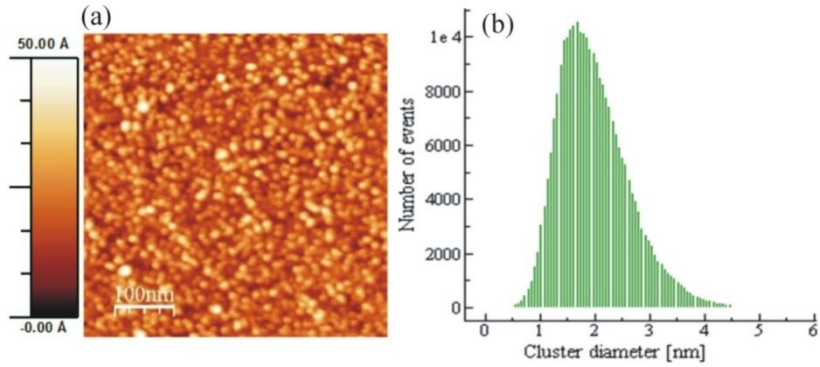

Fig. 4.5. (a) AFM image of gold clusters deposited on a Si wafer (with grown oxide layer). (b) The gold nanocluster diameter (height) distribution gained by the WSxM program [70].

Silicium wafer with grown oxide layer was chosen as substrate for the AFM visualization of the gold nanoparticles because the adhesion is stronger and therefore the nanoparticles withstand the AFM force better.

The clusters deposited on the glass substrate were immersed in the NaOH and $C_6H_8O_7$ solution. The uncoated gold nanoclusters could have been vulnerable to some additives of the purchased pH buffers. Therefore, we have been altering the pH value by introducing different concentrations of NaOH and $C_6H_8O_7$ (citric acid) in solution. The pH values ranged between 3 and 6.2. An advantage of this method is a strong adsorption of citrate at the metal surface which hinders interaction of gold with other ions [186, 187, 188]. In addition, the pH value was altered in a non-monotonic manner by which reversibility of the procedure could be tested.

4.3.2 Results and discussion

Fig. 4.6(a) shows the normalized plasmon peak of 2 nm sized nanoclusters at three different pH values. The background signal is considerable since the tiny gold clusters deposited on a surface were immersed in a solution within a cuvette. The number of excited clusters in the optical beam was about three

orders of magnitude lower as compared to the number of the 5 nm sized colloidal gold nanoparticles which were used for the experiments reported in sec. 4.2. Although clear plasmonic peaks at different pH can be identified, the plasmonic shift by pH variation cannot be resolved. However, the observed small broadening in the spectra could be an indication of flocculation, see the red and blue arrows in Fig. 4.6(a). Although the background signal is large, it might be that the floc elongation is extended for larger pH, leading to a redshift of the longitudinal plasmon peak. For the corresponding pH, the flocculation parameter was calculated, as explained in sec. 4.1, and is shown in Fig. 4.6(b). A linear decrease (represented by the red line) of the flocculation parameter with increasing pH can be noticed. Mayya et al. [158] reported that by decreasing the pH around gold nanoparticles, there is saturation of the flucculation process at pH≈4.3, leaving this phenomenon unexplained. The data reported here would be consistent with the same saturation (see black line in Fig. 4.6(b)).

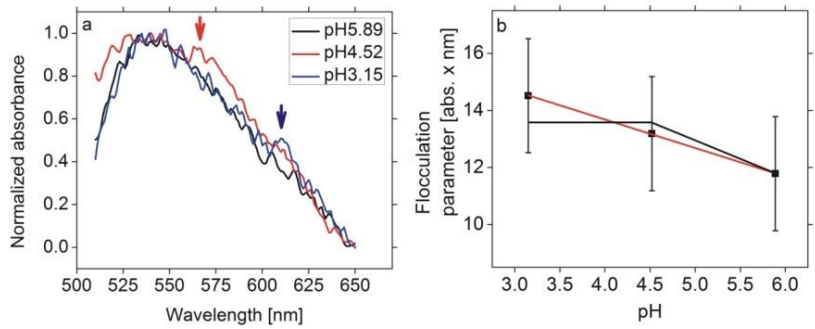

Fig. 4.6. (a) Absorption spectrum of gold nanoclusters within solution for three different pH values. The red and blue arrows in the spectrum indicate broadening which could result from cluster flocculation for different pH. (b) The calculated flocculation parameter, based on the experimental results, for three different pH values (black dots), with a linear (red line) and saturated fit (black line) corresponding to incessant or saturated (stopped) flocculation, respectively.

Mayya et al. [158] have also shown that the flocculation process in case of capped gold nanoparticles is irreversible, whereas our non-monotonic variation of pH, along with the consistent shift of the longitudinal wavelengths, suggests that the process may be reversible. As such, flocculation for our gold clusters may be designated as agglomeration according to its definition in sec. 4.1. Agglomeration likely takes place since the nanoclusters are surrounded by citrate. It is well-known that citrate anions coordinate to the metal surface by inner-sphere complexation of the carboxylate groups [155, 189, 190] and this process is likely affected by pH change which introduces and facilitates new charges, i.e. reversible attraction and repulsion of the clusters, which may lead to flocculation, as plotted in Fig. 4.6. However, why a low pH causes an enhanced flocculation of 2 nm sized gold nanoclusters, similar to ref. [158], being in contrast to both ref. [153] and our 5 nm sized colloidal gold nanoparticles, remains still unknown. This loosely adsorbated citrate layer at the gold nanocluster is also sensitive to changes of the surrounding properties, and gold clusters can thus reversibly disintegrate from the agglomerates in smaller units due to the same surface charges which act via repelling forces [153, 181], leading to the reversible effect. More elaborative quantitative interpretation of plasmonic sensing caused by surrounding adsorbates may be found elsewhere [173].

Further experiments are necessary to fully understand this complex process since the electric and optical properties with pH change differ for diverse metals and surroundings [158, 191, 192, 193, 194]; for example, whereas the plasmon resonance of gold nanoparticles redshifts with increasing pH, in silver particles it blueshifts [194]. This indicates that not only the ligand, but also the nanoparticle core plays a key role in response to the pH change of the surrounding. However, flocculation and stability of the particles primarily depend on ligands bound to the nanoparticles [155, 195, 196, 197].

Also, exceptional care should be directed to the exposition time of appropriate pH [158]. Namely, as long as appropriate acidic pH is applied to the clusters, flocculation is not stagnant, but has a trend of moving the longitudinal absorption peak further to the red and to its increase [158], while

the transverse peak tends to slightly reduce [198]. In this respect, we have been applying different pH under approximately the same exposition time to rule out this effect in our experiment.

4.4 Conclusions

We have compared the pH-induced optical behaviour of capped and ligand-free gold nanoparticles. While the plasmon resonance peak is pH-dependent in 5 nm sized ligand-capped gold nanoparticles, in case of 2 nm sized uncapped gold nanoclusters, the plasmon resonance peak shift could not be resolved, likely due to the significant background signal. The 2 nm sized clusters may exhibit (reversible) flocculation, i.e. agglomeration, likely resulting from a loosely adsorbed surrounding citrate which introduces and facilitates new charges and thus enables attraction/repulsion of the clusters. The pH-induced plasmon resonance shift in the ligand-protected nanoparticles (5 nm sized) reflects change of the electron density in the core, indirectly, via altering the dipole moment of the ligand; the flocculation here occurs due to the van der Waals forces of the neighbouring particles when the dipole moment reaches the length of the citrate cap around the gold core.

Fabrication of a pH-nanosensing device with 2 nm sized uncoated nanoclusters could be questionable owing to their "unprotectedness", although, at the same time, this unprotectedness likely enables repeatability, as well as a more direct and sensitive sensing, since there is no medium between the clusters and their environment.

Our experiments thus demonstrate that pH-induced shifts of the plasmon resonance position and band width could be harnessed to make a plasmonic biosensor which would for example detect cellular and conformational changes [199, 200]. Great challenges to achieve a state-of-the-art device are to increase the plasmon shift and to build highly stable samples with more uniform particle size. For example, further observation of the larger uncapped particles would also help understand these systems; investigation of the electro-optical

properties of smaller uncapped nanoclusters, although very attractive for sensing in very small changes of diverse biomolecules, like DNA and RNA, is still a challenge due to the great background absorption [201].

Finding a way to increase the optical sensitivity of the 2 nm sized gold clusters would be a great incentive in building nanosensing systems. For example, a well-controlled subnanometer distance between such small nanoparticles would likely help this aim owing to plasmonic coupling which gives rise to enhanced optical fields [117, 118, 119]; in this way, plasmonic shifts would certainly be seen. Further research on this pH nanosensors (nanotransducers) is certainly necessary to make a finely controllable nanodevice suitable for a wider application, which can open new avenues to more imminent application of such system in new biophysics and medicine technology [201, 202].

Chapter 5

Photoluminescence as a probe of the electrical charge dependence of gold nanoparticles

The results presented in this chapter are based on:

Photoluminescence as a Probe of the Electrical Charge Dependence of Gold Nanoparticles

Milan Obradovic, Marcel Di Vece, Inge Asselberghs, Didier Grandjean, Koen Clays and Peter Lievens
J. Nanosci. Nanotechnol. **15**, 9766 (2015)

This chapter contains an investigation of the photoluminescence of gold nanoparticles as a function of charge. Electro-optical switching can be achieved by changing the optical absorption of metal nanoparticles by adding or removing electrical charge which results from increased/decreased electron density onto gold nanoparticles. In this work a different approach is taken, namely the variation of

photoluminescence properties as a function of electrical charge on gold nanoparticles. The experiment reported in this chapter shows a significant dependence on the electrical potential, which was measured by averaging multiple photoluminescence changes after a potential step. This work thus presents a further step in the study of changing optical properties as a function of charge, first of its kind. A relation between the optical absorption and the photoluminescence revealed the influence of the charge state on the electronic properties and therefore the optical transition probability. This is of technological interest, opening a new way for electro-optical switching and bio-sensing.

5.1 Introduction

The optical properties of noble metal nanoparticles have attracted much attention over the last years and have been extensively studied from many perspectives [11, 110]. One of the striking properties of metal nanoparticles is the ability to change their optical response by tuning their size, shape, and environment [39]. This optical response is caused by the surface plasmon resonance with its resonance frequency in the visible part of the electromagnetic spectrum. The effect of electrical charge on the optical properties of metal nanoparticles is of high technological relevance as it may for example allow electro-optical switching. It is also important for nanoparticle-based signal amplification for biosensing, widely used during recent years as versatile and sensitive tracer for the electronic, optical, and microgravimetric transduction of different biomolecular recognition events [24, 203, 204].

One of the first experiments reported the electro-reflectance effect for bulk metals [204, 205], which is around 100 times weaker than for a nanoparticles ensemble [206]. For metal nanoparticles with a size 3-50 nm in diameter, there is a strong surface plasmon resonance in the absorption spectrum [207]. Static charge transfer between a silver nanoparticle and a matrix leads to a shift of the plasmon resonance frequency [110]. This frequency, which corresponds to the plasmon

resonance of a metal nanoparticle, depends on the electron density and therefore shifts considerably upon electrical charging. The dependence of the Drude plasma frequency $\omega^2_p = ne^2/m\varepsilon_o$ (with n=electron density, e=electron charge, m=effective electron mass and ε_o= the vacuum permittivity) on the electrical charge was confirmed by several investigations. Electrochemical studies of gold [108] and silver [207] nanoparticles of a diameter of about 10 nm show that the optical absorption changes as a function of the applied electrical potential, i.e. the charge-state. The plasma frequency has a blue shift for negative potentials, and red shift for positive potentials because the charge on the particle increases or decreases the electron density respectively [156, 208, 209, 210].

Very small gold nanoparticles (< 2 nm) are capable of efficient photoluminescence in the blue [77, 78], and other parts of the visible and infrared part of the spectrum [79, 80, 86]. Photoluminescence from larger gold particles (colloids) up to 5 nm, stabilized with non-fluorescent ligands was reported for the first time by Wilcoxon et al. [211]. Such photoluminescence originates from the direct recombination of conduction-band electrons below the Fermi energy with holes in the *d*-band [72]. Very strong photoluminescence was observed in gold nanorods as compared to nano-spheres by Mohamed et al. [212]. Quantum effects are also of fundamental importance in photoluminescence generation [88]. A higher quantum yield as compared to thin films can be attributed to local field enhancement [74]. Whereas dependence of photoluminescence (plasmon-modulated) on the shape and size of Au nanostructures have been demonstrated [213], photoluminescence dependence on potential has not been studied so far, except for potential dependence of the electroluminescence of individual gold nanoclusters at room temperature [214]. The possibility that charge is influencing the plasmon properties of metal nanoparticles in microscopy has been suggested by Bouhelier [215]. Since both the effect of an electrical charge on the optical absorption of metal nanoparticles and luminescence of gold nanoparticles has been observed, the combination of both properties may reveal new physics.

The electronic structure of noble metal clusters is not yet completely understood [86, 216] and hence it is still not well-known at what cluster sizes the transition from discrete levels due to quantum confinement to collective oscillations for non-quantum confined particles occurs. Silver nanoparticles embedded in silica show photoluminescence (excited at 250 nm), with two bands attributed to interband transition and plasmon resonance; the former being independent on particle size (peaking at ~340 nm) and the latter being size dependent (however, this size dependence was less significant for the smallest measured nanoparticles (11 nm and 8 nm), peaking at ~410 nm) [217]. Zakaria et al. [218] have reported that 20-30 nm sized silver nanoparticles show three photoluminescence peaks: at 780 nm, 591 nm and 440 nm. Recent study reports that photoluminescence of 9 nm sized silver nanoparticles peaks at ~440 nm (excited at 366 nm), showing also that for sizes below 15 nm, photoluminescence peak position is poorly size-dependent, although correlated plasmon and emission spectra [219]. To date, there are diverse reports on emission of gold nanoparticles of different sizes [86, 167, 211, 220, 221], not only as a function of cluster size, but also due to different ligands surrounding the gold cores [222, 223]. The photoluminescence of smaller gold nanoparticles is considerably stronger with respect to the larger particles [225]. There are several reports which studied emission energies as a function of cluster size with interpretations based on free-electron models [80, 86, 222, 226]. For example, 28-atom gold clusters show emission onset at about 950 nm [80], while 55-atom gold clusters, excited by 350-390 nm, show a broad emission between 440 nm and 660 nm peaking at about 500 nm [225]. It was shown that 6-mercapto-1-hexanol-capped gold nanoparticles fluorescence at different wavelengths from 510 to 600 nm while the particle size remains within the the 2–3 nm size range [227]; 2.5 nm thiolate-protected gold nanoparticles have also shown emission at different wavelengths in spite of their identical size [228], indicating that the particle size happens not to be a crucial factor in determining the emission wavelength [228]. On the other hand, for very small size, gold nanoclusters change their optical properties abruptly in a non-

scalable way with size [80, 86, 222] which starts when reaching the size <2 nm [11, 90], which also depends on particle environment [229]. Although emission of nanoparticles may be size-dependent [86], different environments of the particles may affect this dependence to a greater extent, as was shown in chapter 4 [222]. A broader overview of up-to-date research on electro-optical properties of very small nanoparticles, with a particular size and ligand density, can be found elsewhere [228, 229]. In this work the photoluminescence of gold nanoparticles is investigated as a function of the electrical charge state. With an electrical voltage in an electrochemical cell nanoparticles with sizes of 2, 5 and 10 nm of diameter were charged, which subsequently resulted in varying luminescence intensity. This electro-optical effect may have technological consequences in the field of optical switching, as well as in biosensing applications in biological tissues [230] and fluids at a molecular level [223].

5.2 Experimental

Three samples were prepared by attaching gold nanoparticles to a conductive ITO substrate. A commercially available ITO slide (surface resistivity, 5-15 Ω/sq, supplied from Delta Technologies Ltd.) was rinsed by immersing it in a basic piranha solution (30% hydrogen peroxide solution in 1:1 ratio with 30% ammonia) for 15 minutes. The slides were rinsed with copious amounts of Milli-Q water and methanol. The sample was subsequently immersed in CH_3OH + 3-aminopropyl-triethoxysilane ($C_9H_{23}NO_3Si$) for 15-20 minutes in order to prepare an amine-terminated siloxane (APSiO)-monolayer modified electrode. After rinsing with methanol, it was immersed in Au colloidal solution (Sigma Aldrich (10 and 5 nm) and TedPella (2 nm), citrate stabilized) for a period of 40-60 minutes, followed by rinsing with Milli-Q water. The gold nanoparticles were imaged with AFM and processed in the WSxM program [70] as shown in Fig. 5.1. For the AFM visualization of the gold nanoparticles, silicium wafer with

grown oxide layer was chosen as substrate as the adhesion is stronger and therefore the nanoparticles withstand the AFM force better. The individual gold nanoparticles are clearly visible and remain firmly attached despite the wiping force of the AFM tip.

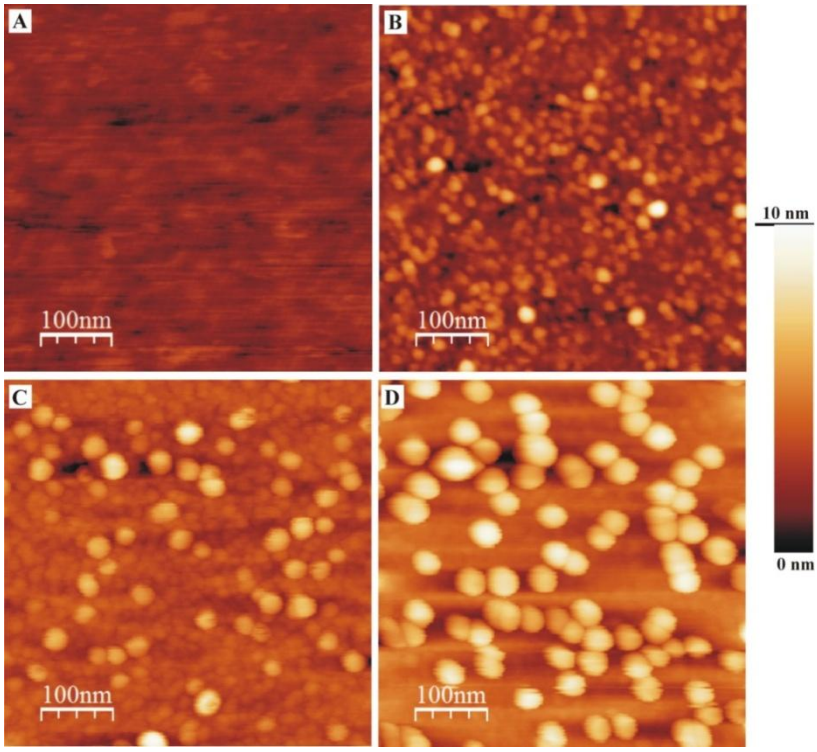

Fig. 5.1. AFM images of (A) pure silica wafer, (B) 2 nm sized gold nanoparticles, (C) 5 nm sized gold nanoparticles, and (D) 10 nm sized gold nanoparticles.

Both the optical absorption and the photoluminescence of the APSiO-modified ITO electrode with immobilized gold nanoparticles were measured at several constant potentials while immersed in a 0.1 M Na_2SO_4 aqueous solution in an electrochemical cell (Fig. 5.2).

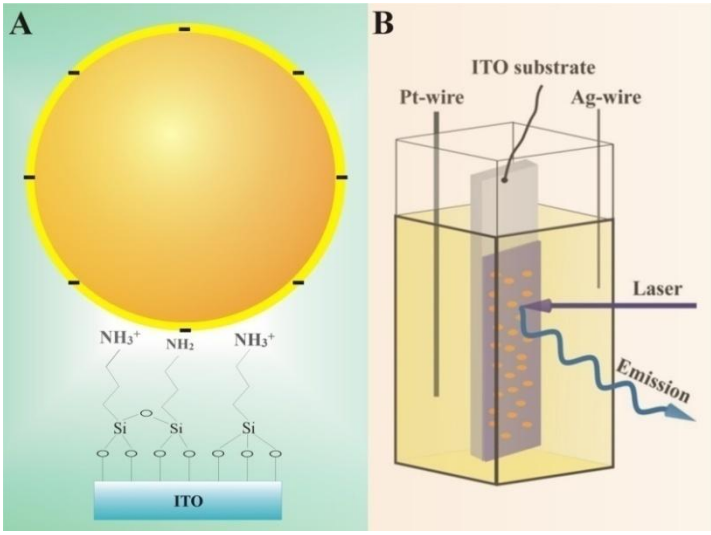

Fig. 5.2. Schematic illustration of (A) a gold nanoparticle attached to ITO (not to scale) and (B) the electrochemical cell with the sample measured in the photoluminescence setup.

Applying electrical potential charges the gold nanoparticle by adding or removing electrons [224]. Cyclic voltammetry experiments and electrical charging were performed by a potentiostat/galvanostat 263A (Princeton Applied Research). Three electrodes were used: an Ag-wire acted as pseudo-reference, a Pt-wire as counter electrode and ITO as working electrode. Voltammograms were measured with a constant sweep rate of 25 mV/s.

Characterization of the ITO electrode surface after modification with the nanoparticles by cyclic voltammetry showed that applying electrical potentials between -1.2 and +1.1 V is charging the gold nanoparticle by adding or removing electrons [224] without inducing any redox reaction. For example, Fig. 5.3 shows the voltammogram obtained for the deposited 5 nm sized gold nanoparticles on ITO working electrode with a well-resolved anodic peak (oxidation peak) at 1.15 V and a cathodic peak (reduction peak) at -1.25 V at which hydrogen is being developed.

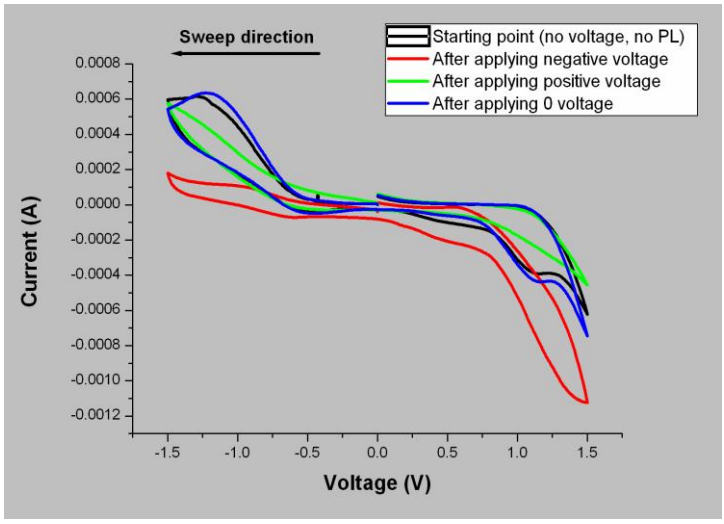

Fig. 5.3. Cyclic voltammetry for the sample with 5 nm sized gold nanoparticles in the following sequence: before applying potential (the black curve), after applying ~1.2 V (the red curve), after applying 1.1 V (the green curve) and after again applying 0 V (the blue curve) (this is the sequence of applying the potential).

It exhibits a good repeatability as the sample was cycled with diverse potentials supporting the fact that there were still not redox reactions. The voltammogram also shows that a purely capacitive current was obtained between -0.5 V and 0.5 V. This suggests that the potential window from -0.5 V to 0.5 V, i.e. double layer potential region, occurs purely due to the capacitance of the gold nanoparticles rather than to the redox (faradaic) reactions. Therefore, this potential window was chosen to charge gold nanoparticles while observing their photoluminescence, excluding any redox reaction and hydrogen gas evolution. In this manner, the applied electrical potential is fully employed for particle charging rather than for redox reactions and thus the photoluminescence changes can be attributed to alternation of electrical charge on gold nanoparticles via the double layer around them. Importantly,

within the potential window, some unavoidable ion adsorption occurs.

Photoluminescence spectra were recorded using a homebuilt setup based on a pulsed Nd:YAG laser (GCR-11-2, Spectra Physics) operated at the third harmonic wavelength of 355 nm, with a pulse duration of 7 ns and a repetition rate of 10Hz. Samples were investigated in a front-face excitation geometry and a monochromator (HR 640, Jobin Yvon) is used to spectrally resolve the luminescence. Further details about this setup are described in sec. 2.3.1 and in ref. [231].

All emission spectra were recorded at room temperature with a wavelength increment of 2 nm and averaged more than 10 times. The spectra were corrected by subtracting the photoluminescence of the cell, ITO and electrolyte from the measurement with nanoparticles. These spectra were thereafter corrected for the spectral sensitivity of the setup. Since the gold photoluminescence has decay times in the order of picoseconds [74], with the here employed setup having a time resolution of nanoseconds, luminescence decay times were not measured.

5.3 Results and discussion

The optical absorption spectra as a function of electrochemical potential are plotted in Fig. 5.4 A and B for gold particles of 5 and 10 nm, respectively (no plasmon signal could be measured for the 2 nm nanoparticles). Without bias, the optical absorption of the gold nanoparticles attached to ITO has a broad range, covering the range from 400 to 800 nm with a maximum at around 530 nm for 5 nm sized gold nanoparticles (Fig. 5.4A) and 520 nm for 10 nm sized nanoparticles (Fig. 5.4B) in agreement with known values of the gold nanoparticle plasma frequency [232]. A slight red shift with respect to ref. [232] is likely caused by the presence of ligands which accept electrons, thereby lowering the plasma frequency [88, 210, 220, 221]. This effect strongly depends on the size of the nanoparticle, i.e. surface-volume ratio, which determines the number of ligands per gold atom and therefore the degree of electron exchange [167]. However, since the plasmon resonance

wavelength shifts to the blue for smaller nanoparticles, obtaining the origin of the optical absorption shift is not straightforward.

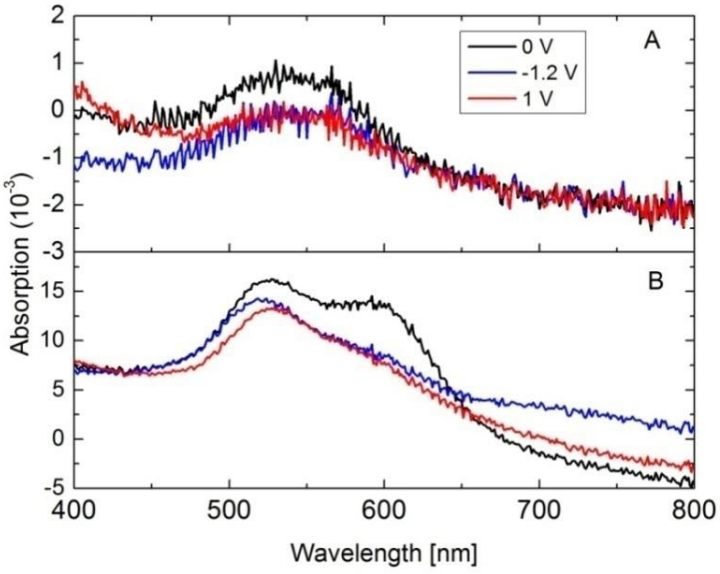

Fig. 5.4. The optical absorption spectrum of (A) 5 nm sized gold nanoparticles; and (B) 10 nm sized gold nanoparticles tethered on ITO and immersed in an aqueous 0.1 M Na_2SO_4 solution and charged at 0, 1.0 and -1.2 V.

The optical absorption at 0V has a pronounced shoulder at around 600 nm. This is likely due to agglomeration, which results in objects with larger dimensions. Increasing the size of a gold object results in a longer plasmon resonance wavelength which explains the shoulder around 600 nm. Remarkably, a non-zero potential removes the shoulder at the wavelength of 600 nm, resulting in a single distinctive peak. This is the result of a repulsive Coulomb interaction between the particles which have identical electrical charge. This repulsive Coulomb force disconnects the agglomerates into individual particles, causing a single sharp optical absorption peak. This effect appears to be irreversible since the shoulder did not reappear upon changing the potentials back and forth. Once the particles are disconnected, they remain separated.

Upon bias, the 10 nm particles exhibit a clear blue (6 nm) and red (4 nm) shift in the optical absorption for negative and positive potential, respectively (Fig. 5.4 B), which is in good agreement with literature [39]. By applying a positive (1 V) or negative (-1.2 V) potential, the amplitude of the absorption is only slightly reduced.

In contrast to the 10 nm nanoparticles, a strong dependence of the optical absorption on the potential is apparent for the 5 nm particles (Fig. 5.4A). This is clear by comparing the amount of change in absorption with respect to the maximum absorption. The optical absorption has significantly decreased at a positive and negative voltage as compared to the higher absorption at 0V. Considering the lower absorption of small particles [232], the relative change in absorption in the smaller nanoparticles is more significant. On going from negative to positive voltages the optical absorption peak at around 530 nm does not shift. This is caused by the combined effect of a much broader plasmon resonance peak and a poorer signal to noise ratio which obscures a wavelength shift with the used experimental sensitivity.

While the 10 nm gold nanoparticles, featuring bulk-like properties, showed insignificant photoluminescence in agreement with literature [79, 80, 88, 211], a clear photoluminescence signal was observed for the 5 nm and the 2 nm gold nanoparticles as shown in Fig. 5.5. This signal was obtained despite the strong background signal (mainly glass) over a wide range. The different spectral signatures of the gold particle luminescence and the background signal confirm the gold particle luminescence origin. The signal was smoothened to increase readability as the noise level (indicated by the bar) was high due to restricted measurement time. The measurement time is kept relatively short in order to allow for a sequence of measurements at different applied voltages while limiting degradation by the laser light exposure. The photoluminescence peaked around 450 nm, in good agreement with literature [79, 211, 225], although some studies show photoluminescence at around 550 nm [74] for much larger particles, as well as in visible and infrared part of the spectrum for smaller nanoparticles (< ~1 nm) [79, 80].

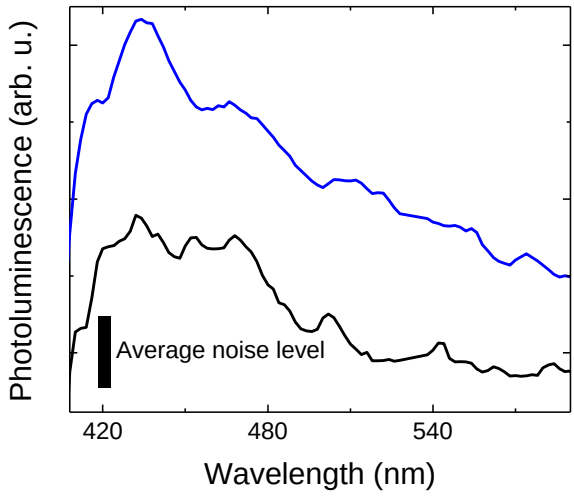

Fig. 5.5. Photoluminescence of 5 nm (black) and 2 nm (blue, shifted for clarity) sized gold nanoparticles tethered on ITO and immersed in an aqueous 0.1 M Na_2SO_4 solution at 0 V.

A broad wavelength range of the photoluminescence peak in small nanoparticles occurs because the dielectric function (refractive index) becomes strongly size-dependent since this size is comparable with the Fermi wavelength [86]; furthermore, optical, electrical and chemical properties of the gold and silver nanoclusters are also affected [86, 233, 234, 235].

According to Kubo's predicted model [234], the square-potential-box model [11] and jellium model [11, 233] considerable changes in emission wavelength occur when the particle size decreases down to ~50 and ~10 atoms, respectively [11, 86, 233, 234]. Since our 5 nm and 2 nm sized gold nanoparticles, correspond to ~1800 and ~200 atoms clusters respectively (Table 3.1), an optical effect along these lines is not expected. In addition, recent studies have shown that photoluminescence peak can exhibit insignificant shift when reaching the size below 15 nm [219, 228].

Since the photoluminescence intensity depends on time due to photo-degradation, the potential was alternately changed

with a repetition of at least 6 times to obtain a reliable average. In Fig. 5.6 the photoluminescence at 450 nm is shown at a positive or negative potential over a large number of potential steps.

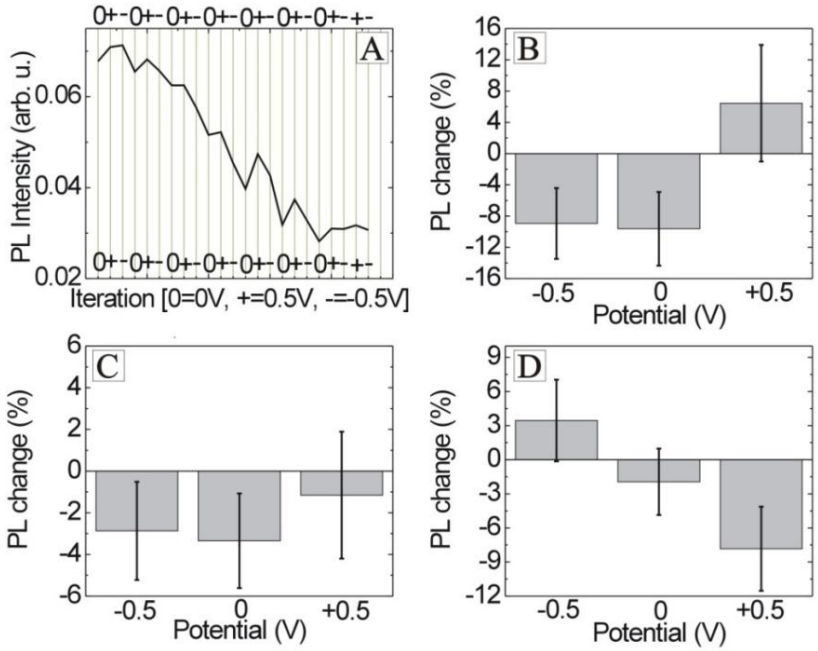

Fig. 5.6. (A) Photoluminescence of 5 nm sized gold nanoparticles tethered on ITO and immersed in an aqueous 0.1 M Na_2SO_4 solution at alternating potentials 0, 0.5 and -0.5 V. Photoluminescence change as a function of potential in % for (B) 2 nm, (C) 5 nm gold nanoparticles tethered on ITO and (D) bare ITO substrate.

The photoluminescence intensity values, either a peak or valley in the signal, are recorded after each potential step. The percentage of photoluminescence change after a potential step for the 2 nm and 5 nm gold nanoparticles, and the bare ITO, are shown in Fig. 5.6 B, C and D as a function of potential (-0.5, 0 and +0.5 V).

The photoluminescence intensity of the 2 nm gold nanoparticles is reduced by about 9% after a step to -0.5 and 0 V, and increases significantly with about 6% after a potential step of +0.5 V. The photoluminescence intensity change of the 5

nm gold nanoparticles is on average always negative without a significant difference between the individual potentials since the error bars are overlapping. The photoluminescence of ITO [236, 237] as control measurement upon changing potentials is markedly different from the gold nanoparticles: increasing at -0.5 V, slightly decreasing at 0 V and a strong decrease at +0.5 V.

This confirms the independent photoluminescence behaviour of the gold nanoparticles with respect to ITO as a function of potential. The negative slope of the photoluminescence, most likely caused by particles disconnecting by thermal stimulation, will only provide an offset of the averaged photoluminescence change. The shape of the photoluminescence spectrum remains unchanged and no peak shifts are observed.

According to Dulkeith et al. [238] the photoluminescence of small gold particles is the result of particle plasmon emission caused by the relaxation of a photoexcited *d*-band hole. To this end, the plasmon-modulated photoluminescence has been profoundly reported also on gold nanofilms [81]. Since the 355 nm (3.5 eV) of the excitation wavelength will excite an electron in the *sp*-band, well above the Fermi level, the electrochemical potential which lifts or lowers this Fermi level will not affect this excitation process. The subsequent relaxation of the hole within the *d*-band, resulting in a plasmon excitation, which radiatively decays, is probably affected by the plasmon properties. Since the optical absorption reduces for the 5 and 10 nm gold nanoparticles at positive and negative potentials (Fig. 5.4), this indicates that the optical transition probability has decreased around the plasmon frequency. The reduced absorption is likely the result of moving the plasmon resonance with respect to interband transitions [110]. Since the 2 nm and 5 nm particles have a plasmon resonance frequency at slightly different positions, this could explain why the 2 nm particles show a slight increase of the photoluminescence signal at positive applied voltage with respect to the 5 nm particles. However, considering the large error bar this is not definitive. The potential therefore also reduces the probability of a plasmon excitation originating from

the d band hole relaxation, thereby reducing the luminescence. Clearly, the effect of charge on the plasmon properties cannot only be explained by the change in electron density. For such small particles the charge also changes the dielectric properties of the particle and in its environment.

Alternative theories about the dependence of gold nanoparticle luminescence on the charge state are for example provided by Wu et al. [167] where the role of the surface and ligands was elaborated; they also found fluorescence enhancement in very small gold nanoparticles (<2 nm) when the electropositivity is increased, which may corroborate the luminescence of our 2 nm gold nanoparticles at positive potential. Although considerable literature exists on electron transfer in very small gold particles [239] and their quantized nature [240] under electrochemical potentials, as well as thorough analysis of quantum and plasmonic properties of very small individual metal nanoparticles [52, 54], a detailed universal theoretical investigation is required to elucidate the described phenomena.

5.4 Conclusions

Since the optical absorption of 10 nm gold nanoparticles showed plasmon peak shifts upon electrical charging, both in literature and in this study, the question arises how the photoluminescence behaves at these different potentials. In this chapter an important step forward, towards controlling luminescence by electrical means, was demonstrated. In an electrochemical setup the optical absorption and photoluminescence of gold nanoparticles was measured as a function of applied potential. Although for 5 nm gold nanoparticles no significant plasmon peak shift was observed, the absolute value of the optical absorption decreased significantly at positive and negative potentials. In line with this change, a dependence of the photoluminescence intensity on potential for 2 nm and 5 nm gold nanoparticles was observed. The photoluminescence was reduced at negative and increased at positive potentials. Both the optical absorption and

photoluminescence dependence on potential are explained by a change in the optical transition probability. Since up to date only the optical absorption was controlled by applying a potential difference, here we have made a next step, first of its kind, by extending this to photoluminescence. The dependence of photoluminescence of gold nanoparticles on charge state is potentially interesting for applications in the field of optical telecommunication and sensor technology.

.

Chapter 6

Charging gold nano-particles in ZnO by electric fields

The results presented in this chapter are based on:

Charging gold nanoparticles in ZnO by electric fields

Milan Obradovic, Marcel Di Vece, Didier Grandjean, Kelly Houben and Peter Lievens
J. Phys. Condens. Matter. **28**, 035303 (2016)

Controlling the plasmon resonance frequency of metal nanostructures holds promise both for fundamental and applied research in optics. The plasmon resonance frequency depends on the number of free electrons in the metal. This dependence is for example reflected in the plasmon resonance frequency shift upon adding or removing electrons to a metal nanoparticle. In this study we indirectly change the number of free electrons in gold nanoparticles by applying an electrical potential difference over a heterostructure consisting of a ZnO layer with embedded gold nanoparticles. The potential difference induces shifts of

defect energy levels in the ZnO by the electric field. This results in an electron transfer between particles and matrix which consequently modifies the gold nanoparticle plasmon properties. In addition, we theoretically support our experimental results and established relations between the number of electrons, voltage, plasmon peak wavelength and Fermi energy. Our results offer a promising way to obtain fast optical switching in a solid state composition.

6.1 Introduction

Optical devices which contain plasmon resonances are of great importance for future high density optical data storage and high-speed signal processing [13]. Plasmonic metal nanostructures are explored to enhance the performance of solar cells [6, 241, 242], increase the sensitivity of detectors [243, 244] and energy-conversion devices and sensors [245], stimulate catalysts [246], etc. Besides the applied interest into plasmonics, much research to the fundamentals of plasmonics is performed [46]. For all these topics, controlling the plasmon resonance energy is a very attractive prospect. The plasmon of a metal nanostructure is affected by the size, structure, and composition of both the metal and its surrounding dielectric medium. Moreover, the coupling between the plasmon resonance of a metal and the quantum size effect of a semiconductor gives rise to new properties: semiconductor quantum dot luminescence enhancement through exciton and plasmon coupling including CdSe/ZnS core/shells on Ag nanoislands [247], CdSe on Au [248], colloidal CdSe/ZnS on nanoperiodic Ag arrays fabricated by electron-beam lithography [249], CdSe on thermal evaporated Au layers [250], and ZnO films embedded with Ag nanoparticles [251]. Instead of these static effects on the plasmon, more dynamic control is desired for many purposes. Work by Toyota et al. [108] shows that the plasmon resonance wavelength of gold nanoparticles can be shifted in an electrochemical cell by applying a voltage. Importantly, the pursuit of more sensitivity of gold nanoparticles to applied voltage can be achieved by decreasing the particle size [91].

Increasing the electron density of the metal nanoparticle blueshifts the plasmon resonance wavelength [108, 156]. Electron transfer to a metal nanoparticle can also occur when the particle is embedded in a semiconductor with appropriate bandgap difference resulting in the Fermi level equilibration and the formation of a nano-Schottky layer. For example, silver nanoparticles on the surface of ZnO nanorods act as a sink for the electrons; they promote interfacial charge-transfer kinetics between the metal and semiconductor, and improve the separation of photogenerated electron-hole pairs, and thus enhance the photocatalytic activity [252]. Dynamically controlling the Schottky layer, by manipulation of the semiconductor bandgap, opens a way to change the charge density on the metal nanoparticle.

Both the Zeeman and Stark effect alter the band structure and change the bandgap of semiconductors. Plasmon-enhanced Stark shifts in Au/CdSe core/shell nanoparticles have been demonstrated by Zhang et al. [248]. Spectral shifting toward lower energy of the exciton of Ag-coated CdS semiconductor quantum dots [253], CdSe/ZnS quantum dots assembled on an Ag nanorod array [254], and the exciton of CdSe/ZnS quantum dots assembled on an Ag island film [247] have been reported. Wang et al. [255] have measured the Stark effect of surrounding molecules via the plasmon resonance of the metallic cores and Miller et al. [256] have observed the bandgap shift for a GaAs-AlGaAs of up to 10^{-5} V/cm; both studies [255, 256] performed the Stark experiments at room temperature.

In this work we embedded gold nanoparticles in ZnO and applied an electric field over the thin film. ZnO is a semiconductor with a bandgap of 3.37 eV (368 nm). It is intrinsically an n-type semiconductor with high electron mobility, high thermal conductivity, wide and direct bandgap and large exciton binding energy (60 meV), making it suitable for a wide range of devices, including transparent thin-film transistors [257], photo-detectors [257] and light-emitting diodes [258]. Here the ZnO defect levels [259], having attractive (nonlinear absorption) properties [260, 261], likely play an important role and are altered by shifting the energy levels under an electric field. This results in a shift of the ZnO exciton peak

toward lower energy. By a shift of the defect level energy close to the conduction band of ZnO, electrons will flow to the gold particle, thereby increasing the electron density on the gold particle. This in turn shifts the plasmon resonance wavelength toward higher energy. This linear dependence points to the first order Stark effect which likely indirectly changes the ZnO bandgap; the electron density on the gold particle therefore dynamically shifts the plasmon resonance wavelength. The controlled dependence of the optical absorption on voltage (electric field) in the heterostructures studied in this work may have an impact on the technology of electro-optical switches.

6.2 Properties of ZnO

ZnO has attracted extensive attention because of its appealing and distinctive electrical, optical and mechanical effects [262]. Its nanoscale mechanical energy can be converted into electrical energy due to the intrinsic piezoelectric features of ZnO; this feature is caused by lack of the centre of symmetry in Wurtzite along with large electromechanical coupling [50, 262, 263, 264]. ZnO can be thus employed as an electromechanical and electrovibrational sensor. Very appealing is the possibility of making powering nanodevices based on converting of the mechanical, vibrational and hydraulic energy onto electricity [265]. Its wide badgap (~3.37 eV) is ideal for electro-optical application in the shorter wavelength region. The large exciton binding energy (60 meV), which can be even increased in diverse ZnO heterostructures [266], enables the detection of physical properties (like excitonic absorption) at room temperature. For example, the Stark effect in ZnO can be detected even at room temperature due to its large binding energy [267]. The Wurtzite crystal structure of ZnO is cartooned in Fig. 6.1.

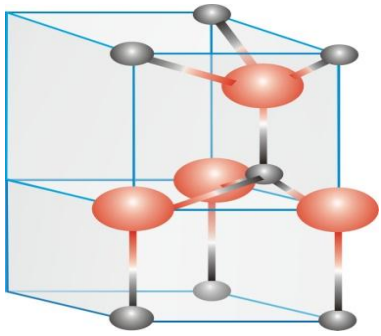

Fig. 6.1. The stick-and-ball representation of the ZnO hexagonal Wurtzite crystal structure (B4). The gray and red spheres denote Zn and O atoms, respectively.

6.3 Experimental

The samples were made within an ultra high vacuum deposition chamber using a laser vaporization source in the CDA setup described in Sect. 2.1. The cluster size distribution was monitored with time-of-flight (TOF) mass spectrometry and is plotted in Fig. 6.2(a) as a function of cluster diameter, hereby assuming a spherical shape of the clusters and using a Wigner-Seitz radius of 0.159 nm for gold.

Gold clusters were deposited on ITO (Präzisions Glas & Optik GmbH) supports which have surface resistivity less than 20 Ω/sq). After the nanoparticles are deposited on ITO, a layer of 100 nm of ZnO, and 100 nm of ITO were subsequently deposited by RF sputtering at 200 W and 300 W, respectively, and in a 5 μbar atmosphere (Kurt Lesker). Properties of the sputtered ZnO layer may be found elsewhere [268]. A cartoon of the entire structure is shown in Fig. 6.2(b). Because of the low reactivity of gold and the high reactivity of zinc, an oxide layer on gold is not expected [269].

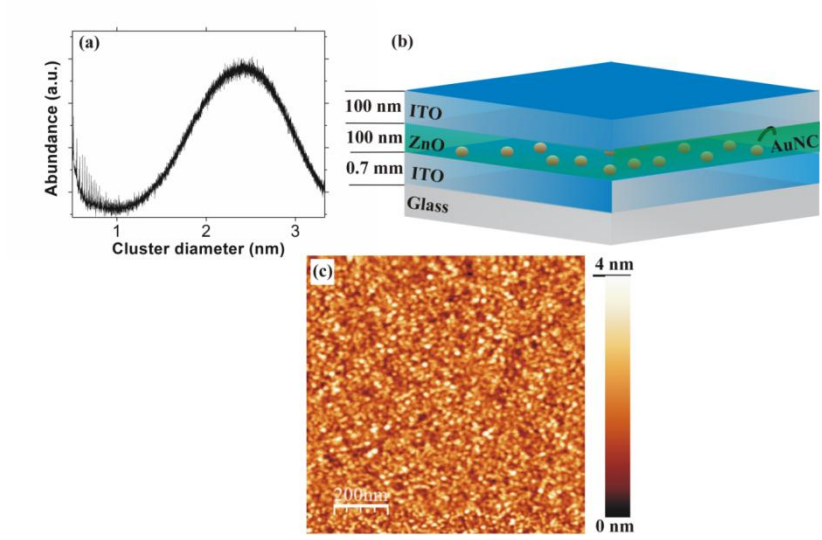

Fig. 6.2. (a) Gold cluster size distribution as measured by a TOF mass spectrometer. The cluster diameter is deduced assuming a spherical cluster shape and a gold Wigner-Seitz radius of 0.159 nm. (b) Schematic diagram depicting the sample. (c) AFM image of gold clusters deposited simultaneously on a Si wafer (with grown oxide layer).

X-ray diffraction (XRD) of all samples on a PANalytical X'Pert PRO X-ray diffractometer (Cu-Kα radiation) showed only the (002) reflection of the ZnO Wurtzite structure pointing out the primary crystallographic orientation along the substrate from the (002) plane. By the Scherrer analysis an average ZnO crystallite size of around 12 nm XRD pattern was measured in grazing incidence. Images of the nanoparticles on silicium wafer with grown oxide layer were obtained by atomic force microscopy (Dimension 3000, Veeco Instruments) and analyzed with the WSxM program [70], see Fig. 6.2(c). Silicium wafer with grown oxide layer was chosen for its superior adhesion properties compared to ITO on which the particles are swept away by the AFM tip.

The ITO electrodes were connected with wires by silver conductive adhesive (E-Solder 3021, Epoxy Produkte). A voltage and a current were applied by a power supply (Thurlby Thunder Instruments, El301). The optical absorption was

measured by a double-beam, double-monochromator spectrometer (Perkin Elmer Lambda 900 UV/VIS/NIR Spectrometer) with a working wavelength range between 175 and 3300 nm with an accuracy of 0.08 nm in the UV-visible region and 0.3 nm in the NIR region. By use of the double beam spectrometer, absorption of the control sample (sample without gold clusters) was subtracted from absorption of the sample of interest, which enabled observing the absorption of gold clusters along with the immediate ZnO surrounding medium. The experiments were performed at room temperature. Fig. 6.3 illustrates how the voltage and current measurement were performed, as well as how the absorption spectrum was obtained.

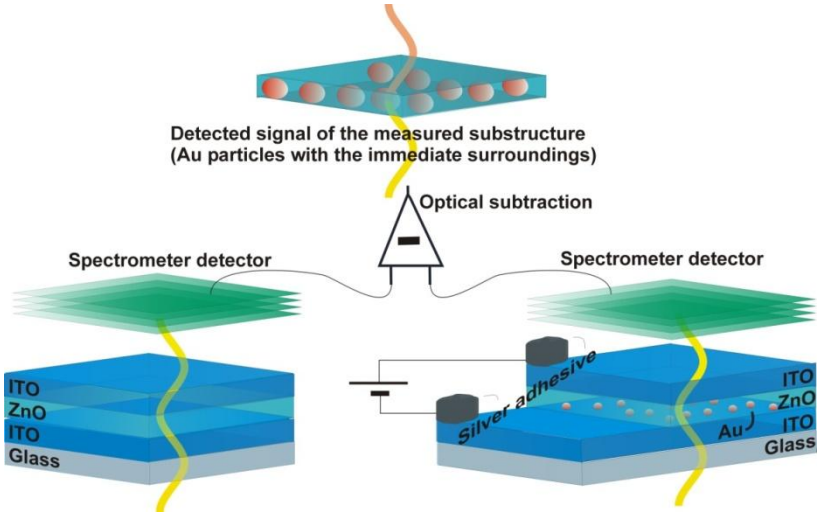

Fig. 6.3. Schematic overview of how the double-channel spectrometer measures absorption of gold nanoclusters and their immediate surroundings. The identical light beams (the yellow wave lines) pass through both samples. There are two samples – the left sample, without particles, as reference, and the right one, with gold nanoclusters. Two spectrometer detectors (the green objects) lead their signals to a subtractor (the triangle) which provides a signal from gold nanoclusters and their immediate ZnO surrounding medium.

6.4 Results and discussion

The optical absorption of the thin ZnO layer with gold nanoclusters, sandwiched between two ITO layers, was measured as a function of applied voltage. Since the gold particles are largely covered by ZnO, the ITO substrate is unlikely to have a strong effect on the properties of the gold particles. And because ITO is more conductive than ZnO, the electric field will mainly be present in the ZnO [259, 270, 271, 272]. Therefore, it is the electric field in the particles and in the immediate ZnO surroundings rather than current that causes the resonance shifts.

On the other hand, the current passing through the sample could increase the temperature of the sample for a few hundreds of degrees which may affect the plasmonic peak. However, the heat is likely dissipated to the conductive ITO [259, 270, 271, 272] and glass sample which have together a much larger volume (orders of magnitude). Calculation of the temperature increase by increasing the potential and following current could be performed with the Stefan-Boltzman law. Hereby it is assumed that the sample is in equilibrium, which means that it adopted the temperature according to the generated heat by the current. At this temperature the generated heat is dissipated to the environment according to the Stefan-Boltzman law.

In Fig. 6.5 the absorption spectrum of gold nanoparticles embedded in ZnO at 0V clearly shows two peaks. The peak at ~550 nm is identified as the plasmon peak of gold nanoclusters in ZnO. The plasmon resonance wavelength depends both on size and surrounding medium. For gold particles of about 2 nm the plasmon resonance wavelength is about 500 nm in vacuum [29], while the refractive index of the surrounding ZnO (~2 around the gold plasmon resonance [273, 274]) causes a significant redshift to 550 nm.

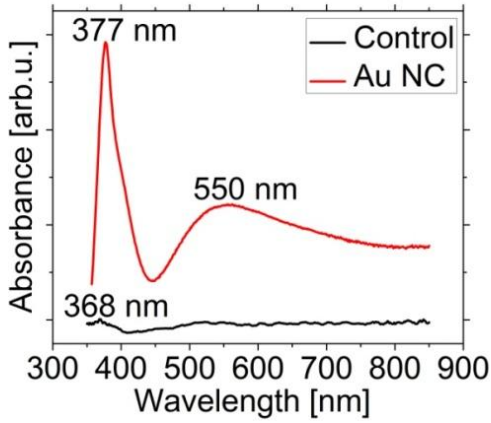

Fig. 6.5. Absorbance spectrum of a thin ZnO layer of a control sample without clusters (black) and of a thin ZnO layer with gold clusters (red) at 0 V.

The peak at 377 nm originates from excitonic absorption [275]. This ZnO peak is much stronger in the presence of gold clusters, which is attributed to a possible enhancement of the ZnO UV peak caused by plasmonic local field enhancement [254]. The intensity ratio between the UV and visible emissions of ZnO is a classical measure of the material quality because the visible emission occurs due to point defects [276]. From the low absorption in the visible, the ZnO must have reasonable quality (cf. XRD results discussed above). However, some defects, i.e. oxygen and/or zinc vacancies, are present which will affect the electron mobility and work function.

The evolution of the absorption spectrum is shown as a function of forward bias, in Fig. 6.6. A voltage of 6 V, taking into account the sample thickness, corresponds to 300 kV/cm. The position of the two main peaks (in energy) as a function of voltage is shown in Fig. 6.7. The relation between peak energy position as a function of voltage shows a linear dependence, see fitting curves, both for the gold plasmon peak and for the ZnO exciton absorption. The linear dependence points to the first order Stark effect which indeed has a linear dependence of ΔE on the electric field and therefore voltage [277].

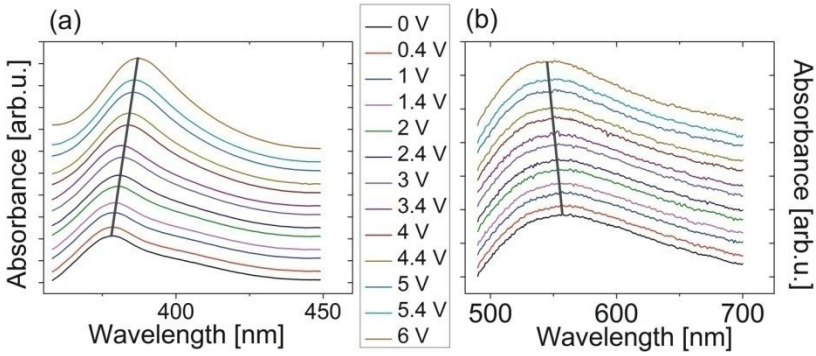

Fig. 6.6. Optical absorption spectra of the thin ZnO layer with embedded gold nanoclusters sandwiched between two ITO layers measured as a function of applied bias. The peak in (a) corresponds to excitonic absorption in ZnO and (b) is the gold nanocluster plasmon peak. A voltage of 6 V, taking into account the sample thickness, corresponds to 300 kV/cm. The dark gray curves, connecting the maxima for zero and 6 V bias, indicate the shifts under bias.

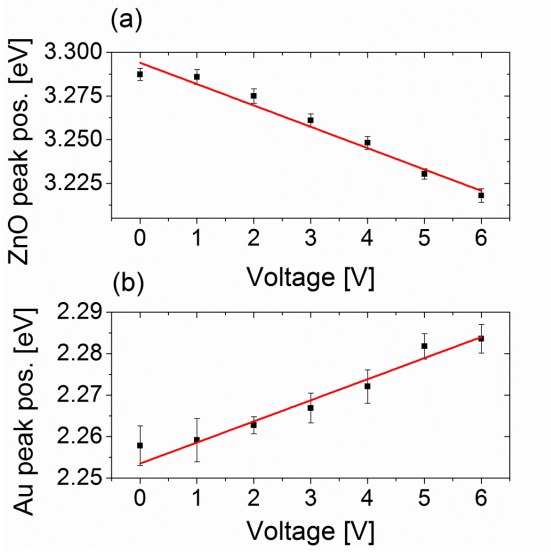

Fig. 6.7. The energy position of (a) the ZnO peak at 3.29 eV (377.2 nm) and (b) the gold peak at 2.26 eV (549.2 nm) as a function of applied voltage. The red curves in both plots are the linear fitting of the measured data.

The data are also compatible with a transition to the second order Stark effect; the optical nonlinearity of similar gold nanoparticles within ZnO surroundings has been demonstrated [269]. In this configuration the Stark effect may act on the defects which are likely introduced around the gold particles.

The position of the ZnO peak shifts to the red by 9 nm (= 69 meV), while this is not the case for the control sample without gold nanoparticles. It is unlikely that this shift is the result of the Franz-Keldysh effect [278, 279] because the electric field is too low and in static electric fields the Franz-Keldysh effect shows a blue shift of the bandgap peak [280], being proportional to a 2/3 power law of the electric field [281]. The observed magnitude of the shift is rather large when considering the ZnO film thickness and applied voltage; according to literature 300 kV/cm could only induce an increase of the ZnO bandgap by 6 meV [282]. Considering a total experimental error of 4 nm on the peak position, such an increase of the wavelength peak position was likely not observable in the control measurement. Since during an optical absorption scan a single wavelength is measured and the gold nanoparticle resonance wavelength is far from the ZnO blue peak, a plasmonically enhanced Stark effect is also unlikely. However, the defects (impurities, dislocations, vacancies), introduced in the ZnO layer [283] by the incorporation of the gold nanoparticles and with energies within the ZnO bandgap, are likely shifted in energy by the Stark effect.

Since many of the defects are close to the Fermi level, a slight shift of the defect level by the Stark effect may result in the release or capture of an electron, for p- and n-type defects respectively. Since these defect levels are of importance to the optical absorption of ZnO, the excitonic peak is shifted as a function of applied electric field. A redshift can be explained by the increase of a p-type defect level energy (2*p*-orbital electrons of oxygen ions within ZnO transferred to gold nanoclusters), which leads to the release of an electron (to the gold particle) [124, 257]. The empty defect level below the conduction band becomes then optically active, leading to the redshifted absorption [284, 285]. Hence, applying the field results in charge transfer from the ZnO to the gold nanoparticle and the

other way around with synergetic effects on both optical properties. Therefore, the redshift of the ZnO peak at 377 nm (3.29 eV) can be explained by the activation of defects with respect to optical transitions through electron release [286, 287].

The measured electric currents through the device (up to 300 mA) could lead to an increase of the device temperature with several hundred of degrees. Since the optical properties of ZnO depend on the temperature [288], a release of electrons from the p-type defects could also be caused by the higher temperature as a result of the flow.

The effect of the electric potential on the gold Fermi level was investigated by reversing the potential polarity. Because the gold particles are only located at one side of the sample, this asymmetry should result in an opposite Fermi level shift upon polarity change. This would translate into either blueshifted or redshifted gold plasmon resonance peaks, which was not observed. Therefore, instead of the effect of potential, it is the electric field which affects the optical response which is schematically illustrated in Fig. 6.8. The independence of the optical response on the polarity makes chemical reactions, induced by the electric field or potential, unlikely since such reactions are sensitive to the voltage sign.

The position of the gold plasmon peak shifts to the blue by 7 nm or 29 meV (which is 1.3% shift of its original value) at the maximum applied voltage. Because of the difference of work function between a metal and semiconductor, charge transfer occurs already without applied voltage and forms a Schottky layer [289, 290]. The work function of gold and ZnO are 5.1 eV [291] and 4.45 eV [292], respectively. This difference in work function results in electron transfer from ZnO to the gold clusters. This mechanism is schematically illustrated in Fig. 6.8. ITO has a work function of 5.53 eV [293] and thus, even if the gold nanoparticles were partially in contact with ITO, electron transfer would occur from gold to ZnO, rather than to ITO.

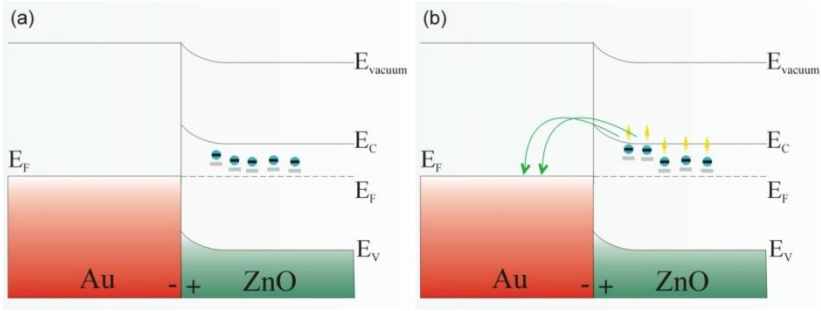

Fig. 6.8. Schematic drawing illustrating the proposed mechanism. (a) The difference in work function between the nanoclusters and the matrix leads to electron transfer from the conduction band of ZnO to the conduction band of gold. (b) Upon applying a voltage via electric field (represented by the vertical yellow arrows) the p-type defect levels shift which results in electron release into the gold particle. As a consequence, the observed optical absorption will be shifted.

Since the electron density on the metal particle determines its plasmon resonance energy [11, 108]: $\omega^2_p = Ne^2/m\varepsilon_o$, with N=electron density, e=electron charge, m=effective electron mass and ε_o= the vacuum permittivity, this charge transfer will change the gold cluster plasmon resonance wavelength. Extrapolating the measurements of Toyota et al. [232] a blueshift of 1.8 nm per electron is estimated for a 2.3 nm gold nanoparticle. Therefore, the shift of 7 nm observed here at maximum applied voltage corresponds to 3.8 electrons per particle on average. The change of the defect energy by about 69 meV is responsible for the transfer of these electrons. According to Zhdanov [294], the electron density on a small metal particle embedded in a semiconductor is much smaller as compared with the metal layer in a conventional Schottky layer because the charge is only located at the surface of the metal nanoparticle. The transfer of 3.8 electrons per particle is realistic when compared with this Zhdanov theory [294] where about 4.8 electrons would move from ZnO to the gold particle.

Note that the absorbance of the gold clusters is 3 times smaller as compared to the ZnO peak, see Fig. 6.5. Both peaks also increase in magnitude with increasing voltage and the

absorbance intensity change of the ZnO peak is about twice larger than for the plasmon peak. Because the plasmon resonance frequency shifts away from the interband transitions, it increases the oscillator strength [109, 110]. This in turn will increase the absorption cross section and the plasmonic strength, explaining the increase in absorption.

An alternative explanation could be found in the dependence of the refractive index on the electric field. Although not much literature is available, Nagata et al. [295] show that the refractive index of a doped ZnO film does not change under an applied electric field. The decrease of the plasmon absorption intensity could be caused by the shift of the plasmon resonance closer to the interband transitions. In a wet electrochemical experiment it was proposed that plasmon dampening by the presence of adsorbates on gold nanoparticles is causing the shifts [296]. In our case with gold clusters embedded in a stable ZnO matrix, it is unlikely that surface effects are responsible.

6.5 Theoretical aspects

The Fermi energy of very small clusters differs from the value of its bulk counterpart. For gold particles of about 2 nm, the Fermi energy is about 4.02 eV, as extrapolated from ref. [297]. The effective mass of an electron of gold clusters is $0.99 \cdot m_e$ [84], where m_e is the electron mass. The dielectric constant of ZnO is $\varepsilon_r = 4.415$, which is close to the reported values [273, 274].

The electron density, *n*, of the neutral state is calculated from equation (1.40). Knowing the free electron density, *n*, one can get the total number of electrons and the number of electrons transferred to a gold nanocluster by inserting the measured plasmon wavelengths from Fig. 6.7B in equation (1.38). Our densely populated gold nanoclusters induce a strong inherent capacitance coupling, as is detailed in appendix A.1. The number of free electrons, *N*, was calculated by multiplying the volume of a gold cluster with the electron density, *n*, as in

equation (1.39). All these values are shown for six different electric potential applied, see Table 6.1.

Table 6.1. The calculation results for both the number of electrons per gold cluster (N) for the appropriate electric potential (*V*) and the number of transferred electrons per gold cluster with respect to the neutral electric potential (ΔN). The last row represents the average number of transferred electrons in a gold nanocluster (ΔN_{Zh}) under electric charging according to Zhdanov [294] (an estimate of the number of atoms in 2 nm sized gold clusters is ~300 [97], which is also congruent with our calculations).

V	**0**	**1**	**2**	**3**	**4**	**5**	**6**
N	294.2	294.5	295.5	296.5	297.9	300.4	300.9
ΔN	0	0.35	1.29	2.37	3.73	6.28	**6.75**
ΔN_{Zh}	**0**	**0.13**	**0.54**	**1.21**	**2.15**	**3.36**	**4.83**

The average number of transferred electrons in a gold nanocluster, ΔN_{Zh}, is compared with its expectations according to Toyota's [232] and Zhdanov's [294] experimental results, see Fig. 6.9. One can see from Table 6.1 and in Fig. 6.9 that 6 V gives rise to the transfer of 6.75 electrons according to our calculations based on our experimental results, which is very close to the value of 3.8 electrons which we calculated from Toyota's [232] extrapolated values (yellow columns in Fig. 6.9), as well as to the value of 4.83 electrons, based on the Zhdanov theory [294] (the blue columns in Fig. 6.9). A slight overestimation could explain that the second order Stark effect contributes to the defect level shift.

Comparing the number of transferred electrons from ZnO to a gold cluster at 6 V (our calculation) with the results based upon Zhdanov theory [294], where only about 4.8 electrons would move, and a conventional Schottky model where thousands of electrons could move, it is clear that our experimental results are closer to the values (within a factor of 2) reported by Zhdanov [232]. Importantly, the number of a few hundred of transferred electrons, originating form the conventional Schottky model, is not certain and real as long as

the capacity of such a small cluster is considered and may be the result of the ill-defined depletion region within the Schottky region in small particles where the depletion region is comparable to the distances between donors [294].

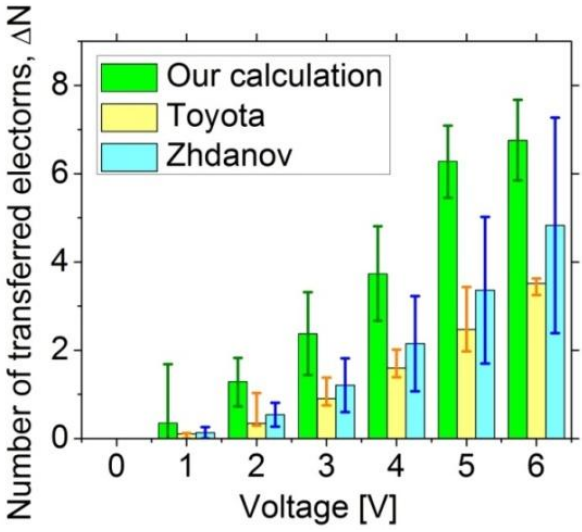

Fig. 6.9. Quantification of the number of transferred electrons when the external potential is applied based on: our experiment-supported calculation (the green columns), extrapolated values from Toyota's experimental results (the yellow columns) [232] and Zhdanov's theory (the blue columns) [294].

Not only the number of transferred electrons can be calculated by electric charging, but also the Fermi energy shift, via equation (1.41). Namely, inserting the number of free electrons for different voltages in equation (1.41) provides a relationship between the electric potential (and electric field) and the Fermi level, Fig. 6.10.

As already mentioned, it is the electric field which affects the absorption, rather then electric potential, where a voltage of 6 V corresponds to an electric field of 300 kV/cm. Our experiments thus show a possibility to tune the Fermi energy of the Au/ZnO heterostructure by applying an electric field which is reflected in the plasmonic features of the

nanodevice. This mechanism of dependence can be utilized in a wide range of optical and sensing devices. For such an optical device to be built, one has to find the relation between the Fermi energy of the material and voltage or the number of transferred free electrons.

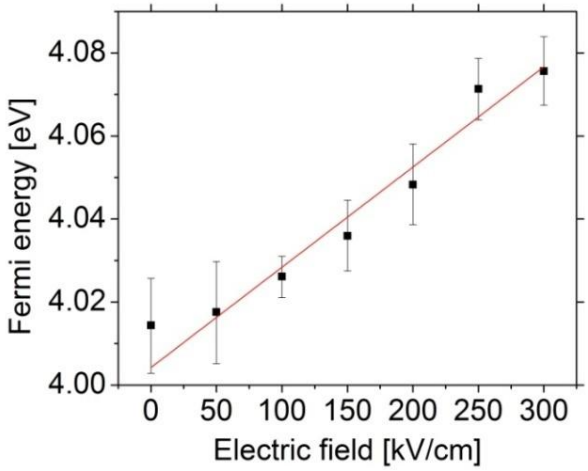

Fig. 6.10. The Fermi energy as a function of the applied electric potential, based on our experimental results and on calculation from equation (1.41). The red curve is a linear fit of the measured data.

The red fitting curve establishes the following linear dependence:

$$E_F = E_{F_0} + \eta \cdot F \tag{6.1}$$

where the initial Fermi energy, i.e. the Fermi energy at 0 V is $E_{F_0} = 4\,meV$, and η is *"the Fermi energy shift strength constant"* which accounts for the reaction of the Fermi level shift upon the electric field and depends on diverse parameters: geometry, size, material and surrounding (unit is as for electric dipole moment). For our Au/ZnO heterostructure, this constant has the value of $\eta_{Au/ZnO} = 0.000241\,em$, which is retrieved from the fitting curve origininating from our electro-optical experimental results.

Another relation being of interest expresses the dependence between applied voltage to a nano-heterostructure and the number of transferred electrons. From the red curve in Fig. 6.11, a relation between the number of transferred electrons and the Fermi energy can be inferred and quantified:

$$E_F = E_{F_0} + \xi \cdot \Delta N \tag{6.2}$$

ξ is *"the Fermi energy shift strength"* which describes how much the Fermi level of a material shifts according to the number of transferred electrons for an appropriate electric charging. This constant also varies depending on geometry, size, material and surrounding of a heterostructures. In case of our Au/ZnO device, according to our calculation, $\xi_{Au/ZnO}$= 0.0091 meV. The greater these two constants, ξ and η, in Fig. 6.10 and Fig. 6.11, respectively, the faster changes for an appropriate voltage occurs.

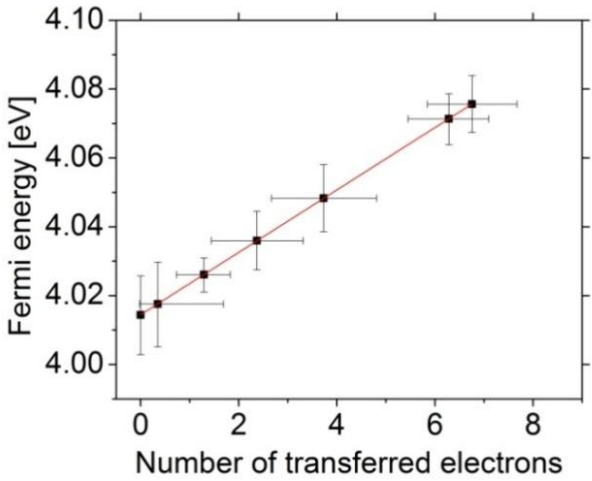

Fig. 6.11. Linear proportion between the Fermi energy, E_F and number of transferred electrons, ΔN. The black dots and red curve represent measurement and fitted curve, respectively.

Extending this research with diverse heterostructures and making the systematic parametric tables of these constants open a way to looking at the intrinsic electro-optical features of the

heterostructures. Knowing both ξ and η for different materials, one can employ appropriate heterostructure for a specific sensing or switching application.

Novoselov et al. [298] have shown the 2D nature of charge carriers in a few layers graphene upon applying an electric field, reflected by the linear proportion of the Fermi energy, E_F and electron concentration n, in contrast to the 3D well-known $E_F \sim n^{2/3}$ proportionality in equation (1.41). We have detected a linear behaviour in our Au/ZnO structure by applying electric potential (via electric field), see Fig. 6.11. This congruence of the data suggests that the region measured in our experiment is really the gold nanoclusters sourrounded by the immediate ZnO layer, thus resembling the 2D nanostructure.

6.6 Conclusions

Experimentally, we have seen that by applying an electric field over a ZnO layer with embedded gold clusters, electrons flow from ZnO to the gold particles whereby the electron density on the embedded gold clusters is increased. This transfer is likely a result of the Stark effect acting on the defect energy levels which are likely introduced within the immediate surroundings of the gold nanoparticles. However, elevated temperature could also have an influence on the defect energy levels. The change in electron density by just 3.8 electrons per particle on average shifts the gold particle plasmon resonance wavelength by about 7 nm. The positive charge in the ZnO matrix shifts its optical absorption peak at 377 nm to lower energy. The interdependent change of both exciton and plasmon wavelength of a heterostructure based on a metal-semiconductor contact provides a controlled way of electrical charging of metal nanoparticles which may be a promising method to investigate the plasmon properties of metal nanoparticles which for example exhibit quantum effects. Changing the strength of the optical interaction with the metal nanoparticle and shifting the plasmon resonance wavelength are interesting for a wide range of optical devices such as electro-optical switches for telecommunication.

Based on our experimental results, we have estimated the number of transferred electrons in the Au/ZnO nanostructure. A comparison with other studies was also made. A relation between the number of transferred electrons and the Fermi energy of the nanostructure was established, supporting the electro-optical switching prospects of this nano-heterostructure via changing the strength of the optical interaction with the metal nanoparticle and shifting the plasmon resonance wavelength.

Chapter 7

Charging silver nano-clusters in ZnO

This chapter observes the absorption spectrum of silver nanoclusters deposited by the CDA and embedded in a ZnO layer (Ag-Ag_2O/ZnO), as well as its changes upon electrical charging. This nanostructure is promising since there is an overlap of the plasmonic peak of silver and the excitonic peak of ZnO. This overlap may give rise to very interesting optical properties. However, dealing with silver clusters introduces a problem of oxidation. Yet, we have here demonstrated that the vulnerability of silver nanoparticles to oxidation may be harnessed as a semiconductor shell (Ag_2O) around silver particles, upon which a layer of ZnO is deposited, thus forming a sort of core/multishell-like structure with its prospective technological interest. We have theoretically accounted for the absorption spectrum and its changes. The combined plasmon-exciton absorption peak of this nanostructure linearly shifts upon voltage variation. This nanostructure can be of great interest in both fundamental and applied research in optics and catalysis. In addition to the promising optical switching properties of the device reported here, further research may substantiate feasibility of variation of the oxide layer around small silver nanoparticles by external electrical potential.

7.1 Experimental

Silver nanoclusters were embedded in a ZnO layer in an analogous way as for gold nanoclusters, see sec. 6.3. The samples were made with the CDA (Sect. 2.1) within an ultra high vacuum deposition chamber, using a high vacuum laser vaporization source, as presented in chapter 2, which was also described elsewhere [64]. The silver cluster size distribution was monitored with TOF mass spectrometry and is plotted in Fig. 7.1(a) as a function of cluster diameter, hereby assuming a spherical shape of the clusters and using a Wigner-Seitz radius of 0.159 nm for silver.

Silver clusters were deposited on ITO (Präzisions Glas & Optik GmbH) supports which have surface resistivity less than 20 Ω/sq). After the nanoparticles are deposited on ITO, a layer of 100 nm of ZnO, and 100 nm of ITO were subsequently deposited by RF sputtering at 200 W and 300 W, respectively, and in a 5 μbar atmosphere (Kurt Lesker). This structure is analogous to the structure shown in Fig. 6.2(b).

X-ray diffraction (XRD) of all samples on a PANalytical X'Pert PRO X-ray diffractometer (Cu-Kα radiation) showed only the (002) reflection of the ZnO Wurtzite structure pointing out the primary crystallographic orientation along the substrate from the (002) plane. The ITO electrodes were connected with wires by silver conductive adhesive (E-Solder 3021, Epoxy Produkte). A voltage and a current were applied by a power supply (Thurlby Thunder Instruments, El301). Images of the nanoparticles on a silicium wafer with grown oxide layer were obtained by atomic force microscopy (Dimension 3000, Veeco Instruments) and analyzed with the WSxM program [70], see Fig. 7.1(b). Silicium wafer with grown oxide layer was chosen for its superior adhesion properties compared to ITO on which the particles are swept away by the AFM tip. Both characterization techniques (Fig. 7.1) have shown that the average size of deposited clusters was around 1.5 nm.

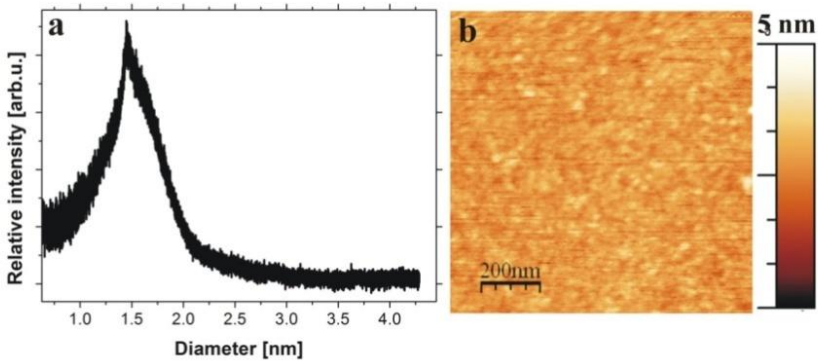

Fig. 7.1. (a) Silver cluster size distribution as measured by a TOF spectrometer. The cluster diameter is deduced assuming a spherical cluster shape and a gold Wigner-Seitz radius of 0.159 nm. (b) AFM image of silver clusters deposited simultaneously on a silicium wafer with grown oxide layer.

The optical absorption was measured by a double-beam, double-monochromator spectrometer (Perkin Elmer Lambda 900 UV/VIS/NIR Spectrometer) with a working wavelength range between 175 and 3300 nm with an accuracy of 0.08 nm in the UV-visible region and 0.3 nm in the NIR region. By use of the double beam spectrometer, absorption of the control sample (sample without silver clusters) was subtracted from absorption of the sample of interest, which enabled observing the absorption of silver clusters along with the immediate ZnO surrounding medium. The experiments were performed at room temperature. The sample configuration with respect to the application of the voltage and measuring the current and how the optical absorption spectrum was obtained is illustrated in Fig. 6.3.

Whereas gold clusters are inert to oxidation, silver (Ag), although a noble metal, is yet reactive to oxide:

$$4Ag + O_2 \rightarrow 2Ag_2O \tag{7.1}$$

Importantly, in the ambient and sub-ambient (vacuum) conditions, silver corrodes on the surfaces [299, 300, 301]. Traces of oxide layers are already present during the very cluster

deposition, which is ascertained by TOF mass spectrometry and plotted in Fig. 7.2.

7.2 Theoretical

Since the silver nanoclusters were embedded in a ZnO layer in an analogous way as for the nanostructure in chapter 6, it is thus electric field which affects the optical response (absorption). Independence of the optical response on the polarity also makes chemical reactions induced by the electric field (via electric potential) unlikely since such reactions are sensitive to the voltage sign (polarity).

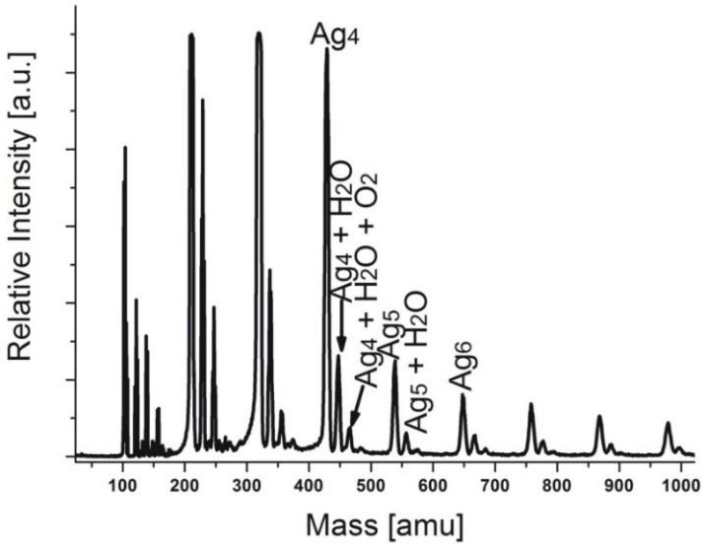

Fig. 7.2. Cluster centres composition based on the mass spectrum obtained by a TOF mass spectrometer.

Since between Ag and a ZnO layer an additional layer of Ag_2O is formed, looking from the immediate surroundings of the clusters, we can approximate this flat layer to a series of the concentric nanoshell structures represented in Fig. 7.3. This concentric nanoshell structure is in literature commonly designated as “nanomatryushka” [35, 302, 303]. After silver deposition, the oxide layer is further appended by RF sputtering

of ZnO upon silver clusters. However, the oxide layer is likely not much extended due to an already established oxide layer during the very silver clusters deposition which acts as a protective layer from the further oxidation [304].

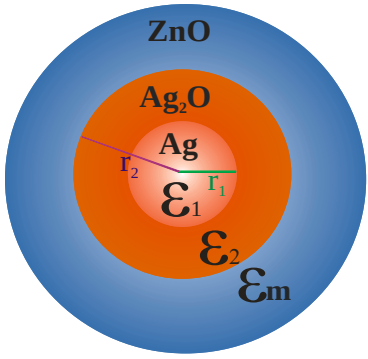

Fig. 7.3. Schematic illustration of electro-optical region of interest around a silver nanocluster (In the real nanostructure, ZnO layer is two orders of magnitude thicker than the Ag/Ag_2O nanoparticle, but here was represented as the electro-optical region of interest, i.e. Ag_2O/ZnO contact).

If the plasmon and exciton resonance peaks are overlapping, they are strongly coupled; otherwise, they are weakly coupled. Gold clusters have the plasmon resonance peak well apart from the ZnO exciton peak, making these resonances weakly coupled. However, silver and ZnO have their resonances close to each other which can be finely tuned to full overlap. Both the weak and the strong coupling have their application in science and technology: the weak coupling, i.e. the nonresonance regime, can lead to enhancement of absorption, plasmon resonance shifts, exciton-plasmon energy transfer [305, 306] and the strongly coupled resonances have peculiar and unprecedented technological applications [305, 307, 308, 309].

7.3 Results and Discussion

7.3.1 The plasmon resonance at 0V

The absorption spectrum of the Ag-Ag_2O/ZnO system is plotted in Fig. 7.4 (black dots) where a peak at 387 nm is identified. Both the plasmon peak of silver [113] and the exciton peak of ZnO [251] approximately correspond to this wavelength.

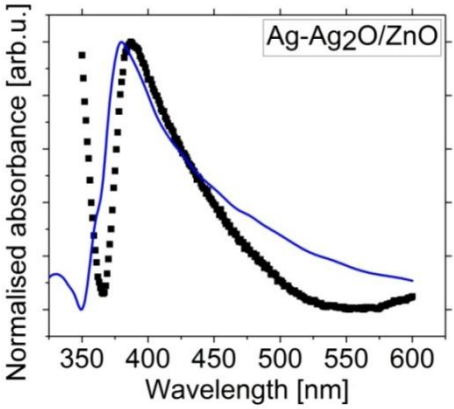

Fig. 7.4. Absorption spectrum of a thin Ag-Ag_2O/ZnO heterostructure; according to measurements (black dots) and calculation (blue line) at 0 V.

Hence, this overlap may give rise to strongly coupled resonances. Strongly coupled plasmon and exciton resonances (hybridized resonance) have already been designated as a *plexciton* (PLasmon-eXCITON). The electro-optical behaviour of the plexciton resonance is distinct from either of its component subsystems [306], where the carrier of the oscillator strength and thus the absorption changes mainly depends on the plasmon mode [307]. However, neither of these two modes has technological predominance since both have their technological significance and application [305, 310, 311, 312].

7.3.2 Calculation of the measured resonance peak at 0V

For a spherical particle with a shell embedded in another medium (Fig. 7.3) for which the radius, r meets the condition $\lambda \gg r$, the polarizability can be written as [58, 313]:

$$\alpha = 4\pi r_2^3 \frac{(\varepsilon_2 - \varepsilon_m)(\varepsilon_1 + 2\varepsilon_2) + f(\varepsilon_1 - \varepsilon_2)(\varepsilon_m + 2\varepsilon_2)}{(\varepsilon_2 + 2\varepsilon_m)(\varepsilon_1 + 2\varepsilon_2) + f(2\varepsilon_2 - 2\varepsilon_m)(\varepsilon_1 - \varepsilon_2)} \quad (7.2)$$

where $r_1$and r_2 are the radii of Ag and Ag/Ag_2O clusters, respectively, $f = (r_1/r_2)^3$ is the ratio between inner and outer radius of the Ag core and Ag_2O shell, respectively [313]. This ratio is not the same as the usual filling factor (when an inclusion is induced), since the Ag nanoparticle (with the radius, r_1) is surrounded by a Ag_2O shell (with a thickness of $r_2 - r_1$) and embedded in another medium (ZnO). Strictly speaking, the Maxwell-Garnett approximation holds for real volume (filling) factors, $f < 0.15$ [314]. The volume factor of the core/shell nano-structure in this work is $f = ({r_1}^3/({r_2}^3 - {r_1}^3)) = 0.14$ which meets the upper requirement, particularly since the core/shell nanostructures are estimated (from the AFM image in Fig. 7.1(b)) to be more than 5-6 nm apart from each other which make the ZnO layer dominated which is important to make equation (7.2) applicable. Importantly, we have not accurately measured the oxide thickness and the Maxwell-Garnett approximation may certainly give a meaningful result with a small deviation of the filling factor, as it was shown in Fig. 7.4 (the blue curve) where the calculated absorption almost perfectly matches the measured data. $\varepsilon_1 = \varepsilon_1(\lambda, r)$ and $\varepsilon_2 = \varepsilon_2(\lambda)$, in equation (7.2), are the complex dielectric functions of silver and silver oxide, respectively, and ε_m is the dielectric constant of the surrounding ZnO.

Based on the experimental results, to calculate the absorption, we have assumed that in Fig. 7.3, $r_1 = 0.75$ nm and $r_2 = 1.3$ nm. It should be noted that the thickness of the passivating oxide in the larger silver nanoparticles for high O_2

exposures and relatively high temperatures can be as large as ~ 2 nm [299, 300]. For example, Kuzma et al. [304] have shown that 7.5 nm sized silver nanoparticles are likely covered with an about ~1.2 nm thick oxide layer. For our calculation, the silver oxide thickness is taken to be $(r_2 - r_1) = 100\%\, r_1$; this oxide thickness is justifiable with respect to the core size and represents a saturated oxide thickness [313], i.e. a protective passivating oxide layer. Moreover, further broadening of the thickness would not significantly affect the plasmonic peak [313, 315]; namely, the plasmon peak steadily shifts as soon as the shell thickness reaches about half of the core radius; this shift rate decreases thereafter and "saturates" when the thickness reaches the radius of the core.

The static dielectric constant of ZnO is $\varepsilon_m(ZnO) \approx 8$ [271, 316]. The complex dielectric function of appropriate silver oxide layer is taken from ref. [317] and is corresponding to the oxygen flow of 5 SCCM (standard cubic centimeters per minute), which is the most similar to both ambient and sub-ambient oxygen conditions in our experiment, as shown in Fig. 7.5. The complex dielectric constant of the silver cluster is calculated using the modified Drude model [37]:

$$\varepsilon(\omega) = \varepsilon_\infty - \frac{\omega_1^2}{\omega^2 + \Gamma^2} + i\frac{\omega_1^2 \Gamma}{\omega(\omega^2 + \Gamma^2)} \qquad (7.3)$$

Inserting the constants from ref. [37] and ref. [58] in equation (7.3) renders the complex dielectric function of the silver core. Factor *A*, which is the constituing parameter in the damping constant, Γ, was taken to be 0.8 [29, 58, 313]. Eventually, the calculated absorption for the plasmon of the Ag-Ag_2O/ZnO heterostructure is presented in Fig. 7.4 (the blue curve), which is congruent with the experimental data.

The exciton peak of ZnO lies at 368 nm (3.37 eV), which is redshifted when in contact with gold nanoparticles (377 nm, i.e. 3.29 eV), see chapter 6, in accordance with literature [318]. Gold nanoparticles embedded in ZnO induce a shift of 0.08 eV; in case of silver nanoparticles, the ZnO exciton peak shift is likely stronger (to the red) due to an oxide layer around silver [304, 313], thus being closer to 387 nm (3.2 eV), see Fig. 7.4.

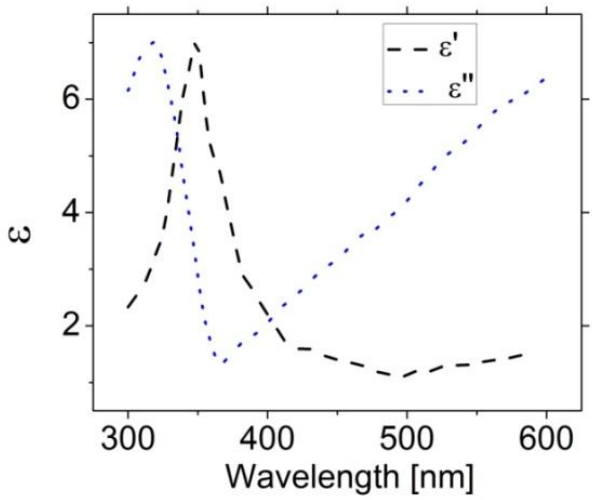

Fig. 7.5. The complex dielectric function for the appropriate silver oxide layer corresponding to 5 SCCM of oxygen flow according to ref. [317].

The expected plasmon peak of silver nanoparticle (*d*= 3 nm and 7 nm) is at ~390 nm (3.18 eV) [313]. Since our silver nanoparticles are smaller, a blueshift should be expected [11], but also a redshift as a result of the oxide layer [304, 313]. Since we do not see two distinctive peaks in the absorption spectrum, it is very likely that the excitonic and the plasmonic peaks overlap. Moreover, slight shape difference between the measurement and the calculation in Fig. 7.4 may be the result of unanticipated strong plasmon-exciton coupling in our calculation, but also of the plasmon dispersion caused by oxide thickness dispersion [304].

Contrary to common belief, it has been recently demonstrated that the oxidized metal nanoparticles can have certain advantages for plasmonic applications; the plasmon position can be markedly enhanced and finely tuned by varying the thickness of the oxide layer [313, 319], which can act as a mediator between metal nanoparticle and its environment, i.e. as an intensifier of light-matter strongly coupling interaction [319, 320].

Deeper understanding of this coupling demands further broader research. In addition, our calculation is based upon the Drude approximation which could fail to account for the plasmonic behaviour when the particle dimensions are sufficiently small (<2 nm) and therefore the quantum mechanics calculation in the plasmonic description should be inserted [52, 54], leading to the appropriate employment of *quantum plasmonics*, different from all other fields of modern plasmonics [321, 322, 323].

7.3.3 Charging the Ag-Ag_2O/ZnO heterostructure by electric fields

The evolution of the absorption spectrum of the nanostructure as a function of forward bias is shown, in Fig. 7.6(a). A voltage of 6 V, taking into account the sample thickness, corresponds to 300 kV/cm. In addition to the shift of the resonance peak, its narrowing by increasing the electric field can be also noticed. The position of the resonance peak (in energy) as a function of voltage is shown in Fig. 7.6(b). The relation between the resonance peak position as a function of voltage shows a linear dependence.

The linear dependence may be the result of the Stark effect [277], although the data are not compatible with a transition to the second order Stark effect, as it is the case for gold nanoparticles (chapter 6). Since the silver particles are largely covered by ZnO, the ITO substrate is unlikely to have an effect on the properties of the silver particles. Moreover, ITO is more conductive than ZnO and therefore the electric field will mainly be present in the ZnO [259, 270, 271, 272]. However, temperature change, caused by current passing through the sample, could increase the temperature of the sample a few hundreds of degrees (estimated) which could affect the plasmonic peak, via temperature-dependent variation of the silver oxide thickness around silver nanoparticles [324]. The generated heat is likely mainly dissipated to the glass with ITO [259, 270, 271, 272]. Since it is mainly ZnO that is in contact

with ITO, it is ZnO through which the current passes from one to the other ITO electrode, [259, 270, 271, 272].

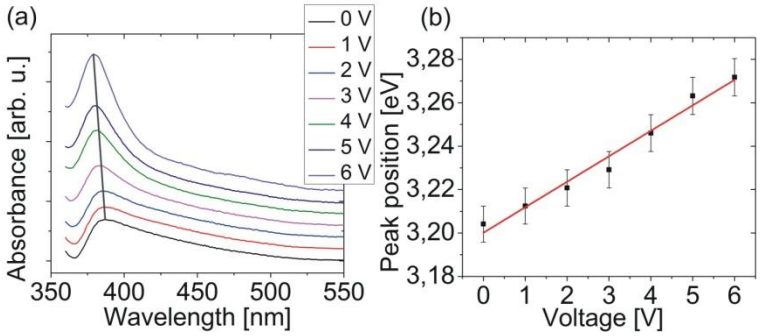

Fig. 7.6. (a) The optical absorption spectra of the thin ZnO layer with embedded silver nanoclusters sandwiched between two ITO layers, measured as a function of applied bias. A voltage of 6 V, taking into account the sample thickness, corresponds to 300 kV/cm. The dark gray curve, connecting the maxima for zero and 6 V bias, indicates the shifts under bias. (b) The energy position of the resonance peak at 3.2 eV (387 nm) as a function of applied voltage. The red curve in the plot is the linear fitting of the measured data.

The silver oxide layer between Ag and the ZnO layer likely affects the plasmon peak shift. Furthermore, since the FWHM of the silver plasmon peak is markedly dependent on the thickness of Ag_2O around the core [313, 324], it may be that the thickness of the oxide layer is varied due to voltage or temperature change; in addition, the currents, up to 300 mA, could lead to a temperature increase (several hundred of degrees) in this nanostructure, which may also change the thickness of the oxide layer. In this way, the voltage change can be used as an easy method for fine control of the oxide layer around silver which is outstandingly important in enhancing the plasmon resonance [313, 319, 320]. Fine control of the oxide layer has even greater importance in fine tuning of the exciton and the plasmon resonances, to overlap them and achieve the plexciton resonance (strongly coupled resonances).

The number of transferred electrons has been calculated in the same manner as it was done for Au/ZnO in chapter 6. The number of transferred electrons in the Ag-Ag_2O/ZnO heterostructure also changes linearly with the bias, see Fig. 7.7.

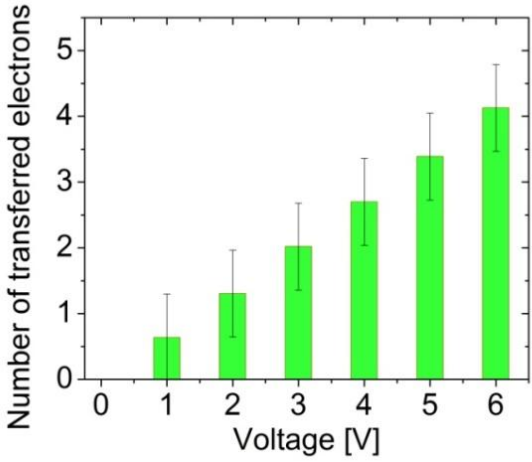

Fig. 7.7. Quantification of the number of transferred electrons as a function of forward bias, based on our experimental-supported calculation for Ag-Ag_2O/ZnO heterostructure.

Silver oxide affects the p-type defects in ZnO layer (around silver nanoparticles) which were likely introduced during deposition of the ZnO layer. However, the electron transfer to the silver core may be hindered due to the oxide layer [325], which is indicated by a more linear dependence of the plasmon shift on voltage (Fig. 7.6(b)) with respect to the analogous structure with gold nanoparticles in which the data were also compatible with a transition to a slight nonlinearity. It is thus the oxide layer that likely hinders the Stark effect to remarkably affect the plasmonic shift in this nanostructure. Since the resonance in Fig. 7.4 mainly depends upon the plasmon mode [307], it is likely that the resonance shift as a function of forward bias is the result of the plasmonic response of the silver clusters, i.e. the Ag-Ag_2O/ZnO.

Since it is not the size, but the shell thickness of the oxide layer in Ag/Ag_2O core/shell nanostructure which

markedly influences the plasmon width (FWHM) [313], variation of the oxide layer via electric potential in our heterostructure could be very interesting in a broader field of nanotechnology, especially catalysis. However, to fully grasp the mechanisms in this heterostructure, further and broader research is necessary.

7.4 Prospects and application

In the Ag-Ag_2O/ZnO heterostructure, its electro-optical switching may be influenced by the oxide layer thickness. The thickness is strongly dependent on the external bias [313] which may have technological implications in catalysis or in the field of molecule (biomolecule) detection [326]. The plasmon (plexciton) resonance can be employed to detect the thickness of oxide layer [327]. To achieve this goal, a broader research on how silver oxide depends upon core size should be taken, similar to ref. [313, 325, 328, 329]. The further and broader research would unravel some "hidden" properties interwoven within the electro-optical features reported here.

The fact that the bandgap is dependent not only on particle size [265], but also on electric field [282], allows for employment of the electric field as a means to tune the bandgap instead of changing the nanodevice size in technological fields where it is demanded; for example, for making nanogenerator self-powering devices [265]. In this chapter we emphasized advantages of the strong coupling, i.e. plexciton resonance and compared the electro-optical properties of gold (reported in chapter 6) and silver (this chapter) embedded in a ZnO layer and have derived some conclusions. However, further research in this direction would give more insights which, for example, would help in finding a controllable way of adding the oxide layer to silver nanoparticles. Additional electrochemical experiments would certainly help in this respect [313, 325].

As a suggestion, making alloys and embedding them in the analogous heterostructures can help understand the optical behaviour of these nanodevices. We have thus also deposited an alloy structure ($AuAg_2$) by the CDA and embedded it in an

analogous ZnO layer. The absorption spectrum of $AuAg_2$ nanostructure and its immediate ZnO surrounding is shown in Fig. 7.8. One can see that the $AuAg_2$/ZnO nanostructure has a plasmon peak at ~428 nm which lies in between the plasmon resonance of gold (~550 nm) [11, 304] and silver (~387 nm) [304, 330]; this is expected since the alloy consists of these two noble metals. The exciton resonance of the ZnO layer peaks at 386 nm (between the ZnO exciton resonances at 377 nm and 387 nm when respectively gold and silver were embedded in ZnO); having more silver than gold in the alloy, the peak is closer to the peak at 387 nm. In addition, different concentration of gold and silver within an alloy may also help in fine tuning of the plasmon with respect to the ZnO exciton. Variation of the electric potential to this and similar alloys and the noble metal nanostructures could help in understanding the electro-optical changes upon voltage variation.

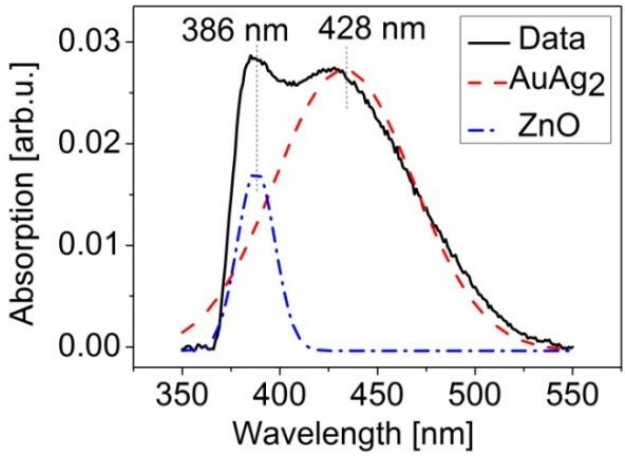

Fig. 7.8. Absorption spectrum of the $AuAg_2$ alloy embedded in the ZnO surrounding at 0 V, the black curve (measurement), which is decomposed to two fitting peaks: ZnO (the blue curve) and $AuAg_2$ (the red curve).

7.5 Conclusions

We have fabricated an Ag-Ag_2O/ZnO nanostructure, whose resonance characteristics, although linear with the bias variation, differs from the Au/ZnO nanostructure described in chapter 6. This distinction is the result of vulnerability of silver clusters to oxidation, as well as of an overlap of the silver plasmon and the ZnO exciton resonances. Based on our experimental results, we have calculated the number of transferred electrons from ZnO to silver clusters, which is lower as compared to the number of transferred electrons in the Au/ZnO nanostructure, described in chapter 6. It is likely that the oxide layer around the silver clusters impedes the possible Stark effect, in contrast to the Au/ZnO nanostructure. Temperature effects induced by the current can also not be excluded. To fully unravel the origin of the distinction between these two structures, further research is needed where the employment of different gold/silver alloys would certainly be a proper direction to investigate. Changing the strength of the electro-optical interaction within these heterostructures and shifting the hybride plasmon-exciton resonance wavelengths are very interesting for a wide range of technological applications, but also for fundamental understanding of the here studied electro-optical phenomena.

Chapter 8

General conclusions and perspectives

This research lies in the field of both experimental and applied physics. The aim was the study and use of electro-optical properties of nanomaterials, particularly electro-optical switching properties of noble metal nanoparticles, in building capacitor-like nanodevices. Interestingly, this work is performed after more than 100 years from the time when Einstein was awarded the Noble Prize for his contribution to understand the photoelectric effect. Electrical and optical properties of diverse materials have been developing and advancing, and understanding has since progressed at large. Investigations based on plasmon resonance become increasingly attractive and have nowadays proved to be one of the highlights of nanotechnology, particularly in applied physics since plasmons represent a kind of the light fingerprints of nanostructures. This fingerprint strongly depends on various parameters which could be used as a means to detect small changes in a nanostructure or nanoenvironment. In addition to chemical deposition of nanoparticles, the Leuven cluster beam deposition apparatus was also employed in this work to produce very small uncoated nanoclusters (nanoparticles) in a fine island-like pattern, allowing for constructing a bottom-up nanodevice with specific electro-optical features.

Conclusions

This thesis describes the optical and electrical properties of noble metal nanoparticles with various sizes and attempts to explain how electrical charging variation on nanodevices alters their optical properties (achieved by diverse techniques). Nanoparticles of different sizes, mainly gold but also silver, with and without surrounding ligands were considered. Whereas the ligand-capped gold nanoparticles were deposited by chemical means, based on the siloxination of amine-termination, uncapped gold and silver clusters were deposited by cluster beam deposition with sizes ranging around 1.5-2.3 nm. This size of nanoparticles is very important because it represents a frontier between the continuous and the discrete quantum world. To find the size frontier where the continuous levels abruptly become discrete levels was not straightforward because nanoparticles were not deposited by the same technique and it is also dependent on the environment of the nanoparticles. To study the electronic and optical properties of small gold particles, they were deposited with a size of about 1.5 nm and subsequently studied by optical absorption spectrometry. A clear plasmon resonance peak was observed, which appeared to consist of two adjoining peaks. Although to understand the origin of the observed double peak in the optical spectrum for these clusters requires a more detailed study, several explanations about the origin of these peaks are provided and substantiated by some recent studies in the field. Plasmonic coupling of the neighbouring particles, prospectively oblate particle shape or interband transition near the L point of the first Brillouin zone, or an overlap of the plasmon resonance of the particles with the interband transition threshold may explain the observed double peak.

A study about the effect of a changing pH around the gold particles resulted in distinctive changes in the absorption spectrum. These particles differed in size and the immediate surroundings. While the clusters were uncapped, chemical

deposition of the gold nanoparticles was based upon the protective ligand layer around the particles. The pH variation gave rise to an electronic change of the nanoparticles resulting in changes of the optical spectrum. Along with some recent studies, based on the changes in the optical spectrum of both systems, we have provided possible mechanisms which result in distinctive changes of the optical spectrum of both ligand-protected and unprotected gold nanoparticles upon pH variation. The pH-induced optical behaviour of capped and ligand-free gold nanoparticles were compared. While gold colloidal solution (5 nm sized gold nanoparticles) shows pH-dependent plasmonic shifts as a result of the electron density change in the core via the dipole moment, gold clusters (2 nm sized gold nanoparticles) do not show detectable wavelength shifts upon pH variation. This is likely since they are smaller, thus having a much weaker plasmon resonance. Although the fabrication of a pH-nanosensing device with 2 nm sized uncoated nanoclusters could be questionable owing to their "unprotectedness", at the same time, this unprotectedness likely enables repeatability, as well as a more direct and sensitive sensing, since there is no solid medium between the clusters and their environment.

In both protected and unprotected gold nanoparticles, pH-induced flocculation occurs. The pH-induced shifts of the plasmon resonance position and band width could be used to make a plasmonic biosensor (transducer), enabling for example in situ detection of cellular and conformational changes. For this to come true, further research in this direction would help to better understand our findings. For example, a well-controlled subnanometer distance between small nanoparticles would likely help this end, owing to plasmonic coupling which gives rise to enhanced optical fields [117, 118, 119].

Because our main aim was to supply a system with electrons in an all-solid-state device, via direct electron supply, we used an electrical potential variation on a capacitor-like nanostructure with embedded gold nanoparticles. Depositing gold nanoparticles of different sizes (2, 5 and 10 nm in diameter) on an ITO substrate, by immersing it in an electrolyte, a capacitor-like nanostructure was built. The optical absorption

and photoluminescence of gold nanoparticles was measured as a function of applied potential in an electrochemical setup. By applying electric potential to the nanosystem consisting of gold nanoparticles embedded in a capacitor-like structure, we have observed changes of both absorption and photoluminescence upon voltage alteration. An important observation is that in the smallest gold nanoparticles, photoluminescence was reduced at negative and increased at positive potentials. Since up to date only the optical absorption was controlled by applying a potential difference, here we have made a next step by extending this to photoluminescence which may be of an important guide to future research. The dependence of photoluminescence of gold nanoparticles on their charge state is potentially interesting for applications in the field of optical telecommunication and sensor technology. However, although the system was straightforward due to its simplicity, both electrolyte and ligands around nanoparticles make this system more complex to understand. Further research in this field would provide a more profound understanding of the here studied photoluminescence change.

We have then employed the cluster beam deposition to produce very small uncoated nanoclusters (nanoparticles) in a fine island-like pattern (gold, silver and gold/silver alloy). They were embedded in a ZnO layer and sandwiched between ITO layers (electrodes). These nanostructures represent a capacitor-like system whose electric properties and changes upon applying the voltage were observed by optical spectroscopy. The plasmon peak of gold clusters is relatively distant in the spectrum with respect to the exciton peak of ZnO layer, while in case of silver clusters the plasmon peak overlaps with the exciton ZnO peak. This explains the different optical behaviour upon voltage variation which was observed. By applying an electric field over a ZnO layer with embedded gold clusters, electrons flow from ZnO to the gold particles whereby the electron density on the embedded gold clusters is increased, likely as a result of the Stark effect acting on the defect energy levels. However, elevated temperature (due to presence of the current) could also have an influence on the defect energy levels. In both Au/ZnO

and Ag/ZnO nanostructures the plasmon peak dependence on electrical potential is linear. The temperature-dependent properties of the silver-oxide layer may play a great role in electron transfer between silver and ZnO. We have shown that applying a field via potential change results in charge transfer from the ZnO to the noble metal nanoparticles and the other way around with synergetic effects on optical properties. Our calculation of the number of transferred electrons on island-like-distributed gold and silver nanoparticles supported Zhdanov's theory [294] which reports on a commonly overestimated number of the transferred electrons by many researchers. In our case there are only a few rather than many electrons that were transferred from the surrounding medium to the nanoparticle. A comparison with other studies was also made. A relation between the number of transferred electrons and the Fermi energy of the nanostructure was established, supporting the electro-optical switching prospects of this nano-heterostructure via changing the strength of the optical interaction with the metal nanoparticle and shifting the plasmon resonance wavelength. The interdependent change of both exciton and plasmon wavelength of a heterostructure based on a metal-semiconductor contact provides a controlled way of electrical charging of metal nanoparticles which may be a promising method to investigate the plasmon properties of metal nanoparticles. Changing the strength of the optical interaction with the metal nanoparticle and shifting the plasmon resonance wavelength are interesting for a wide range of optical devices such as electro-optical switches for telecommunication.

We have suggested and theoretically supported our findings concerning the capacitor-like nanostructures and proposed the further direction of the experiments toward full elucidation of the peculiar optical changes upon voltage variation. Further research is especially desirable in the light of unravelling of the origin of the silver-based nanostructure. All the observed nanodevices, which also acted as capacitor-like structures, could have a very significant importance in new technology for opto-electronic and sensitive devices. For example, our nano-capacitor devices may be of importance to

fine control the frequency in plasmonic nano-antennas [331, 332]. Importantly, to achieve this goal in its full meaning of the real application, further study is required to gain better sensitivity of the nanodevice which may be achieved by studying different materials and their sizes in various environments. To this end, our absorption spectroscopy could be complemented by spectroscopic ellipsomentry to determine the optical constants (dielectric constant) of the nanolayered structures, but also to determine the film thicknesses. In addition, if implemented during the deposition process, spectroscopic ellipsometry could accurately measure the oxide thickness during the process of silver and ZnO deposition, for example [333]. Smaller nanoclusters have a greater potential in detecting as low as the single-electron transfer processes, having in the same time a decreased plasmon peak detectability. Therefore, in addition to both the fundamental and application findings, our research has also urged for the broader fundamental research of the here studied nano-heterostructures for the full use in the new technology resulted from the directed application study.

Outlook

The everyday life is full of opto-electrical devices which are further increasingly employed. However, with further increasing their use, emerging questions about the better sensitivity and performance arise. Nanotechnology is increasingly governed by sensitive nano-changes; for example, the size of the used nanoparticles, and small groups of electrons whose number varies and markedly depends upon small changes of the environment or physical pressure which is reflected in the electric properties of the material, changing consequently the number of electrons. All these interwoven physical features could be observables for which we have to build very sensitive sensors and detection tools. The thesis deals with such miniscule nanodevices whose prospect lies in great sensitivity of the local nanoenvironment. The thesis also shows that the challenge of a

sensitive nanodevice may be achieved by building a nanolayered heterostructure with embedded noble metal nanoparticles, thus harnessing unbeatable intrinsically storing/memory effect of these particles. The results presented in the thesis facilitate a better grasp of the electrical and optical phenomena of such nanostructures with the prospective place located in the core of the rapidly developing nanotechnology, ranging from biological to technological use. In the near future fast-advancing progress in this field will change everyday life. This thesis gave a detectable imprint and prospective pathways for future employment of cluster based nanostructures and nanodevices. However, there are still many puzzles to be unravelled such as the properties of noble metal nanoalloys. The use of various noble metal nanoclusters, as well as diverse surrounding media, within a capacitor heterostructure could lead to an even better understanding of the electro-optical nanoprocesses which take place at the interface between noble metal and the surrounding medium. While there is significant research in the field of how light causes electrical transitions in diverse nanostructures, in this study, the construction of a nanodevice which changes the light response by the electronic structure could be utilized as a proper and highly-controllable sensing tool. This could have applications, not only in the field of photovoltaics, transistors and catalysis, but also in the field of medicine and biology.

Nederlandse samenvatting

Dit onderzoek betreft experimentele en toegepaste natuurkunde. Het bestudeert en werd ingericht tot gebruik van electro-optische eigenschappen van nanodeeltjes, in het bijzonder de electro-optische schakeling van eigenschappen van edelmetaalnanodeeltjes ingebracht binnen gelaagde condensator nanodevices. De nanodeeltjes werden geproduceerd op verschillende manieren: met het gebruik van chemische methoden, maar ook met clusterbundeldepositie. Deze laatste methode was heel doelmatig om eiland achtige nanodeeltjes te deponeren zodat het eindproduct een bottom-up nanodevice werd met gewenste specifieke en fijne electro-optische eigenschappen. Het onderzoek berust op de plasmon resonantie, welke heel aantrekkelijk is want plasmons zijn een soort van lichtgebaseede vingerafdruk van de nanodeeltjes die sterk afhangt van verschillende parameters zoals de grootte en vorm welke als detectiemiddel gebruikt zouden kunnen worden voor fijne nanoveranderingen in een nanoruimte.

In deze thesis wordt het duidelijk hoe belangrijk de afmeting van de nanodeeltjes en hun omgeving zijn. Daarnaast leidt het electrische laden van deze nanodevices tot bepaalde georganizeerde veranderingen in het optische spectrum van de nanostructuren. Dit is het hoogtepunt van dit doctoraat: deze veranderingen te bepalen, te onderzoeken en proberen te begrijpen. De eerste hoofdstukken geven een theoretische en experimentele basis van waaruit dit bestuderen ontspringt. Een hoofdstuk wordt gewijd aan het begrip van nanostructuren die gedeponeerd zijn op verschillende manieren. Tevens wordt aangetoond hoe belangerijk het is om te begrijpen wat de juiste

afmetingsgrens is voor heel kleine nanodeeltjes die kwantum eigenschappen vertonen. Goud nanodeeltjes met afmetingen van ~ 1.5 nm hebben de juist afmeting voor dit gedrag. Niettemin is verder onderzoek om kleine electro-optische veranderingen volledig te begrijpen noodzakelijk.

In deze doctoraatsthesis wordt verder bestudeerd hoe de pH waarde van de omgeving met het gebruik van goud nanodeeltjes gedetecteerd kan worden. Dit onderzoek werd uitgeoefend met het gebruik van zowel beschermde alsook niet beschermde goud nanodeeltjes. Een ligand beschermt en maakt het nanodeeltje inert voor veranderingen, maar hoe meer het beschermdwordt hoe minder de eigenschappen van goud nanodeeltjes zich manifesteren. Dit is een soort trade-off waarmee men rekening dient te houden.

Een bijzonder veelbelovende ontdekking was dat fotoluminescentie van kleine goud nanodeeltjes van de toegevoegde elektrische lading afhangt. In dit werk werden voor de eerste keer verschillende grootten van nanodeeltjes bestudeerd. Voortbouwend op eerder uitgevoerd onderzoek in het domein van fotoabsorptie en lading van metalen nanodeeltjes, wordt hier verder onderzocht hoe de fotoluminescentie van goud nanodeeltjes verandert met aangelegde toegevoegde elektrische spanning. Dit is belangrijk want goud wordt al gebruiktals fluorescent materiaal in lichaamsweefsel.

De laatste hoofdstukken betreffen edelmetaal-nanodeeltjes die ingebed werden in een gelaagde nanostructuur (condensator) en hun elektrische en optische eigenschappen die sterkverbonden zijn. Over deze gefabriceerde nano-condensatoren hebben we elektrische spanning aangelegd. Deze elektrische verandering veroorzaakte plasmonische (in Au en Ag nanodeeltjes) en excitonische (ZnO laag) veranderingen in het nanodevice, wat we hebben verklaard gebruik makend van eerdere onderzoeksresultaten. Een schatting van het aantal getransporteerde elektronen is ook gemaakt. Daaruit bleek dat in overeenstemming met de resultaten van andere onderzoekers,

slechts enkele elektronen overgingen van ZnO naar de goud en zilver nanodeeltjes. De optische veranderingen van de nanostructuren gemaakt van goud nanodeeltjes worden veroorzaakt door het Stark effect. De nanostructuren met zilver, waar een oxidelaag gevormd wordt, kan ook door een temperatuureffect zijn veroorzaakt. Hiermee is meteen een toekomstige onderzoekspiste aangegeven. Hopelijk kunnen de hier onderzochte systemen gebaseerd op nanodeeltjes in interactie met licht bijdragen tot applicaties voor licht manipulatie of sensor technologie, misschien zelfs wel in disciplines zoals biologie en geneeskunde.

Appendix

A.1 Calculation of the mutual capacitance of gold nanoclusters

Comparison of Ung's formula and our calculations for the capacitances and surface capacitances

Ung et al. [156] have determined a correlation between the plasmon resonance shift and the surface capacitance of a particle as:

$$K = \frac{(1 - (\lambda_f / \lambda_i)^2 rF}{3V_m \Delta P} \qquad \text{(A1.1)}$$

This calculation is mainly devoted to chapter 6 of the thesis. In that experiment, the measured plasmon wavelength resonance at 6 V and 0 V was λ_f = 549.2 nm (final) and λ_i = 543 nm (initial), respectively, where r=1.15 nm is the radius of the spherical gold nanocluster. F=96487 C/mol is Faraday constant, V_m=10.26 cm^3/mol is the molar volume of gold. The surface capacitance for our nanosystem equals, K=1.35 μF/cm^2.

If there is a spherical metal particle in a dielectric environment, the capacitance of the metal nanoparticle can be calculated as:

$$C = 4\pi\varepsilon_0\varepsilon_m r \qquad \text{(A1.2)}$$

where ε_0 is the vacuum permittivity, ε_m is the dielectric constant of the surrounding medium, and r is the radius of the spherical metal nanoparticle. The surface capacitance can thereof be obtained as:

$$K = C/(4\pi r^2)\,. \qquad \text{(A1.3)}$$

Using equation (A1.2) and (A1.3), the surface capacitance of our gold nanoclusters in chapter 6 significantly differs when compared with the result obtained by formula (A1.1).

According to the AFM image of the deposited gold clusters (Fig. 6.2(c)), the cluster density is estimated to be a half of the surface, i.e. 50%. Such densely populated gold nanoparticles lead to a significant contribution of the mutual capacitance among the clusters to the overall capacitance, i.e. the nanostructure capacitance. The coverage of 50% means that the interparticle distance is ~4r, where r represents the particle radius. The particles are assumed to have the same electric charge and to be of the same diameter (~2.3 nm) and at the equidistant rows and columns which form a matrix, see Fig. A1-1.

Method developed by E. Pisler et al. [334] was used to calculate the capacitance enriched by the mutual capacitance contribution to the self-capacitance of a cluster. In addition, we have extended the calculation from two to four metal (gold) spheres, although we should have included as many spheres as they were present in the entire nanostructure.

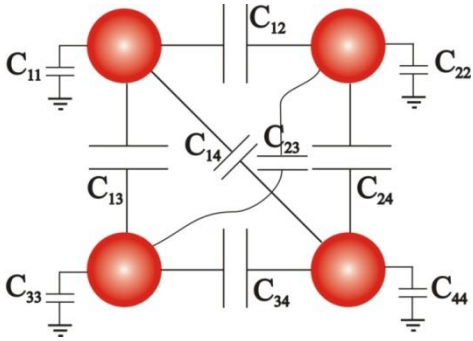

Fig. A1-1. Mutual capacitance of a set of clusters which is for the sake of simplicity reduced to four gold clusters (the red spheres).

However, due to simplicity, we have chosen only a 4x4 matrix, as illustrated in Fig. A1-1. The capacitance of four metal (gold) particles can be described by the Maxwell capacitance matrix [335]:

$$\begin{bmatrix} C_{11}+C_{12}+C_{13}+C_{14} & -C_{12} & -C_{13} & -C_{14} \\ -C_{21} & C_{21}+C_{22}+C_{23}+C_{24} & -C_{23} & -C_{24} \\ -C_{31} & -C_{32} & C_{31}+C_{32}+C_{33}+C_{34} & -C_{34} \\ -C_{41} & -C_{42} & -C_{43} & C_{41}+C_{42}+C_{43}+C_{44} \end{bmatrix} =$$

$$= \begin{bmatrix} 0.25 & 0.33 & 0.33 & 0.22 \\ 0.33 & 0.25 & 0.22 & 0.33 \\ 0.33 & 0.22 & 0.25 & 0.33 \\ 0.22 & 0.33 & 0.33 & 0.25 \end{bmatrix} \{aF\}$$

(A1.4)

The capacitances in matrix (A1.4), expressed in aF, were calculated employing equation (A1.2). Only the main diagonal in this matrix is important because it comprises both self- and mutual capacitance of a gold cluster. Inserting the values of capacitance within the main diagonal into equation (A1.3), the surface capacitance of a gold particle equals K=1.53 μF/cm^2. This value deviate only 10% from the value obtained by use of equation (A1.1). If the matrix were greater in rows and columns, the two values would even better overlap.

Herewith, we have shown that the calculated capacitances of gold particles are the same whether they are calculated via Ung's formula, by knowing the plasmon resonance position or by employing numerical calculation method [334] via matrices inserting the particle radius, which enables using the change of the plasmon resonance of small metal nanoparticles in detecting the capacitance change. In addition, our relatively dense cluster coverage induces a strong mutual capacitance, i.e. there is a strong capacitance coupling.

A.2 Spill-out effect and its application in experiments in chapters 6 and 7

We have performed a calculation based on the measured plasmon peak position at 0V. This calculation emphasizes not only the interband contribution to the plasmon peak position, but also the surface effect, i.e. the spill-out effect [57]. The alkali metals show the redshift of the plasmon as the size is decreasing [11, 336], as a result of the spill-out effect. The noble metals mainly exhibit blueshift of the plasmon resonance as the particle size decreases [11, 52, 113], due to an enhanced role of the deeper energy levels to the free electrons, i.e. interband transition - although there are to a less extent conflicting results, mainly caused by the underestimation of the spill-out effect [337].

For particles lower than 10 nm, Mie theory does not hold. In addition to validity of the Drude model in such nanoparticles, we now employ a model developed by R. C. Monreal et al. [57], which involves the surface effect, in addition to the interband contribution, i.e. both the spill-out and the quantum size effect. In such small particles, electrons can spill out of the metal surface due to finite potential barriers which for very small nanoparticles can give rise to the redshift or additionally to the blueshift [57]. Namely, there is a competition between contributions of the spin-out and quantum size effect which is significantly pronounced for very small particles. This fact may reduce the matching of the experimental and theoretical results in very small particles; for example, in our 1.5 nm sized silver nanoclusters in chapter 7. Therefore, expected experimental plasmon blueshift of individual small

silver particles could not match the theoretical expectations [52]. There is also a lack of theoretical articles dealing with the spill-out effect so far. This lack is even stronger for the experiments supported by theoretical descriptions [57].

The quantum size and the surface mutual effects in small metal nanoparticles

The polarizability of a metal sphere of radius *R*, with a bulk dielectric function *ε(ω)* can be written as [338, 339, 340]:

$$\alpha = R^3 \frac{(\varepsilon(\omega) - \varepsilon_m)\left(1 - \frac{d_r(\omega)}{R}\right)}{\varepsilon(\omega) + 2\varepsilon_m + 2(\varepsilon(\omega) - \varepsilon_m)\frac{d_r(\omega)}{R}}, \qquad \text{(A2.1)}$$

where $d_r(\omega)$ is related to the electron density, $\rho(r,\omega)$ as:

$$\frac{d_r(\omega)}{R} = \frac{\int r(R-r)\rho(r,\omega)dr}{\int r^2\rho(r,\omega)dr} \qquad \text{(A2.2)}$$

where *r* is the radial coordinate [57].

Surface plasmon resonance frequency, involving both the spill-out and the quantum size effect, can be represented as [57]:

$$\omega_{s=}^2 = \omega_p^2 \left(\frac{\left(\frac{R_0}{R}\right)^2}{1 + 2Re\left\{\frac{d_r(\omega_s)}{R}\right\}} + \frac{}{\varepsilon_d(\omega_s) + 2\varepsilon_m + 2(\varepsilon_d(\omega_s) - \varepsilon_m)Re\left\{\frac{d_r(\omega_s)}{R}\right\}} \right). \qquad \text{(A2.3)}$$

If $Re\{d_r(\omega)\} < 0$, electrons have the main weight outside the surface, i.e. spill out, and if $Re\{d_r(\omega)\} > 0$, electrons spill in. These inequalities determine the red- or blue-shift, respectively, asociated with the spill-out effect [57].

The classical theory is accounted for by bulk dielectric properties, giving rather good estimates for the particles larger than 10 nm. Monreal's model [57] appends the surface effect via

a frequency-dependent complex length scale $d_r(\omega)$ [338]. Since the *d*-band electrons are very localized, they are not very much present at the surface and $d_r(\omega) \approx d_\perp(\omega)$ [57]. A calculation for $d_\perp(\omega)$ for a planar jellium surface of the effective free electron density parameter of gold and silver, r_s=3.01 and r_s=3.02, respectively, was given by Feibelman [341], Fig. A2-1.

$$R_0 = 1.1 a_0 \sqrt{r_s}\,, \tag{A2.4}$$

where a_0 is the Bohr radius of a cluster.

$\varepsilon_d(\omega)$, in equation (A2.3), is obtained from the reported experimental data [84, 342]. Dielectric constant of the surrounding ZnO was taken to be 4.415, being very close to the reported values [273, 274]. Monreal et al. [57] have not used the expected bulk plasma frequencies for gold and silver, 9.1 and 9.2 eV [37], respectively, but 5.99 and 3.81 eV, respectively [57], due to screening of the d-electron of bulk gold and silver.

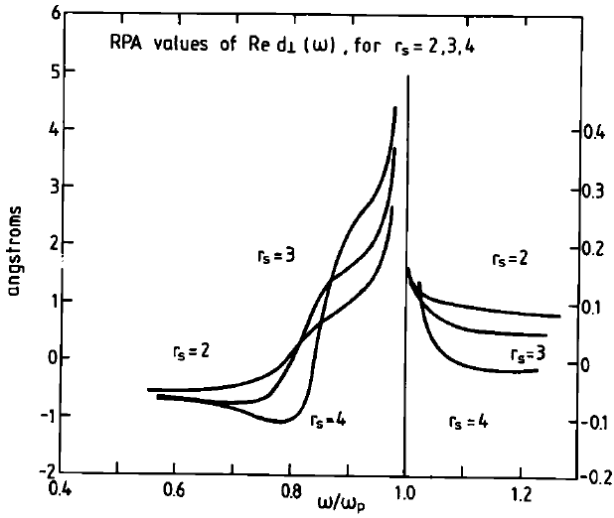

Fig. A2-1. $Re\{d_\perp(\omega)\}$ as a function of ω within the random phase approximation for r_s=2, 3 and 4 [341].

Gold

In our experiment in chapter 6, 2.3 nm sized gold nanoclusters embedded in ZnO layer gives a plasmon wavelength of 548.62 nm (ω_s=2.26 eV). When we insert the bulk plasma frequency for gold of 4.2 eV in equation (A2.3), it renders just the measured value of the surface plasma frequency.

Silver

Polarizability of the core-shell/shell silver nanostructure from Fig. A2-2 can be calculated as [37]:

$$\alpha = 4\pi r_2^3 \cdot \frac{(\varepsilon_2 - \varepsilon_m)(\varepsilon_1 + 2\varepsilon_2) + f(\varepsilon_1 - \varepsilon_2)(\varepsilon_m + 2\varepsilon_2)}{(\varepsilon_2 + 2\varepsilon_m)(\varepsilon_1 + 2\varepsilon_2) + f(2\varepsilon_2 - 2\varepsilon_m)(\varepsilon_1 - \varepsilon_2)} \quad \text{(A2.5)}$$

where ε_1, ε_2 and ε_m represents respectively the complex dielectric function of the core, the complex dielectric function of the subsequent shell and the dielectric constant of the outer shell (in our case ZnO).

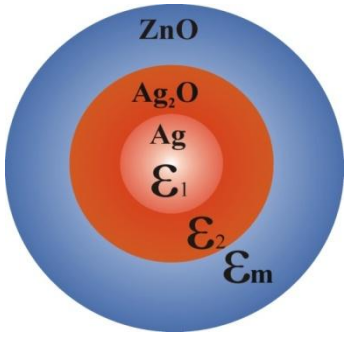

Fig. A2-2. A silver particle in chapter 7, having two layers around itself (Ag_2O and ZnO), builds a matryushka-like structure, i.e. the outermost ZnO flat layer was approximated by a shell structure for easier representation (in real nanostructure, ZnO layer is two orders of magnitude thicker than the Ag/Ag_2O nanoparticle, but here was represented as the electro-optical region of interest, i.e. Ag_2O/ZnO contact).

By applying analogous calculation with equation (A2.3) to obtain the surface plasma frequency for the silver/double shell (nanomatryushka) structure, the denominator of equation (A2.5) must equal zero which gives the following formula (based on the reasoning like for gold [57]):

$$\omega_s = \omega_p \sqrt{\frac{A+B}{C+D}} \tag{A2.6}$$

where:

$$A = \Bigg((2\varepsilon_2(\varepsilon_m - \varepsilon_2)(\varepsilon_{1d} - 1)f + 2\varepsilon_2(2\varepsilon_m + \varepsilon_2)) \cdot \left(\frac{R_0}{r_1}\right)^2 + 2\varepsilon_2(\varepsilon_m - \varepsilon_2)f + 2\varepsilon_2(2\varepsilon_m + \varepsilon_2) \Bigg) \cdot Re\left\{\frac{d_r}{r_1}\right\}$$

$$B = (2(\varepsilon_2 - \varepsilon_m)(\varepsilon_{1d} - \varepsilon_2)f + (\varepsilon_2 + 2\varepsilon_m)(2\varepsilon_2 + \varepsilon_{1d})) \cdot \left(\frac{R_0}{r_1}\right)^2 + 2(\varepsilon_2 - \varepsilon_m)f + 2\varepsilon_m + \varepsilon_2$$

$$C = (2\varepsilon_2(\varepsilon_m - \varepsilon_2)(\varepsilon_{1d} - 1)f + 2\varepsilon_2(\varepsilon_m + \varepsilon_2)(\varepsilon_{1d} - 1)) \cdot Re\left\{\frac{d_r}{r_1}\right\}$$

$$D = 2(\varepsilon_2 - \varepsilon_m)(\varepsilon_{1d} - \varepsilon_2)f + (2\varepsilon_m + \varepsilon_2)(2\varepsilon_2 + \varepsilon_{1d})$$

where all the terms are dependent upon ω_s.

In case of Ag-Ag_2O/ZnO samples, the plasmon peak at 0 V appears at around 387 nm (3.203 eV). Inserting the bulk

plasma frequency for silver of 6.52 eV in equation (A2.5), it renders the measured value of the surface plasma frequency (387 nm).

In the upper calculations, it is important to mention that the ratio between the surface and the bulk plasmon resonance (ω/ω_p in Fig. A2-1) for both gold and silver is lower than 0.6. Since this value is beyond the range that Fig. A2-1 shows, we had to extrapolate the function for r_s=3 (Au and Ag) to obtain $Re\{d_\perp(\omega)\}$.

In addition, the work of Monreal et al. [57], which calculates the surface plasmon peak position depending on the metal nanoparticle size, could be a theoretical basis for the analogous calculation depending on the electric field applied to the metal/semiconductor heterostrucutre, since the parameters in equation (A2.3) and (A2.5) depend upon applied electric potential. In addition, further mutual experimental and theoretical investigation should be led to unravel in which way the bulk plasma frequency and $Re\{d_r(\omega)\}$ depend upon the applied electric potential.

Bibliography

[1] M. Radivojević, T. Rehren, E. Pernicka, D. Sljivar, M. Brauns and D. Borić, On the origins of extractive metallurgy: new evidence from Europe, J. Archeol. Sci. **37**, 2775 (2010).
[2] I. Freestone, N. Meeks, M. Sax and C. Higgitt, *The Lycurgus Cup – A Roman Nanotechnology*, Gold Bulletin **40/4**, 270 (2007).
[3] P. R. Sajanlal and T. Pradeep, Gold Nanoparticles, Kirk-Othmer Encyclopedia of Chemical Technology, 1 (2012).
[4] T. L. Stone, *Color Design Workbook*, Rockport Publishers, 2006.
[5] B. Hammer and J. K. Norskov, Why gold is the noblest of all the metals, Nature **376**, 238 (2002).
[6] H. A Atwater and A. Polman, Plasmonics for improved photovoltaic devices, Nature Mater. **9**, 205 (2010).
[7] J. J. Mock, M. Barbic, D. R. Smith, D. A. Schultz and S. Schultz, Shape effects in plasmon resonance of individual colloidal silver nanoparticles, J. Chem. Phys. **116**, 6755 (2002).
[8] A. Trügler, Optical Properties of Metallic Nanoparticles, PhD thesis, University of Graz, Austria (2011).
[9] P. Seneor, N. Lidgi, J. Carrey, H. Jaffres, F. N. Van Dau, A. Friederich and A. Fert, Principle of a variable capacitor based on Coulomb blockade of nanometric-size clusters, Europhys. Lett. **65**, 699 (2004).
[10] J. Carrey, P. Seneor, N. Lidgi, H. Jaffrès, F. Nguyen Van Dau, A. Fert, A. Friederich, F. Montaigne, and A. Vaurès, Capacitance variation of an assembly of clusters in the Coulomb blockade regime, J. Appl. Phys. **95**, 1265 (2004).
[11] U. Kreibig and M. Vollmer, *Optical Properties of Metal Clusters*, Springer, Berlin, 1995.

[12] M. Orrit, Nano-optics: Quantum light switch, Nat. Phys. **3**, 755 (2007).
[13] W. L. Barnes, A. Dereux and T. W. Ebbesen, Surface plasmon subwavelength optics, Nature **424**, 824 (2003).
[14] A. Partovi, D. Peale, M. Wuttig, C. A. Murray, G. Zydzik, L. Hopkins, K. Baldwin, W. S. Hobson, J. Wynn, J. Lopata, L. Dhar, R. Chichester and J. H-J. Yeh, High-power laser source for near-field optics and its application to high-density optical data storage, Appl. Phys. Lett. **75**, 1515 (1999).
[15] S. Shinada, F. Koyama, N. Nishiyama, M. Arai and K. Iga, Analysis and fabrication of microaperture GaAs-GaAlAs surface-emitting laser for near-field optical data storage, IEEE J. Sel. Top. Quantum Electron. **7**, 365 (2001).
[16] T. Yatsui, M. Kourogi and M. Ohtsu, Plasmon waveguide for optical far/near-field conversion, Appl. Phys. Lett. **79**, 4583 (2001).
[17] E. M. Larsson, S. Langhammer, I. Zoric and B. Kasemo, Nanoplasmonic Probes of Catalytic Reactions, Science **326**, 1091 (2010).
[18] R. J. Tseng, C. L. Tsai, L. P. Ma, J. Y. Ouyang, C. S. Ozkan and Y. Yang, Digital memory device based on tobacco mosaic virus conjugated with nanoparticles, Nat. Nanotechnol. **1**, 72 (2006).
[19] W. Cai, J. S. White and M. L. Brongersma, Compact, High-Speed and Power-Efficient Electrooptic Plasmonic Modulators, Nano Lett. **9**, 4403 (2009).
[20] D. C Look and K. D. Leedy, ZnO plasmonics for telecommunications, Appl. Phys. Lett. **102**, 182107 (2013).
[21] J. W. M. Chon, *Nanoplasmonics: Advanced Device Applications*, CRC Press, 2013.
[22] S. Lal, S. E. Clare and N. J. Halas, Nanoshell-enabled photothermal cancer therapy: impending clinical impact, Acc. Chem. Res. **41**, 1842 (2008).
[23] M. A. El-Sayed, Some Interesting Properties of Metals Confined in Time and Nanometer Space of Different Shapes, Acc. Chem. Phys. **34**, 257 (2001).
[24] C. M. Niemeyer, Nanoparticles, Proteins, and Nucleic Acids: Biotechnology Meets Materials Science, Angew. Chem. Int. Ed. **40**, 4128 (1999).

[25] T. Sannomiya, H. Dermutz, C. Hafner, J. Vörös and A. B. Dahlin, Electrochemistry on a Localized Surface Plasmon Resonance Sensor, Langmuir **26**, 7619 (2010).
[26] A. G. Brolo, Plasmonics for future biosensors, Nature Photon. **6**, 701 (2012).
[27] S. Pud, D. Verschueren, N. Vukovic, C. Plesa, M. Jonsson and C. Dekker, Self-Aligned Plasmonic Nanopores by Optically Controlled Dielectric Breakdown, Nano Lett. **15**, 7112 (2015).
[28] V. Trajković and Z. Marković, *Nanomedicina: stanje i perspective [Nanomedicine: state and prospects]*, in: D. Rakovic and D. Uskokovic (Eds.), *Biomerijali [Biomaterials]*, Institut tehničkih nauka SANU, Društvo za istraživanje materijala, Beograd, 2010.
[29] M. M. Alvarez, J. T. Khoury, T. G. Schaaff, M. N. Shafigullin, I. Vezmar and R. L. Whetten, Optical Absorption Spectra of Nanocrystal Gold Molecules, J. Phys. Chem. B **101**, 3706 (1997).
[30] H. Hövel, S. Fritz, A. Hilger, U. Kreibig and M. Vollmer, Width of cluster plasmon resonances: bulk dielectric functions and chemical interface damping, Phys. Rev. B **48**, 18178 (1993).
[31] U. Kreibig and L. Genzel, Optical absorption of small metallic particles, Surf. Sci. ***156***, 678 (1985).
[32] A. B. Dahlin, Plasmonic biosensors: An integrated view of refractometric detection, IOS Press, 2012.
[33] P. Winsemius, Temperature Dependence of the Optical Properties of Au and Ag, PhD thesis, Rijksuniversiteit Leiden, The Netherlands (1973).
[34] T. Pakizeh, Optical Absorption of Plasmonic Nanoparticles in Presence of a Local Interband Transition, J. Phys. Chem. C **115**, 21826 (2011).
[35] H. Wang, F. Tam, N. K. Grady and N. J. Halas, Cu Nanoshells: Effects of Interband Transitions on the Nanoparticle Plasmon Resonance, J. Phys. Chem. B **109**, 18218 (2005).
[36] A. Derkachova, K. Kolwas and I. Demchenko, Dielectric Function for Gold in Plasmonics Applications: Size Dependence of Plasmon Resonance Frequencies and Damping Rates for Nanospheres, Plasmonics, 1, DOI 10.1007/s11468-015-0128-7 (2015).

[37] W. Cai and V. Shalaev, *Optical Metamaterials: Fundamentals and Applications*, Springer, New York, 2010.
[38] K. L. Kelly, E. Coronado, L. L. Zhao and G. C Schatz, The Optical Properties of Metal Nanoparticles: The Influence of Size, Shape, and Dielectric Environment, J. Phys. Chem. B **107**, 668 (2003).
[39] C. Noguez, Surface Plasmons on Metal Nanoparticles: The Influence of Shape and Physical Environment, J. Phys. Chem. C **111**, 3806 (2007).
[40] P. G. Etchegoin, E. C. L. Ru and M. Meyer, An analytic model for the optical properties of gold, J. Chem. Phys. **125**, 164705 (2006).
[41] A. Vial, A. -S. Grimault, D. Macias, D. Barchiesi and M. de la Chapelle, Improved analytical fit of gold dispersion: application to the modeling of extinction spectra with a finite-difference time-domain method, Phys. Rev. B **71**, 085416 (2005).
[42] T. Laroche and C. Girard, Near-field optical properties of single plasmonic nanowires, Appl. Phys. Lett. **89**, 233119 (2006).
[43] R. v. Baltz, *Plasmons and Surface Plasmons in Bulk Metals, Metallic Clusters, and Metallic Heterostructures*, in: B. Di Bartolo and S. Kyrkos (Eds.), *Spectroscopy and Dynamics of Collective Excitations in Solids*, NATO ASI Series **356**, Springer US, 1997, p. 303-338.
[44] R. H. Ritchie, Plasma Losses by Fast Electrons in Thin Films, *Phys. Rev.* **106**, 874 (1957).
[45] C. Xia, C. Yin and V. V. Kresin, Photoabsorption by Volume Plasmons in Metal Nanoclusters, *Phys. Rev. Lett.* **102**, 156802 (2009).
[46] L. Novotny and B. Hecht, *Principles of Nano-Optics*, Cambridge University Press, Cambridge, 2008.
[47] F. -P. Schmidt, H. Ditlbacher, U. Hohenester, A. Hohenau, F. Hofer and J. R. Krenn, Universal dispersion of surface plasmons in flat nanostructures, Nat. Commun. **5**, 3604 (2014).
[48] M. Guasoni, Analytical approximations of the dispersion relation of the plasmonic modes propagating around a curved dielectric-metal interface, J. Opt. Soc. Am. B **28**, 1396 (2011).

[49] J. W. Liaw, Simulation of surface plasmon resonance of metallic nanoparticles by the boundary-element method, J. Opt. Soc. Am. A **23**, 108 (2006).
[50] M. Willatzen, Electromagnetic-wave propagation along curved surfaces, Phys. Rev. **80**, 043805 (2009).
[51] S. B. Ogale, V. N. Bhoraskar and P. V. Panat, Surface plasmon dispersion relation for spherical metal particles, Pramana **11**, 135 (1978).
[52] J. A. Scholl, A. L. Koh and J. A. Dionne, Quantum plasmon resonance of individual metallic nanoparticles, Nature **483**, 421 (2012).
[53] Y. Fang and X. Tian, Resonant surface plasmons of a metal nanosphere can be considered in the way of propagating surface plasmons, arXiv:1412.2664 [physics.optics] (2014).
[54] A. Moradi, Plasmon modes of spherical nanoparticles: The effects of quantum nonlocality, Surf. Sci. **637**, 53 (2015).
[55] M. Dressel and G. Gruener, *Electrodynamics of Solids: Optical Properties of Electrons in Matter*, Cambridge University Press, Cambridge, 2002, p. 114.
[56] D. Bedeaux and J. Vlieger, *Optical Properties of Surfaces*, Imperial College Press, London, 2004, p. 38.
[57] R. C. Monreal, T. J. Antosiewicz and S. P. Apell, Plasmons do not go that quantum, New J. Phys. **15**, 083044 (2013).
[58] C. F. Bohren and D. R. Huffman, *Absorption and Scattering of the Light by Small Particles*, Wiley, New York, USA (1998).
[59] J. M. Pitarke, V. M. Silkin, E. V. Chulkov and P. M. Echenique, Theory of surface plasmons and surface-plasmon polaritons, Rep. Prog. Phys. **70**, 1 (2007).
[60] J. W. Rohlf, *Modern Physics from α to Z^0*, John Wiley & Sons Inc, Canada, 1994.
[61] L. Patterson, The Scherrer Formula for X-Ray Particle Size Determination, Phys. Rev. **56**, 978 (1939).
[62] C. P. Romero Vieyra, Physical properties of hybrid cluster assembled nanomaterials, PhD thesis. KU Leuven, Belgium (2012).
[63] G. Verschoren, *Transport and magnetic properties of cluster-assembled nanogranular gold-cobalt films*, PhD thesis, KU Leuven, Belgium (2005).

[64] W. Bouwen, P. Thoen, F. Vanhoutte, S. Bouckaert, F. Despa, H. Weidele, R. E. Silverans and P. Lievens, Production of bimetallic clusters by a dual-target dual-laser vaporization source, Rev. Sci. Instrum. **71**, 54 (2000).
[65] R. C. Wiley and I. H. McClaren, Time-of-Flight Mass Spectrometer with Improved Resolution, Rev. Sci. Instrum. **26**, 1150 (1955).
[66] R. N. Jagtap and A. H. Ambre, Overview literature on atomic force microscopy (AFM): Basics and its important applications for polymer characterization, IJEMS **13**, 368 (2006).
[67] W. Liu, V. Montana, J. Bai, E. R. Chapman, U. Mohideen and V. Parpura, Single Molecule Mechanical Probing of the SNARE Protein Interactions, Biophys. J. **91**, 744 (2006).
[68] G. Binnig and C. F. Quate, C. Gerber, Atomic Force Microscopy, Phys. Rev. Lett. **56**, 930 (1986).
[69] M. Gysemans, Atomic force microscopy of self-assembled biomolecular structures and their interaction with metallic nanoparticles, PhD thesis, KU Leuven, Belgium (2009).
[70] I. Horcas, R. Fernández, J. M. Gomez-Rodríguez, J. Colchero, J. Gómez-Herrero and A. M. Baro, WSxM: A software for Scanning probe microscopy and a tool for nanotechnology, Rev. Sci. Instrum. **78**, 013705 (2007).
[71] C. Kittel, *Introduction to Solid State Physics*, 8th edition, John Wiley and Sons, USA, 2005.
[72] A. Mooradian, Photoluminescence of metals, Phys. Rev. Lett. **22**, 185 (1969).
[73] M. R. Beversluis, A. Bouhelier and L. Novotny, Continuum generation from single gold nanostructures through near-field mediated intraband transitions, Phys. Rev. B **68**, 115433 (2003).
[74] O. P. Varnavski, T. Goodson, T. M. B. Mohamed and M. A. El-Sayed, Femtosecond excitation dynamics in gold nanospheres and nanorods, Phys. Rev. B **72**, 235405 (2005).
[75] H. Ehrenreich and H. P. Philipp, Optical Properties of Ag and Cu, Phys. Rev. **128**, 1622 (1962).
[76] G. T. Boyd, Z. H. Yu and Y. R. Shen, Photoinduced luminescence from the noble metals and its enhancement on rough surfaces, Phys. Rev. B **33**, 7923 (1986).

[77] Z. Liu, L. Peng and K. Yao, Intense blue luminescence from self-assembled Au-thiolate clusters, Mat. Lett. **60**, 2362 (2006).
[78] J. Zheng, J. T. Petty and R. M. Dickson, High Quantum Yield Blue Emission from Water-Soluble Au_8 Nanodots, J. Am. Chem. Soc. **125**, 7780 (2003).
[79] V. A. Sinani, P. Podsiadlo, J. Lee, N. A. Kotov and K. Kempa, Gold nanoparticles with stable yellow-green luminescence, Int. J. Nanotechnology **4,** 239 (2007).
[80] S. Link, A. Beeby, S. FitzGerald, M. A. El-Sayed, T. G Schaaff and R. L. Whetten, Visible to Infrared Luminescence from a 28-Atom Gold Cluster, J. Phys. Chem. B **106**, 3410 (2002).
[81] L. L. T. Ngoc, J. Wiedemair, A. van den Berg and E. T. Carlen, Plasmon-modulated photoluminescence from gold nanostructures and its dependence on plasmon resonance, excitation energy, and band structure, Opt. Express **23**, 5547 (2015).
[82] V. Hubenthal, Increased Damping of Plasmon Resonances in Gold Nanoparticles Due to Broadening of the Band Structure, Plasmonics **8**, 1341 (2013).
[83] C. Sönnichsen, Plasmons in metal nanostructures, PhD thesis, University of Munich, Germany (2001).
[84] P. B. Johnson and R. W. Christy, Optical Constants of the Noble Metals, Phys. Rev. B **6**, 4370 (1972).
[85] U. Kreibig, *Optics of nanosized metals*, in: R. Hummel and P. Wissmann (Eds.), *Handbook of Optical Properties: Optics of Small Particles, Interfaces and Surfaces*, CRS Press, Broca Raton, FL, 1997, p. 39.
[86] J. Zheng, P. R. Nicovich and R. M. Dickson, Highly Fluorescent Noble Metal Quantum Dots, Annu. Rev. Phys. Chem. **58**, 409 (2007).
[87] A. Fernando, K. L. Dimuthu, M. Weerawardene, N. V. Karimova and C. M. Aikens, Quantum Mechanical Studies of Large Metal, Metal Oxide, and Metal Chalcogenide Nanoparticles and Clusters, Chem. Rev. **115**, 6112 (2015).
[88] L. Prodi, G. Battistini, L. S. Dolci, M. Montalti and N. Zaccheroni, *Luminescence of Gold Nanoparticles*, in: D. L. Andrews, Z. Gaburro (Eds.), *Frontiers in Surface*

Nanophotonics: Principles and Applications, Springer-Verlag, Berlin, 2007, p. 99-128.
[89] D. Gall, Electron mean free path in elemental metals, J. Appl. Phys. **119**, 085101(2016).
[90] O. Varnavski, G. Ramakrishna, J. Kim, D. Lee and T. Goodson, Critical Size for the Observation of Quantum Confinement in Optically Excited Gold Clusters, J. Am. Chem. Soc. **132**, 16 (2010).
[91] Y. Huang, M. C. Pitter and M. G. Somekh, Morphology-Dependent Voltage Sensitivity of a Gold Nanostructure, Langmuir **27**, 13950 (2011).
[92] E. Roduner, Size matters: why nanomaterials are different, Chem. Soc. Rev. **35**, 583 (2006).
[93] H. Eckardt, L. Fritsche and J. Noffke, Self-consistent relativistic band structure of the noble metals, J. Phys. F: Met. Phys. **14**, 97 (1984).
[94] X. Li and R. L. Whetten, Ultraviolet absorption bands of ionic compound clusters: Onset of crystalline structures in $[Cs_{n+1}I_n]^+$, n=1-13, J. Chem. Phys. **98**, 6170 (1993).
[95] M. C. Daniel and D. Astruc, Gold Nanoparticles: Assembly, Supramolecular Chemistry, Quantum-Size-Related Properties, and Applications toward Biology, Catalysis, and Nanotechnology, Chem. Rev. **104**, 293 (2004).
[96] G. Schmid and B. Corain, Nanoparticulated Gold: Syntheses, Structures, Electronics, Reactivities, Eur. J. Inorg. Chem. **2003**, 3081 (2003).
[97] S. L. Logunov, T. S. Ahmadi, M. A. El-Sayed, J. T. Khoury and R. L. Whetten, Electron Dynamics of Passivated Gold Nanocrystals Probed by Subpicosecond Transient Absorption Spectroscopy, J. Phys. Chem. B **101**, 3713 (1997).
[98] G. Schmid, M. Bäumle, M. Geerkens, I. Heim, C. Osemann and T. Sawitowski, Current and future applications of nanoclusters, Chem. Soc. Rev. **28**, 179 (1999).
[99] H. Zhang, G. Schmid and U. Hartmann, Reduced Metallic Properties of Ligand-Stabilized Small Metal Clusters, Nano Lett. **3**, 305 (2003).
[100] K. J. Taylor, C. L. Pettiette-Hall, O. Cheshnakovsky and R. E. Smalley, Ultraviolet photoelectron spectra of coinage metal clusters, J. Chem. Phys. **96**, 3319 (1992).

[101] L. -D. Wang, T. Zhang, S. -Q. Zhu, X. -Y. Zhang, Q. -L. Wang, X. Liu and R. -Z. Li, Two-dimensional ultrathin gold film composed of steadily linked dense nanoparticle with surface plasmon resonance, Nanoscale Res. Lett. **7**, 683 (2012).
[102] S. Zhu, T. P. Chen, Z. H. Cen, E. S. M. Goh, S. F. Yu, Y. C. Liu and Y. Liu, Split of surface plasmon resonance of gold nanoparticles on silicon substrate: a study of dielectric functions, Opt. Express **18**, 21926 (2010).
[103] V. N. Rai, A. K. Srivastava, C. Mukherjee and S. K. Deb, Surface enhanced absorption and transmission from dye coated gold nanoparticles in thin films, Appl. Opt. **51**, 2606 (2012).
[104] F. Hubenthal, *Noble metal nanoparticles: Synthesis and applications*, in: D. L. Andrews, G. D. Scholes and G. P. Wiederrecht (Eds.), *Comprehensive Nanoscience and Technology*, Oxford Academic Press: New York, NY, USA, 2011, p. 375–435.
[105] V. B. Svetovoy, P. J. van Zwol, G. Palasantzas and J. Th. M. De Hosson, Optical properties of gold films and the Casimir force, Phys. Rev. B **77**, 035439 (2008).
[106] I. Pirozhenko, A. Lambrecht and V. B. Svetovoy, Sample dependence of the Casimir force, New J. Phys. **8**, 238 (2006).
[107] P. Yu. Kuryoz, L. V. Poperenko and V. G. Kravets, Correlation between dielectric constants and enhancement of surface plasmon resonances for thin gold films, Phys. Status Solidi A **210**, 2445 (2013).
[108] A. Toyota, N. Nakashima and T. Sagara, UV–visible transmission–absorption spectral study of Au nanoparticles on a modified ITO electrode at constant potentials and under potential modulation, J. Electroan. Chem. **565**, 335 (2004).
[109] M. Guerrisi, R. Rosei and P. Winsemius, Splitting of the interband absorption edge in Au, Phys. Rev. B **12**, 557 (1975).
[110] U. Kreibig, *Optics of nanosized metals*, in: R. Hummel and P. Wissmann (Eds.), *Handbook of Optical Properties: Optics of Small Particles, Interfaces and Surfaces*, CRS Press, Broca Raton, FL, 1997, p. 145.
[111] M. Pelton and G. W. Bryant, *Introduction to Metal-Nanoparticle Plasmonics* (*Measuring: Characterization of Plasmons in Metal Nanoparticles*), Wiley-Science Wise Publishing Co-Publication, New Jersey, 2013.

[112] F. Hubenthal, D. B. Sánchez and F. Träger, Determination of Morphological Parameters of Supported Gold Nanoparticles: Comparison of AFM Combined with Optical Spectroscopy and Theoretical Modeling versus TEM, Appl. Sci. **2**, 566 (2012).
[113] S. Raza, N. Stenger, S. Kadkhodazadeh, S. V. Fischer, N. Kostesha, A. -P. Jauho, A. Burrows, M. Wubs and N. A. Mortensen, Blueshift of the surface plasmon resonance in silver nanoparticles studied with EELS, Opt. Express **21**, 27344 (2013).
[114] T. Pradeep, *A Textbook of Nanoscience and Nanotechnology*, in *Advanced Nanomaterials* McGraw-Hill Offices, New Delhi, 2012, p. 294.
[115] K. -H. Su, Q. -H. Wei, and X. Zhang, J. J. Mock, D. R. Smith, and S. Schultz, Interparticle Coupling Effects on Plasmon Resonances of Nanogold Particles, Nano Lett. **3**, 1087 (2003).
[116] X. Wang, P. Gogol. E. Cambril and B. Palpant, Near- and Far-Field Effects on the Plasmon Coupling in Gold Nanoparticle Arrays, J. Phys. Chem. C **116**, 24741 (2012).
[117] P. Song, P. Nordlander and S. Gao, Quantum mechanical study of the coupling of plasmon excitations to atomic-scale electron transport, J. Chem. Phys. **134**, 074701 (2011).
[118] H. Duan, A. I. Fernàndez-Domìnguez, M. Bosman, S. A. Meier and J. K. W. Yang, Nanoplasmonics: Classical down to the Nanometer Scale, Nano Lett. **12**, 1683 (2012).
[119] K. J. Savage, M. M. Hawkeye, R. Esteban, A. G. Borisov, J. Aizpurua and J. J. Baumberg, Revealing the quantum regime in tunnelling plasmonics, Nature **491**, 574 (2012).
[120] M. Zhu, C. M. Aikens, F. J. Hollander, G. C. Schatz and R. Jin, Correlating the Crystal Structure of A Thiol-Protected Au25 Cluster and Optical Properties, J. Am. Chem. Soc. **130**, 5883 (2008).
[121] F. Stietz and F. Träger, Surface plasmons in nanoclusters: elementary electronic excitations and their applications, Philos. Mag. B **9**, 1281 (1999).
[122] J. Bosbach, D. Martin, F. Stietz, T. Wenzel and F. Träger, Laser-based method for fabricating monodisperse metallic nanoparticles, Appl. Phys. Lett. **18**, 2605 (1999).

[123] T. Wenzel, J. Bosbach, A. Goldmann, F. Stietz and F. Träger, Shaping nanoparticles and their optical spectra with photons, Appl. Phys. B **69**, 513 (1999).
[124] A. Janotti and C. G. Van de Walle, Native point defects in ZnO, Phys. Rev. B **76**, 165202 (2007).
[125] C. E. Talley, L. Jusinski, C. W. Hollars, S. M. Lane and T. Huser, Intracellular pH Sensors Based on Surface-Enhanced Raman Scattering, Anal. Chem. **76**, 7064 (2004).
[126] S. Zong, Z. Wang, J. Yang and Y. Cui, Intracellular pH Sensing Using p-Aminothiophenol Functionalized Gold Nanorods with Low Cytotoxicity, Anal. Chem. **83**, 4178 (2011).
[127] P. Zijlstra, P. M. R. Paolo and M. Orrit, Optical detection of single non-absorbing molecules using the surface plasmon resonance of a gold nanorod, Nat. Nanotechnol. **7**, 379 (2012).
[128] S. Yang, Y. Wang, Q. Wang, R. Zhang and B. Ding, UV irradiation induced formation of Au nanoparticles at room temperature: The case of pH values, Colloids Surf. A**301**, 174 (2007).
[129] J. Piella, N. G. Bastús and V. Puntes, Size-Controlled Synthesis of Sub-10-nanometer Citrate-Stabilized Gold Nanoparticles and Related Optical Properties, Chem. Mater. **28**, 1066 (2016).
[130] H. Zhang and D. Wang, Controlling the Growth of Charged-Nanoparticle Chains through Interparticle Electrostatic Repulsion, Angew. Chem. Int. Ed. **47**, 3984 (2008).
[131] X. Li, K. Tamada, A. Baba and M. Hara, pH-controlled two dimensional gold nanoparticle aggregates for systematic study of local surface plasmon coupling, J Nanosci. Nanotechnol. **9**, 408 (2009).
[132] S. A. Maier, P. G. Kik, H. A. Atwater, S. Meltzer, E. Harel, B. E. Koel and A. A. G. Requicha, Local detection of electromagnetic energy transport below the diffraction limit in metal nanoparticle plasmon waveguides, Nat. Mater. **2**, 229 (2003).
[133] M. Pillers, V. Goss and M. Lieberman, Electron-Beam Lithography and Molecular Liftoff for Directed Attachment of DNA Nanostructures on Silicon: Top-down Meets Bottom-up, Acc. Chem. Res. **47**, 1759 (2014).

[134] Y. M. Georgiev, N. Petkov, B. McCarthy, R. Yu, V. Djara, D. O'Connell, O. Lotty, A. M. Nightingale, N. Thamsumet, J. C. deMello, A. Blake, S. Das, J. D. Holmes, Fully CMOS-compatible top-down fabrication of sub-50 nm silicon nanowire sensing devices, Microelectronic Engineering **118**, 47 (2014)].
[135] A. M. Hung, C. M. Micheel, L. D. Bozano, L. W. Osterbur, G. M. Wallraff and J. N. Cha, Large-area spatially ordered arrays of gold nanoparticles directed by lithographically confined DNA origami, Nat. Nanotechnol. **5**, 121 (2010).
[136] S. Schultz, D. R. Smith, J. J. Mock, D. A. Schultz, Single-target molecule detection with nonbleaching multicolor optical immunolabels, PNAS **97**, 996 (2000).
[137] Y. C. Cao, R. Jin, C. A. Mirkin, Nanoparticles with Raman spectroscopic fingerprints for DNA and RNA detection, Science **30**, 1536 (2002).
[138] D. A. Schultz, Plasmon resonant particles for biological detection, Curr. Opin. Biotech. **14**, 13 (2003).
[139] S. K. Ghosh and T. Pal, Interparticle Coupling Effect on the Surface Plasmon Resonance of Gold Nanoparticles: From Theory to Applications, Chem. Rev. **107**, 4797 (2007).
[140] K. Saha, S. S. Agasti, C. Kim, X. Li and V. M. Rotello, Gold Nanoparticles in Chemical and Biological Sensing, Chem. Rev. **112**, 2739 (2012).
[141] K. Aslan, J. R. Lakowicz and C. D. Geddes, Nanogold-plasmon-resonance-based glucose sensing, Anal. Biochem. **330**, 145 (2004).
[142] L. Novotny, R. X. Bian and X. S. Xie, Theory of Nanometric Optical Tweezers, Phys. Rev. Lett. **79**, 645 (1997).
[143] N. Calander and M. Willander, Optical trapping of single fluorescent molecules at the detection spots of nanoprobes, Phys. Rev. Lett. **82**, 143603 (2002).
[144] P. C. Chaumet, A. Rahmani and M. Nieto-Vesperinas, Optical Trapping and Manipulation of Nano-objects with an Apertureless Probe, Phys. Rev. Lett. **88**, 13601 (2002).
[145] H. Xu and M. Käll, Surface-Plasmon-Enhanced Optical Forces in Silver Nanoaggregates, Phys. Rev. Lett. **89**, 246802 (2002).

[146] C. Cheniclet, S. Garzon and M. Bendayan, *In Situ Detection of Nucleic Acids by the Nuclease-Gold Method*, in: G. Morel (Ed.), *Vizualization of Nucleic Acids*, CRC Press, Broca Raton, FL, 1995.
[147] L. A. E. Leal and O. Lopez-Acevedo, A theoretical study of the interaction between DNA/RNA and the noble metal atoms of gold and silver - Ground-state properties, Nanotechnology Reviews **4**, 173 (2015).
[148] Y. Ding, Z. Jiang, K. Saha, C. S. Kim, S. T. Kim, R. F. Landis and V. M. Rotello, Gold Nanoparticles for Nucleic Acid Delivery, Mol. Ther. **22**, 1075 (2014).
[149] C. Lee, C. Takagi, T. Truong, Y. Chen and A. Ostafin, Luminescent Au Nanoparticles with a pH-Responsive Nanoparticle-Supported Molecular Brush, J. Phys. Chem. C 114, 12459 (2010).
[150] J. Nam, N. Won, H. Jin, H. Chung and S. Kim, pH-Induced Aggregation of Gold Nanoparticles for Photothermal Cancer Therapy, J. Am. Chem. Soc. **131**, 13639 (2009).
[151] A. K. Covington, R. G. Batesa and R. A. Durst (1985), Definitions of pH scales, standard reference values, measurement of pH, and related terminology, Pure Appl. Chem. **57**, 531 (1985).
[152] C. Pfeiffer, C. Rehbock, D. Hühn, C. Carrillo-Carrion, D. J. de Aberasturi, V. Merk, S. Barcikowski and W. J. Parak, Interaction of colloidal nanoparticles with their local environment: the (ionic) nanoenvironment around nanoparticles is different from bulk and determines the physico-chemical properties of the nanoparticles, J. R. Soc. Interface **11**, 20130931 (2014).
[153] Y. R. Toh, P. Yu, X. Wen, J. Tang and T. Hsieh, Induced pH-dependent shift by local surface plasmon resonance in functionalized gold nanorods, Nanoscale Res. Lett. **8**, 103 (2013).
[154] A. J. Haes, S. Zou, G. C. Schatz and R. P. Van Duyne, Nanoscale Optical Biosensor: Short Range Distance Dependence of the Localized Surface Plasmon Resonance of Noble Metal Nanoparticles, J. Phys. Chem. B **108**, 6961 (2004).
[155] J. -W. Park and J. S. Shumaker-Parry, Structural Study of Citrate Layers on Gold Nanoparticles: Role of Intermolecular

Interactions in Stabilizing Nanoparticles, J. Am. Chem. Soc. **136**, 1907 (2014).
[156] T. Ung, M. Giersig, D. Dunstan and P. Mulvaney, Spectroelectrochemistry of Colloidal Silver, Langmuir **13**, 1773 (1997).
[157] S. Ross and I. D. Morrison, *Colloidal System and Interfaces*, John Wiley and Sons: New York, 1988, p. 4.
[158] K. S. Mayya, V. Patil and M. Sastry, On the Stability of Carboxylic Acid Derivatized Gold Colloidal Particles: The Role of Colloidal Solution pH Studied by Optical Absorption Spectroscopy, Langmuir **13**, 3944 (1997).
[159] R. S. Periathai, S. Abarna, G. Hirankumar, N. Jeyakumaran and N. Prithivikumaran, Effect of pH on the electrical properties and conducting mechanism of SnO_2 nanoparticles, Physica B Condens. Matter. **509**, 62 (2017).
[160] V. Ratchagar and K. Jagannathan, Effect of pH on magnetic, thermal and dielectric properties of SnO_2 nanomaterials, J. Alloy. Comp. **689**, 1088 (2016).
[161] R. Chintaparty, B. Palagiri, R. R. Nagireddy, V. s. R. Immareddy, M. W, Effect of pH on structural, optical and dielectric properties of nano-zirconium oxide prepared by hydrothermal method, Mat. Lett. **161**, 770 (2015).
[162] J. W. Pitera, M. Falta and W. F. van Gunsteren, Dielectric Properties of Proteins from Simulation: The Effects of Solvent, Ligands, pH, and Temperature, Biophys. J. **80**, 2546 (2001).
[163] T. Ahuja, D. Wang, Z. Tang, D. A. Robinson, J. W. Padelford and G. Wang, Electronic coupling between ligand and core energy states in dithiolate-monothiolate stabilized Au clusters, Phys. Chem. Chem. Phys. **17**, 19342 (2015).
[164] M. A. H. Muhammed, S. Ramesh, S. S. Sinha, S. K. Pal and T. Pradeep, Two Distinct Fluorescent Quantum Clusters of Gold Starting from Metallic Nanoparticles by pH-Dependent Ligand Etching, Nano Res. **1**, 333 (2008).
[165] E. W. Elliott, P. M. Haben and J. E. Hutchison, Subnanometer Control of Mean Core Size during Mesofluidic Synthesis of Small (D_{core}< 10 nm) Water-Soluble, Ligand-Stabilized Gold Nanoparticles, Langmuir **31**, 11886 (2015).

[166] Size Control of Gold Nanocrystals in Citrate Reduction: The Third Role of Citrate, J. Am. Chem. Soc. **129**, 13939 (2007).
[167] Z. Wu and R. Jin, On the Ligand's Role in the Fluorescence of Gold Nanoclusters, Nano Lett. **10**, 2568 (2010).
[168] Gold Nanorods: Electrochemical Synthesis and Optical Properties, J. Phys. Chem. B **101**, 6661 (1997).
[169] P. Kannan, S. Sampath and S. A. John, Direct Growth of Gold Nanorods on Gold and Indium Tin Oxide Surfaces: Spectral, Electrochemical, and Electrocatalytic Studies, J. Phys. Chem. C **114**, 21114 (2010).
[170] J. Wiesner and A. Wokaun, Anisometric gold colloids. Preparation, characterization, and optical properties, Chem. Phys. Lett. **157**, 569 (1989).
[171] M. Quinten and U. Kreibig, Optical properties of aggregates of small metal particles, Surf. Sci. **172**, 557 (1986).
[172] C. S. Weisbecker, M. V. Merritt and G. M. Whitesides, Molecular Self-Assembly of Aliphatic Thiols on Gold Colloids, Langmuir **12**, 3763 (1996).
[173] L. S. Jung, C. T. Campbell, T. M. Chinowsky, M. N. Mar and S. S. Yee, Quantitative interpretation of the response of surface plasmon resonance sensors to adsorbed films, Langmuir **14**, 5636 (1998).
[174] D. Stuart, A. Haes, C. Yonzon, E. Hicks and R. P. Van Duyne, Biological applications of localized surface plasmon resonance phenomenae, IEE Proceedings Nanobiotechnology **152**, 13 (2005).
[175] G. Barbillon, J. L. Bijeon, J. S. Bouillard, J. Plain, M. Lamy de la Chapelle, P. M. Adam and P. Royer, Detection in near-field domain of biomolecules adsorbed on a single metallic nanoparticle, J. Microsc. **229**, 270 (2008).
[176] G. Barbillon, J. L. Bijeon, J. Plain, M. L. Chapelle, P. M. Adam and P. Royer, Biological and chemical gold nanosensors based on localized surface plasmon resonance, Gold Bulletin **40**, 240 (2007).
[177] G. Barbillon, A. C. Faure, N. E. Kork, P. Moretti, S. Roux, O. Tillement, M. G. Ou, A. Descamps, P. Perriat, A. Vial, J. L. Bijeon, C. A. Marquette and B. Jacquier, How nanoparticles encapsulating flurophores allow a double

detection of biomolecules by localized surface plasmon resonance and luminescence, Nanotechnology **19**, 035705 (2008).
[178] G. Barbillon, M. G. Ou, A. C. Faure, C. Marquette, J. L. Bijeon, O. Tillement, S. Roux and P. Perriat, Two examples of nanostructured gold surfaces as biosensors. Surface-enhanced chemiluminescence and double detection by surface plasmon resonance and luminescence, Gold Bulletin **41**, 174 (2008).
[179] R. J. Nichols, I. Burgess, K. L. Young, V. Zamlynny, J. Lipkowski, A quantitative evaluation of the adsorption of citrate on Au(111) using SNIFTIRS, J. Electroanal. Chem. **563**, 33 (2004).
[180] M. D. Malinsky, K. L. Kelly, G. C. Schatz and R. P. Van Duyne, Chain Length Dependence and Sensing Capabilities of the Localized Surface Plasmon Resonance of Silver Nanoparticles Chemically Modified with Alkanethiol Self-Assembled Monolayers, J. Am. Chem. Soc. **123**, 1471 (2001).
[181] A. D. McFarland and R. P. Van Duyne, Single silver nanoparticles as real-time optical sensors with zeptomole sensitivity, Nano. Lett. **3**, 1057 (2003).
[182] R. J. Hunter, *Foundations of Colloid Science*, Clarendon Press, Oxford, U.K. (1992).
[183] K. Lee, A. N. Sathyagal and A. V. McCormick, A closer look at an aggregation model of the Stöber process, Colloids Surf. A **44**, 115 (1998).
[184] J. P. Kottmann and O. J. F. Martin, Influence of the cross section and the permittivity on the plasmon-resonance spectrum of silver nanowires, Appl. Phys. B **73**, 299 (2001).
[185] J. H. Kang, D. S. Kim and Q-Han Park, Local Capacitor Model for Plasmonic Electric Field Enhancement, PRL **102**, 093906 (2009).
[186] D. W. Thompson and I. R. Copllins, Electrical Properties of the Gold-Aqueous Solution Interface, J. Colloid Interface Sci. **152**, 197 (1992).
[187] B. V. Enüstün and J. Turkevich, Coagulation of Colloidal Gold, J. Amer. Chem. Soc. **85**, 3317 (1963).
[188] C. J. Sandroff and D. R. Herschbach, Kinetics of displacement and charge transfer reactions probed by SERS:

evidence for distinct donor and acceptor sites on colloidal gold surfaces, Langmuir **1**, 131 (1985).
[189] S. Biggs, P. Mulvaney, C. F. Zukoski and F. Grieser, Study of Anion Adsorption at the Gold-Aqueous Solution Interface by Atomic Force Microscopy, J. Am. Chem. Soc. **116**, 9150 (1994).
[190] M. K. Chow and C. F. Zukoski, Gold Sol Formation Mechanisms: Role of Colloidal Stability, J. Colloid Interface Sci. **165**, 97 (1994).
[191] B. R. Panda and A. Chattopadhyay, A water-soluble polythiophene-Au nanoparticle composite for pH sensing, J. Colloid Interface Sci. **316**, 962 (2007).
[192] A. M. El Badawy, T. P. Luxton, R. G. Silva, K. G. Scheckel, M. T. Suidan and T. M. Tolaymat, Impact of Environmental Conditions (pH, Ionic Strength, and Electrolyte Type) on the Surface Charge and Aggregation of Silver Nanoparticles Suspensions, Environ. Sci. Technol. **44**, 1260 (2010).
[193] C. Xue and C. A. Mirkin, pH-Switchable Silver Nanoprism Growth Pathways, Angew. Chem. **119**, 2082 (2007).
[194] T. C. Prathna, N. Chandrasekaran and A. Mukherjee, Studies on aggregation behaviour of silver nanoparticles in aqueous matrices: Effect of surface functionalization and matrix composition, Colloids Surf. A **390**, 216 (2011).
[195] S. P. Ramnani, J. Biswal and S. Sabharwal, Synthesis of silver nanoparticles supported on silica aerogel using gamma radiolysis, Rad. Phys. Chem. **76**, 1290 (2007).
[196] D. Long, G. Wu and S. Chen, Preparation of oligochitosan stabilized silver nanoparticles by gamma irradiation, Rad. Phys. Chem. **76**, 1126 (2007).
[197] S. A. Kumar, A. Kazemian, S. W. Gosavi, K. K. Sulabha, P. Renu, A. Ahmad and M. I. Khan, Nitrate reductase-mediated synthesis of silver nanoparticles from $AgNO_3$, Biotech. Lett. **29**, 439 (2007).
[198] C. G. Blatchford, J. R. Campbell and J. A. Creighton, Plasma resonance - enhanced Raman scattering by adsorbates on gold colloids: The effect of aggregation, Surf. Sci. **120**, 435 (1982).

[199] G. Navarra, C. Peres, M. Contardi, P. Picone, P. L. San Biagio, M. Di Carlo, D. Giacomazza and V. Militello, Heat- and pH-induced BSA conformational changes, hydrogel formation and application as 3D cell scaffold, Arch. Biochem. Biophys. **606**, 134 (2016).
[200] P. Hanč, O. Schulz, H. Fischbach, S. R. Martin, S. Kjær and C. Reis e Sousa, A pH- and ionic strengt h-dependentconformational change in the neck region regulatesDNGR-1 function in dendritic cells, EMBO J **35**, 2484 (2017).
[201] L. Guo, J. A. Jackman, H. -H. Yang, P. Chen, N. -J. Cho and D. -H. Kima, Strategies for enhancing the sensitivity of plasmonic nanosensors, Nano Today **10**, 213 (2015).
[202] J. N. Anker, W. P. Hall, O. Lyandres, N. C. Shah, J. Zhao and R. P. Van Duyne, Biosensing with plasmonic nanosensors, Nat. Mater. **7**, 442 (2008).
[203] P. Alivisatos, The use of nanocrystals in biological detection, Nat. Biotechnol. **22**, 47 (2003).
[204] E. Katz and I. Willner, Integrated nanoparticle-biomolecule hybrid systems: synthesis, properties, and application, Angew. Chem. Int. Ed. Engl. **43**, 6042 (2004).
[205] W. N. Hansen and A. Proshtak, Electroreflectance in Metals, Phys. Rev. **160**, 600 (1967).
[206] W. N. Hansen and A. Proshtak, Electromodulation of the Optical Properties of Gold, Phys. Rev. **174**, 500 (1968).
[207] R. Chapman and P. Mulvaney, Electro-optical shifts in silver nanoparticles films, Chem. Phys. Lett. **349**, 358 (2001).
[208] T. Baum, D. Bethell, M. Brust and D. J. Schiffrin, Electrochemical Charge Injection into Immobilized Nanosized Gold Particle Ensembles: Potential Modulated Transmission and Reflectance Spectroscopy, Langmuir **15**, 866 (1999).
[209] T. Sagara, N. Kato and N. Nakashima, Electroreflectance Study of Gold Nanoparticles Immobilized on an Aminoalkanethiol Monolayer Coated on a Polycrystalline Gold Electrode Surface, J. Phys. Chem. B **106**, 1205 (2002).
[210] A. C. Templeton, J. J. Pietron, R. W. Murray and P. Mulvaney, Solvent Refractive Index and Core Charges Influences on the Surface Plasmon Absorbance of

Alkanethiolate Monolayer-Protected Gold Clusters, J. Phys. Chem. B**104**, 564 (2000).
[211] J. P. Wilcoxon, J. E. Martin, F. Parsapour, B. Wiedenman and D. F. Kelley, Photoluminescence fromnanosized gold clusters, J. Chem. Phys. **108**, 9137 (1998).
[212] M. B. Mohamed, V. Volkov, S. Link and M. A. El-Sayed, The 'lightning' gold nanorods: fluorescence enhancement of over a million compared to the gold metal, Chem. Phys. Lett. **317**, 517 (2000).
[213] H. Hu, H. Duan, J. K. W. Yang and Z. X. Shen, Plasmon-Modulated Photoluminescence of Individual Gold Nanostructures, ACS Nano **6**, 10147 (2012).
[214] J. I. Gonzalez, T. Vosch and R. M. Dickson, Charge Injection into discrete states of individual electroluminescent Au nanoclusters, Phys. Rev. B **74**, 235404 (2006).
[215] A. Bouhelier, Field-enhanced scanning near-field optical microscopy, Microsc. Res. Tech. **69**, 563 (2006).
[216] Surface plasmon resonance and photoluminescence studies of Au and Ag micro-flowers, J. Lumin. **128**, 1635 (2008).
[217] O. A. Yeshchenko, I. Dmitruk, A. Alexeenko and A. Pinchuk, Size-dependent surface-plasmon-enhanced photoluminescence from silver nanoparticles embedded in silica, Phys. Rev. B **79**, 235438 (2009).
[218] A. Zakaria, K. S. Hamdan, S. M. C. Noh, A. Supangat and M. Sookhakian, Surface plasmon resonance and photo-luminescence studies of Au and Ag micro-flowers, Opt. Mater. Express **5**, 943 (2015).
[219] V. Kravets, Z. Almemar, K. Jiang, K. Culhane, R. Machado, G. Hagen, A. Kotko, I. Dmytruk, K. Spendier and A. Pinchuk, Imaging of Biological Cells Using Luminescent Silver Nanoparticles, Nanoscale Res. Lett. **11**, 30 (2016).
[220] T. Huang and R. W. Murray, Visible luminescence of water-soluble monolayer-protected gold clusters, J. Phys. Chem. B **105**, 12498 (2001).
[221] R. Jin, Quantum sized thiolate-protected gold nanoclusters, Nanoscale **2,** 343 (2010).
[222] J. Zheng, C. Zhou, M. Yu and J. Liu, Different sized luminescent gold nanoparticles, Nanoscale **4**, 4073 (2012).

[223] E. Heikkilä, A. A. Gurtovenko, H. Martinez-Seara, H. Häkkinen, I. Vattulainen and J. Akola, Atomistic Simulations of Functional $Au_{144}(SR)_{60}$ Gold Nanoparticles in Aqueous Environment, J. Phys. Chem. C **116**, 9805 (2012).
[224] J. F. Hicks, F. P. Zamborini and R. W. Murray, Dynamics of electron transfer between electrodes and monolayer of nanoparticles, J. Phys. Chem. B **106**, 7751 (2002).
[225] S. H. Yau, O. Varnavski, J. D. Gilbertson, B. Chandler, G. Ramakrishna and T. Goodson, Ultrafast Optical Study of Small Gold Monolayer Protected Clusters: A Closer Look at Emission, J. Phys. Chem. C **114**, 15979 (2010).
[226] S. Link, M. A. El-Sayed, T. G. Schaaff, R. L. Whetten, Transition from nanoparticle to molecular behavior: a femtosecond transient absorption study of a size-selected 28 atom gold cluster, Chem. Phys. Lett. **356**, 240 (2002).
[227] P. -C. Chen, T. -Y. Yeh, C. -M. Ou, C. -C. Shih and H. -T. Chang, Synthesis of Aluminum Oxide Supported Fluorescent Gold Nanodots for the Detection of Silver Ions, Nanoscale **5**, 4691 (2013).
[228] J. Liu, P. N. Duchesne, M. Yu, X. Jiang, X. Ning, R. D. Vinluan III, P. Zhang and J. Zheng, Luminescent Gold Nanoparticles with Size-Independent Emission, Angew. Chem. Int. Ed. **55**, 8894 (2016).
[229] H. Häkkinen and R . L. Whetten, Protected Metallic Clusters, Quantum Wells and Metal-Nanocrystal Molecules, J. Phys. Chem. C **114**, 15877 (2010).
[230] E. Heikkilä, H. Martinez-Seara, A. A. Gurtovenko, M. Javanainen, H. Häkkinen, I. Vattulainen and J. Akola, Cationic Au Nanoparticle Binding with Plasma Membrane-like Lipid Bilayers: Potential Mechanism for Spontaneous Permeation to Cells Revealed by Atomistic Simulations, J. Phys. Chem. C **118**, 11131 (2014).
[231] M. Di Vece, B. Kolaric, K. Baert, G. Schweitzer, M. Obradovic, R. A. L. Vallée, P. Lievens and K. Clays, Controlling the photoluminescence of CdSe/ZnS quantum dots with a magnetic field, Nanotechnology **20**, 135203 (2009).
[232] A. Toyota and T. Sagara, Particle size dependence of the charging of Au nanoparticles immobilized on a modified ITO electrode, Electrochim. Acta **53**, 2553 (2008).

[233] H. Haberland, *Clusters of Atoms and Molecules: Theory Experiment, and Clusters of Atoms*, Springer-Verlag, Berlin (1994).
[234] R. Kubo, Electronic properties of metallic fine particles, J. Phys. Soc. Jpn. **17**, 975 (1962).
[235] T. G. Schaaff, G. Knight, M. N. Shafigullin, R. F. Borkman and R. L. Whetten, Isolation and selected properties of a 10.4 kDa gold: glutathione cluster compound, J. Phys. Chem. B **102**, 10643 (1998).
[236] X. C. Wu, J. M. Hong, Z. J. Han and Y. R. Tao, Fabrication and photoluminescence characteristics of single crystalline In_2O_3 nanowires, Chem. Phys. Lett. **373**, 28 (2003).
[237] H. Zhou, W. Cai and L. Zhang, Photoluminescence of indium-oxide nanoparticles dispersed within pores of mesoporous silica, Appl. Phys. Lett. **75**, 495 (1999).
[238] E. Dulkeith, T. Niedereichholz, T. A. Klar, J. Feldmann, G. von Plessen, D. I. Gittins, K. S. Mayya and F. Caruso, Plasmon emission in photoexcited gold nanoparticles, Phys. Rev. B **70**, 205424 (2004).
[239] Z. Li, Y. Liu, S.F.L. Mertens, I.V. Pobelov and T. Wandlowski, From Redox Gating to Quantized Charging, J. Am. Chem. Soc. **132**, 8187 (2010).
[240] S. Chen and R. W. Murray, Electrochemical Quantized Capacitance Charging of Surface Ensambles of Gold Nanoparticles, J. Phys. Chem. B **103**, 9996 (1999).
[241] D. Derkacs, W. V. Chen, P. M. Matheu, S. H. Lim, P. K. L. Yu and E. T. Yu, Nanoparticle-induced light scattering for improved performance of quantum-well solar cells, Appl. Phys. Lett. **93**, 91107 (2008).
[242] Y. H. Su, Y. F. Ke, S. L. Cai and Q. Y. Yao, Surface Plasmon resonance of layer-by-layer gold nanoparticles induced photoelectric current in environmentally-friendly plasmon-sensitized solar cell, Nat. Nanotechnol. **6**, 28 (2011).
[243] E. Hutter, J. H. Fendler and D. Roy, Surface Plasmon Resonance Studies of Gold and Silver Nanoparticles Linked to Gold and Silver Substrates by 2-Aminoethanethiol and 1,6-Hexanedithiol, J. Phys. Chem. B, **105**, 11159 (2001).

[244] P. Tobiška, O. Hugon, A. Trouillet and H. Gagnaire, An integrated optic hydrogen sensor based on SPR on palladium, Sens. Actuators B **74**, 168 (2001).
[245] A. O. Govorov and I. Carmeli, Hybrid Structures Composed of Photosynthetic System and Metal Nanoparticles: Plasmon Enhancement Effect, Nano Lett. **7**, 620 (2007).
[246] D. B. Ingram, P. Christopher, J. L. Bauer and S. Linic, Predictive Model for the Design of Plasmonic Metal/Semiconductor Composite Photocatalysts, ACS Catal. **1**, 1441 (2011).
[247] I. M. Soganci, S. Nizamoglu, E. Mutlugun, O. Akin and H.V. Demir, Localized plasmon-engineered spontaneous emission of CdSe/ZnS nanocrystals closely-packed in the proximity of Ag nanoisland films for controlling emission linewidth, peak, and intensity, Opt. Express **15**, 14289 (2007).
[248] J. Zhang, Y. Tang, K. Lee and M. Ouyang, Tailoring light–matter–spin interactions in colloidal hetero-nanostructures, Nature **466**, 91 (2010).
[249] J. H. Song, T. Atay, S. Shi, H. Urabe and A. V. Nurmikko, Large Enhancement of Fluorescence Efficiency from CdSe/ZnS Quantum Dots Induced by Resonant Coupling to Spatially Controlled Surface Plasmons, Nano Lett. **5**, 1557 (2005).
[250] K. Okamoto, S. Vyawahare and A. Scherer, Surface-plasmon enhanced bright emission from CdSe quantum-dot nanocrystals, J. Opt. Soc. Am. B **23**, 1674 (2006).
[251] M. Liu, S. W. Qu, W. W. Yu, S. Y. Bao, C. Y. Ma, Q. Y. Zhang, J. He, J. C. Jiang, E. Meletis and C. L. Chen, Photoluminescence and extinction enhancement from ZnO films embedded with Ag nanoparticles, Appl. Phys. Lett. **97**, 231906 (2010).
[252] Y. H. Zheng, L. R. Zheng, Y. Y. Zhan, X. Y. Lin, Q. Zheng and K. M. Wei, Ag/ZnO heterostructure nanocrystals: Synthesis, characterization, and photocatalysis, Inorg. Chem. **46**, 6980 (2007).
[253] K. C. Je, H. Ju, M. Treguer, T. Cardinal and S. H. Park, Local field-induced optical properties of Ag-coated CdS quantum dots, Opt. Express **14**, 7994 (2006).
[254] X. N. Peng, Z. K. Zhou, W. Zhang and Z. H. Hao, Dynamically tuning emission band of CdSe/ZnS quantum dots

assembled on Ag nanorod array: plasmon-enhanced Stark shift, Opt. Express **19**, 24804 (2011).
[255] S. Wang, S. Boussaad, S. Wong and N. J. Tao, High-Sensitivity Stark Spectroscopy Obtained by Surface Plasmon Resonance Measurement, Anal. Chem. **72**, 4003 (2000).
[256] D. A. B. Miller, D. S. Chemla, T. C. Damen, A. C. Gossard, W. Wiegmann, T. H. Wood and C. A. Burrus, Band-Edge Electroabsorption in Quantum Well Structures: The Quantum-Confined Stark Effect, Phys. Rev. Lett. **53**, 2173 (1984).
[257] R. L. Hoffman, B. J. Norris and J. F. Wager, ZnO-based transparent thin-film transistors, Appl. Phys. Lett. **82**, 733 (2003).
[258] A. Janotti and C. G. Van de Walle, Fundamentals of zinc oxide as a semiconductor, Rep. Prog. Phys. **72**, 126501 (2009).
[259] M. Fukuda, *Optical semiconductor devices*, Wiley, New York, 1999, p 268.
[260] J. E. Stehr, S. L. Chen, N. K. Reddy, C. W. Tu, W. M. Chen and I. A. Buyanova, Turing ZnO into an Efficient Energy Upconversion Material by Defect Engineering, Adv. Funct. Mater. **24**, 3760 (2014).
[261] B. Anand, S. R. Krishnan, R. Podila, S. Siva Sankara Sai, A. M. Rao and R. Philip, The role of defects in the nonlinear optical absorption behavior of carbon and ZnO nanostructures, Phys. Chem. Chem. Phys. **16**, 8168 (2014).
[262] Z. L. Wang, Zinc oxide nanostructures: growth, properties and applications, J. Phys: Condens. Matt. **16**, R829 (2004).
[263] Z. L. Wang and J. Song, Piezoelectric Nanogenerators Based on Zinc Oxide Nanowires Arrays, Science **312**, 242 (2006).
[264] M. Kadota and M. Minakata, Piezoelectric Properties of Zinc Oxide Films on Glass Substrates Deposited by RF-Magnetron-Mode Electron Cyclotron Resonance Sputtering System, IEEE Trans. Ultrason. Ferroelectr. Freq. Contr. **42**, 345 (1995).
[265] C. He and W. Zhang, Effect of Electric Field on Electronic Properties of Nanogenerators Based on ZnO Nanowires, Nanosci. Nanotechnol. Lett. **5**, 286 (2013).

[266] S. H. Park, Exciton Binding Energy in Wurtzite ZnO/MgZnO Quantum Wells with Spontaneous and Piezoelectric Polarizations, J. Kor. Phys. Soc. **51**, 1404 (2007).
[267] T. Makino, Y. Segawa, M. Kawasaki and H. Koinuma, Optical Properties of Excitons in ZnO-based Quantum Well Heterostructures, Semicond. Sci. Technol. **20**, S78 (2004).
[268] R. E. I. Schropp and A. Madan, Properties of conductive zinc oxide films for transparent electrode applications prepared by rf magnetron sputtering, J. Appl. Phys. **66**, 2027 (1989).
[269] A. I. Ryasnyanskiy, B. Palpant, S. Debrus, U. Pal and A. L. Stepanov, Optical nonlinearities of Au nanoparticles embedded in a zinc oxide matrix, Opt. Commun. **273**, 538 (2007).
[270] G. B. Palmer, K. R. Poeppelmeier and T. O. Mason, Conductivity and Transparency of ZnO/SnO_2-Cosubstituted In_2O_3, Chem. Mater. **9**, 3121 (1997).
[271] S. J. Pearton, D. P. Norton, K. Ip, Y. W. Heo and T. Steiner, Recent progress in processing and properties of ZnO, Prog. Mater. Sci. **50**, 293 (2005).
[272] F. C. Chiu, Conduction Mechanism in Resistance Switching Memory Devices Using Transparent Boron Doped Zinc Oxide Films, Materials **7**, 7339 (2014).
[273] H. Yoshikawa, S. Adachi, Optical Constants of ZnO, Jpn. J. Appl. Phys. **36**, 6237 (1997).
[274] Z. H. Dai, R. J. Zhang, J. Shao, Y. M. Chen, Y. X. Zheng, J. D. Wu and L. Y. Chen, Optical Properties of Zinc-oxide Films Determined Using Spectroscopic Ellipsometry with Various Dispersion Models, J. Korean Phys. Soc. **5**, 1227 (2009).
[275] S. Dhara and P. K. Giri, Quick single-step mechanosynthesis of ZnO nanorods and their optical characterization: milling time dependence, Appl. Nanosci. **1**, 165 (2011).
[276] T. Pauporte, E. Jouanno, F. Pelle, B. Viana and P. Ashehoung, Key Growth Parameters for the Electrodeposition of ZnO Films with an Intense UV-Light Emission at Room Temperature, J. Phys. Chem. C **113**, 10422 (2009).
[277] J. Stark, *Beobachtungen über den Effekt des elektrischen Feldes auf Spektrallinien*, Sitzungsberichte Königlich

Preussischen Akademie der Wissenschaften: 932-46 (Berlin: Kgl. Akademie d. Wissenschaften Berlin G. Reimer), 1913.
[278] J. D. Dow and D. Redfield, Electroabsorption in Semiconductors: The Excitonic Absorption Edge, Phys. Rev. B **1**, 3358 (1970).
[279] M. S. Leeson, Design of a Franz–Keldysh effect electroabsorption waveguide modulator for millimetre-wave generation, Opt. Laser Technol. **34**, 475 (2002).
[280] W. Xu, Magneto-optical Franz-Keldysh effect of an electron gas subjected to quantizing magnetic fields and intense terahertz laser fields, Phys. Rev. B **64**, 113310 (2001).
[281] D. A. B. Miller, D. S. Chemla and S. Schmitt-Rink, Relation between electroabsorption in bulk semiconductors and in quantum wells: The quantum-confined Franz-Keldysh effect, Phys. Rev. B **33**, 6976 (1986).
[282] K. Sato, T. Abe, R. Fujinuma, K. Yasuda, T. Yamaguchi, H. Kasada and K. Ando, Stark effects of ZnO thin film and ZnO/ZnMgO quantum Wells, Phys. Status Solidi C **9**, 1801 (2012).
[283] H. Alves, D. Pfisterer, A. Zeuner, T. Riemann, J. Christen, D. M. Hofmann and B. K. Meyer, Optical investigations on excitons bound to impurities and dislocations in ZnO, Opt. Mater. **23**, 33 (2003).
[284] D. Pradhan, S. K. Mohapatra, S. Tymen, M Misra and K. T. Leung, Morphology-Controlled ZnO Nanomaterials for Enhanced Photoelectrochemical Performance, Mater. Express **1**, 59 (2011).
[285] M. K. Kavitha, K. B. Jinesh, R. Philip, P. Gopinath and H. John, Defect engineering in ZnO nanocones for visible photoconductivity and nonlinear absorption, Phys. Chem. Chem. Phys. **16**, 25093 (2014).
[286] W. Y. Ching and R. Rulis, *Electronic Structure Methods for Complex Materials: The orthogonized linear combination of atomic orbitals - Application to Impurities Defects and Surfaces*, Oxford University Press, Oxford, 2012, p. 180.
[287] M. F. Thorpe and L. Tichy (Eds.) *Properties and Applications of Amorphous Materials*, Springer Science, Dodrecht, 2001, p. 401.

[288] R. C. Rai, M. Guminiak, S. Wilser, B. Cai and M. L. Nakarmi, Elevated temperature dependence of energy band gap of ZnO thin films grown by e-beam deposition, J. Appl. Phys. **111**, 073511 (2012).
[289] C. Hägglund and V. P. Zhdanov, Charge distribution on and near Schottky nanocontacts, Physica E **33**, 296 (2006).
[290] C. Malagu, V. Guidi, M. Stefancich, M. C. Carotta and G. Martinelli, Model for Schottky barrier and surface states in nanostructured n-type semiconductors, J. Appl. Phys, **91**, 807 (2002).
[291] D. E. Eastman, Photoelectric Work Functions of Transition, Rare-Earth, and Noble Metals, Phys. Rev. B **2**, 1 (1970).
[292] S. Ju, S. Kim, S. Mohammadi, D. B. Janes, Y. Ha, A. Facchetti and T. J. Marks, Interface studies of ZnO nanowire transistors using low-frequency noise and temperature-dependent I-V measurements, Appl. Phys. Lett. **92**, 022104 (2008).
[293] R. Schlaf, H. Murata and Z. H. Kafafi, Work function measurements on indium tin oxide films, J. Electron. Spectrosc. Relat. Phenom. **120**, 149 (2001).
[294] V. P. Zhdanov, nm-sized metal particles on a semiconductor surface, Schottky model, etc., Surf. Sci. **512**, L331 (2002).
[295] T. Nagata, T. Shimura, A. Ashida, N. Fujimura and T. Ito, Electro-optic property of ZnO:X (X=Li,Mg) thin films, J. Cryst. Growth **237–239**, 533 (2002).
[296] S. K. Dondapati, M. Ludemann, R. Müller, S. Schwieger, A. Schwemer, B. Händel, D. Kwiatkowski, M. Djiango, E. Runge and T. A. Klar, Voltage-Induced Adsorbate Damping of Single Gold Nanorod Plasmons in Aqueous Solution, Nano Lett. **12**, 1247 (2012).
[297] T. Kiyonaga, M. Fujii, T. Akita, H. Kobayashi and H. Tada, Size-dependence of Fermi energy of gold nanoparticles loaded on titanium(IV) dioxide at photostationary state, Phys. Chem. Chem. Phys. **10**, 6553 (2008).
[298] K. S. Novoselov, A. K. Geim, S. V. Morozov, D. Jiang, Y. Zhang, S. V. Dubonos, I. V. Grigorieva and A. A. Firsov,

Electric Field Effect in Atomically Thin Carbon Film, Science **306**, 666 (2004).
[299] H. Over and P. Seitsonen, Oxidation of Metal Surfaces, Science **297**, 2003 (2002).
[300] C. I. Carlisle, T. Fujimoto, W. S. Sim and D. A. King, Atomic imaging of the transition between oxygen chemisorption and oxide film growth on Ag{111}, Surf. Sci. **470**, 15 (2000).
[301] M. Bowker, M. A. Bareau, R. J. Madix, Oxygen induced adsorption and reaction of H_2, H_2O, CO and CO_2 on single crystal Ag(110), Surf. Sci. **92**, 528 (1980).
[302] E. Prodan, C. Radloff, N. J. Halas and P. Nordlander, A Hybridization Model for the Plasmon Response of Complex Nanostructures, Science **302**, 419 (2003).
[303] C. Radloff and N. J. Halas, Plasmon Properties of Concentric Nanoshells, Nano Lett. **4**, 1323 (2004).
[304] A. Kuzma, M. Weis, S. Flickyngerova, J. Jakabovic, A. Satka, E. Dobrocka, J. Chlpik, J. Cirak, M. Donoval, P. Telek, F. Uherek and D. Donoval, Influence of surface oxidation on plasmon resonance in monolayer of gold and silver nanoparticles, J. Appl. Phys. **112**, 103531 (2012).
[305] N. T. Fofang, N. K. Grady, Z. Fan, A. O. Govorov and N. J. Halas, Plexciton Dynamics: Exciton-Plasmon Coupling in a J-Aggregate-Au Nanoshell Complexes Provides a Mechanism for Nonlinearity, Nano Lett. **11**, 1556 (2011).
[306] M. Acherman, Exciton-Plasmon Interactions in Metal-Semiconductor Nanostructures, J. Phys. Chem. Lett. **1**, 2837 (2010).
[307] N. T. Fofang, T. H. Park, O. Neumann, N. A. Mirin, P. Nordlander, N. J. Halas, Plexcitonic Nanoparticles: Plasmon Exciton Coupling in Nanoshell-J-Aggregate Complexes, Nano Lett. **8**, 3481 (2008).
[308] N. T. Fofang, *Optical Properties of Strongly Coupled Plasmon-Exciton Hybride Nanostructures*, PhD thesis, Rice University, Huston, Texas, USA (2011).
[309] D. Marinica, H. Lourenço-Martins, J. Aizpurua and A. G. Borisov, Plexcitonic Quenching by Resonant Electron Transfer from Quantum Emitter to Metallic Nanoantenna, Nano Lett. **13**, 5972 (2013).

[310] J. Dintinger, S. Klein, F. Bustos, W. L. Barnes and T. W. Ebbesen, Strong coupling between surface plasmon-polaritons and organic molecules in subwavelength hole arrays, Phys. Rev. B **71**, 035424 (2005).
[311] G. A. Wurtz, P. R. Evans, W. Hendern, R. Atkinson, W. Dickson, R. J. Pollard, A. V. Zayats, W. Harrison and C. Bower, Molecular Plasmonics with Tunable Exciton-Plasmon Coupling Strength in J-Aggregate Hybridized Au Nanorod Assemblies, Nano Lett. **7**, 1297 (2007).
[312] Y. Sugawara, T. A. Kelf, J. J. Baumberg, M. E. Abdelsalam and P. N. Barlett, Strong Coupling between Localized Plasmon and Organic Excitons in Metal Nanovoids, Phys. Rev. Lett. **97**, 266808 (2006).
[313] J. M. J. Santillán, L. B. Scaffardi and D. C. Schinca, Quantitative optical extinction-based parametric method for sizing a single core shell Ag-Ag_2O nanoparticle, J. Phys. D: Appl. Phys. **44**, 105104 (2011).
[314] Z. V. Popović, M. Grujić-Brojčin, N. Paunović, M. M. Radonjić, V. D. Araújo, M. I. B. Bernardi, M. M. de Lima and A. Cantarero, Far-infrared spectroscopic study of CeO_2 nanocrystals, J. Nanopart. Res. **17**, 23 (2015).
[315] D. D. Evanoff, L. R. L. White and G. Chumanov, Measuring the Distance Dependence of the Local Electromagnetic Field from Silver Nanoparticles, J. Phys. Chem. B **108**, 1522 (2004).
[316] K. F. Young and H. P. R. Frederikse, Compilation of the Static Dielectric Constant of Inorganic Solids, J. Phys. Chem. Ref. Data **2**, 313 (1973).
[317] J. Qiu, P. Zhou, X. Gao, J. Yu, S. Wang, J. Li, Y. Zheng, Y. Yang, Q. Song and L. Chen, Ellipsometric Study of the Optical Properties of Silver Oxide Prepared by Reactive Magnetron Sputtering, J. Korean Phys. Soc. **46**, S269 (2005).
[318] E. Mosquera, C. Rojas-Michea, M. Morel, F. Gracia, V. Fuenzalida and R. A. Zárate, Zinc oxide nanoparticles with incorporated silver: Structural, morphological, optical and vibrational properties, Appl. Surf. Sci. **347**, 561 (2015).
[319] O. Peña-Rodriguez and U. Pal, Effects of surface oxidation on the linear optical properties of Cu nanoparticles, J. Opt. Soc. Am. B **28**, 2735 (2008).

[320] F. Todisco, S. D'Agostino, M. Esposito, A. I. Fernàndez-Domìnguez, M. De Giorgi, D. Ballarini, L. Dominici, I. Tarantini, M. Cuscunà, F. Della Sala, G. Gigli, D. Sanvitto, Exciton-Plasmon Coupling Enhancement via Metal Oxidation ACS Nano **9**, 9691 (2015).
[321] A. Cuche, O. Mollet, A. Drezet and S. Huant, "Deterministic" Quantum Plasmonics, Nano Lett. **10**, 4566 (2010).
[322] M. S. Tame, K. R. McEnery¸S. K. Özdemir, J. Lee, S. A. Maier and M. S. Kim, Quantum plasmonics, Nat. Phys. **9**, 329 (2013).
[323] Z. Jacob and V. M. Shalaev, Plasmonics Goes Quantum, Science **334**, 463 (2011).
[324] K. Chatteree, S. Banerjee and D. Chakravorty, Plasmon resonance shifts in oxide-coated silver nanoparticles, Phys. Rev. B **66**, 085421 (2002).
[325] J. Ghilane, F. R. Fan, A. J. Bard and N. Dunwoody, Facile Electrochemical Characterization of the Core/Shell Nanoparticles. Ag Core/Ag_2O Shell Structures, Nano Lett. **7**, 1406 (2007).
[326] J. Lee, P. Hernandez, J. Lee, A. O. Govorov and N. A. Kotov, Exciton-plasmon interactions in molecular springh assemblies of nanowires and wavelength-based protein detection, Nature Mat. **6**, 291 (2007).
[327] J. Bellessa, C. Symonds, J. Laverdant, J. M. Benoit, J. C. Plenet and S. Vignoli, Strong Coupling between Plasmons and Organic Semiconductors, Electronics **3**, 303 (2014).
[328] X. Bao, M. Muhler, Th. Schedel-Niedrig and R. Schlögl, Interaction of oxygen with silver at high temperature and atmospheric pressure: A spectroscopic and structural analysis of a strongly bound surface species, Phys. Rev. B **54**, 2249 (1996).
[329] O. S. Ivanova and F. P. Zamborini, Size-Dependent Electrochemical Oxidation of Silver Nanoparticles, J. Am. Chem. Soc. **132**, 70 (2010).
[330] B. Niesen, B. P. Rand, P. Van Dorpe, H. Shen, B. Maes, J. Genoe and Paul Hereman, Excitation of multiple dipole surface plasmon resonances in spherical silver nanoparticles, Opt. Express **18**, 19032 (2010).

[331] Y. Liu, Y. Park and S. E. Lee, Thermo-responsive mechano-optical plasmonic nano-antenna, Appl. Phys. Lett. **109**, 013109 (2016).
[332] F. Huang, X. Wang, J. Xu, D. Chen and Y. Wang, A plasmonic nano-antenna with controllable resonance frequency: $Cu_{1.94}S$–ZnS dimeric nanoheterostructure synthesized in solution, J. Mater. Chem. **22**, 22614 (2012).
[333] B. D. Johs, J. Hale, N. J. Ianno, C. M. Herzinger, T. E. Tiwald and J. A. Woollam, Recent developments in spectroscopic ellipsometry for in-situ applications, SPIE 4449, p. 41-57 (2001).
[334] E. Pisler and T. Adhikari, Numerical Calculation of Mutual Capacitance between Two Equal Metal Spheres, Phys. Scripta **2**, 81 (1970).
[335] E. Di Lorenzo, The Maxwell Capacitance Matrix, White Paper WP110301 (2011).
[336] T. Reiners, C. Ellert, M. Schmidt and H. Haberland, Size Dependence of the Optical Response of Spherical Sodium Clusters, Phys. Rev. Lett. **74**, 1558 (1995).
[337] S. Peng, J. M. McMahon, G. C. Schatz, S. K. Gray and Y. Sun, Reversing the size-dependence of surface plasmon resonances, Proc. Natl. Acad. Sci. U.S.A. **107**, 14530 (2010).
[338] P. Apell and A. Ljungbert, A General Non-Local Theory for the Electromagnetic Response of a Small Metal Particle, Phys. Scripta **26**, 113 (1982).
[339] P. Apell and D. R. Penn, Optical Properties of Small Metal Spheres: Surface Effects, Phys. Rev. Lett. **50**, 1316 (1983).
[340] D. R. Penn and P. Apell, Anomalous electron energy loss in small spheres, J. Phys. C: Solid State Phys. **16**, 5729 (1983).
[341] P. J. Feibelman, Surface Electromagnetic Field, Prog. Surf. Sci. **12**, 287 (1982).
[342] R. L. Olmon, B. Slovick, T. W. Johnson, D. Shelton, S. H. Oh, G. D Boreman and M. B. Raschke, Optical dielectric function of gold, Phys. Rev. B **86**, 235147 (2012).

Curriculum Vitae

Milan (Stankov) Obradović

Married to: Olga Obradović
Father to: Sava (8), Vasilija (6), Danica (4), … … …

May 5, 1982	Born in Inđija (Инђија) Serbia (Србија)
1989-1997	Elementary School Petar Kočić (“Петар Кочић”) Inđija, Serbia
1997-2001	High School of Mathematics and Natural Sciences “Gimnazija”, Inđija, Serbia High School Thesis Title: “*Matrix inversion*” Award for the best student in class 2001

1999/2000	Young researcher in IYRC “Petnica”, Serbia
2001-2007	Faculty of Electrical Engineering (minor: Physical Electronics) Univeristy of Belgrade, Serbia Diploma Thesis Title: “*Review of methods for polygraphic signals analysis*”
2007	Research Assistant Laboratory for Quantum Optics and Lasers Institute of Physics Belgrade
2008-2017	PhD at the Faculty of Science (Solid State Physics and Magnetism) KU Leuven, Belgium PhD thesis Title: “*Electro-optical switching properties of plasmonic nanoparticles inside capacitor-like nanostructures*”

List of publications

2016 M. Obradovic, M. Di Vece, D. Grandjean, K. Houben, P. Lievens, ***Charging Gold Nanoparticles in ZnO by Electric Fields***, J. Phys. Condens. Matter. **28**, 035303 (2016).

2015 M. Obradovic, M. Di Vece, I. Asselberghs, D. Grandjean, K. Clays, P. Lievens, ***Photoluminescence as a Probe of the Electrical Charge Dependence of Gold Nanoparticles***, J. Nanosci. Nanotechnol. **15**, 9766 (2015).

2009 M. Di Vece, B. Kolaric, K. Baert, G. Schweitzer, M. Obradovic, R. A. L. Valée, P. Lievens, K. Clays, ***Controlling the photoluminescence of CdSe/ZnS quantum dots with a magnetic field***, Nanotechnology **20**, 135203 (2009).

2007 Z. D Grujic, M. M. Mijailovic, B. M. Pantic, M. Minic, A. G. Kovacevic, M. Obradovic, B. M. Jelenkovic, S. Cartaleva, ***Zeeman Coherence Narrowing due to Ramsey Effects Induced by Thermal Motion of Rubidium Atoms***, Acta Phys. Pol. A **112**, 799 (2007).